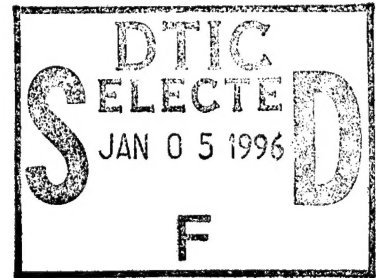


NAVAL POSTGRADUATE SCHOOL

Monterey, California



THESIS

**AN ANALYSIS OF HYPERSPECTRAL IMAGERY
DATA COLLECTED DURING OPERATION
DESERT RADIANCE**

by

Matthew E. Fay

June, 1995

Principal Advisor:
Second Reader:

Richard C. Olsen
Terry Alfriend

Approved for public release; distribution is unlimited.

DTIC QUALITY INSPECTED 1

19960103 133

REPORT DOCUMENTATION PAGE			Form Approved OMB No. 0704-0188	
Public reporting burden for this collection of information is estimated to average 1 hour per response, including the time for reviewing instruction, searching existing data sources, gathering and maintaining the data needed, and completing and reviewing the collection of information. Send comments regarding this burden estimate or any other aspect of this collection of information, including suggestions for reducing this burden, to Washington headquarters Services, Directorate for Information Operations and Reports, 1215 Jefferson Davis Highway, Suite 1204, Arlington, VA 22202-4302, and to the Office of Management and Budget, Paperwork Reduction Project (0704-0188) Washington DC 20503.				
1. AGENCY USE ONLY (Leave blank)		2. REPORT DATE June 1995		3. REPORT TYPE AND DATES COVERED Master's Thesis
4. TITLE AND SUBTITLE An Analysis of Hyperspectral Imagery Data Collected During Operation DESERT RADIANCE				5. FUNDING NUMBERS
6. AUTHOR(S) Matthew E. Fay				
7. PERFORMING ORGANIZATION NAME(S) AND ADDRESS(ES) Naval Postgraduate School Monterey CA 93943-5000				8. PERFORMING ORGANIZATION REPORT NUMBER
9. SPONSORING/MONITORING AGENCY NAME(S) AND ADDRESS(ES)				10. SPONSORING/MONITORING AGENCY REPORT NUMBER
11. SUPPLEMENTARY NOTES The views expressed in this thesis are those of the author and do not reflect the official policy or position of the Department of Defense or the U.S. Government.				
12a. DISTRIBUTION/AVAILABILITY STATEMENT Approved for public release; distribution unlimited				12b. DISTRIBUTION CODE
13. ABSTRACT (<i>maximum 200 words</i>) The utility of hyperspectral imagers for the identification, classification and status of a specific material based on it's spectral characteristics has been demonstrated in the fields of geology, forestry and meteorology. The United States military has an interest in the utility of hyperspectral imagers for a multitude of tactical and strategic purposes. The Hyperspectral MASINT Support to Military Operations Program (HYMSMO) was designed to explore this arena through a series of planned collection operations utilizing the Hyperspectral Digital Imagery Collection Experiment (HYDICE) sensor in addition to other hyperspectral imaging platforms. Operation DESERT RADIANCE explored many of the areas relating to the tactical detection and classification of military targets. Through the use of the Low Probability of Detection and the Principle Components Transformation algorithms contained in the HYDICE Starter Kit and ENVI software package, this thesis shows that the detection of a tactical target by use of it's unique spectral signature is feasible.				
14. SUBJECT TERMS Hyperspectral Imagery, Image Processing, Material Detection Algorithms				15. NUMBER OF PAGES 117
				16. PRICE CODE
17. SECURITY CLASSIFICATION OF REPORT Unclassified		18. SECURITY CLASSIFICATION OF THIS PAGE Unclassified		19. SECURITY CLASSIFICATION OF ABSTRACT Unclassified
				20. LIMITATION OF ABSTRACT UL

NSN 7540-01-280-5500

Standard Form 298 (Rev. 2-89)

Prescribed by ANSI Std. Z39-18

Approved for public release; distribution is unlimited.

**AN ANALYSIS OF HYPERSPECTRAL IMAGERY DATA COLLECTED
DURING OPERATION DESERT RADIANCE**

Matthew Edward Fay
Major, United States Marine Corps
B.S., Norwich University, 1978

submitted in partial fulfillment of the requirements for the degree of

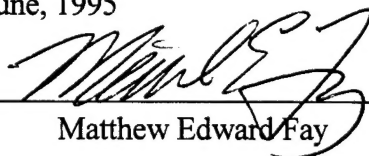
**MASTER OF SCIENCE IN SYSTEMS TECHNOLOGY
(SPACE SYSTEMS OPERATIONS)**

from the

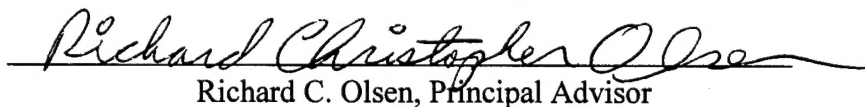
NAVAL POSTGRADUATE SCHOOL

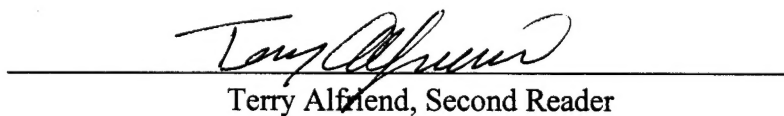
June, 1995

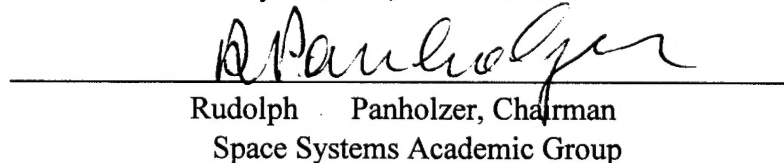
Author:


Matthew Edward Fay

Approved by:


Richard C. Olsen, Principal Advisor


Terry Alfriend, Second Reader


Rudolph Panholzer, Chairman
Space Systems Academic Group

Accession For		
NTIS	CRA&I	<input checked="checked" type="checkbox"/>
DTIC	TAB	<input type="checkbox"/>
Unannounced		<input type="checkbox"/>
Justification		
By		
Distribution /		
Availability Codes		
Dist	Avail and/or Special	
A-1		

ABSTRACT

The utility of hyperspectral imagers for the identification, classification and status of a specific material based on its spectral characteristics has been demonstrated in the fields of geology, forestry and meteorology. The United States military has an interest in the utility of hyperspectral imagers for a multitude of tactical and strategic purposes. The Hyperspectral MASINT Support to Military Operations Program (HYMSMO) was designed to explore this arena through a series of planned collection operations utilizing the Hyperspectral Digital Imagery Collection Experiment (HYDICE) sensor in addition to other hyperspectral imaging platforms. Operation DESERT RADIANCE explored many of the areas relating to the tactical detection and classification of military targets. Through the use of the Low Probability of Detection and the Principle Components Transformation algorithms contained in the HYDICE Starter Kit and ENVI software package, this thesis shows that the detection of a tactical target by use of its unique spectral signature is feasible.

TABLE OF CONTENTS

I. INTRODUCTION	1
II. BACKGROUND	5
A. HISTORY OF HYPERSPECTRAL IMAGING	5
1. Concept	5
2. Evolution	7
a. Airborne Imaging Spectrometer (AIS I/II)	8
b. Airborne Visible/Infrared Imaging Spectrometer (AVIRIS)	9
c. Geophysical Environment Corporation Imaging Spectrometer (GERIS)	14
d. Fluorescence Line Imager (FLI)	14
e. Hyperspectral Digital Imagery Collection Experiment (HYDICE)	15
f. Shuttle Imaging Spectrometer Experiment (SISEX)	16
g. Moderate Resolution Imaging Spectrometer (MODIS)	17
3. Evolution Summary	18
B. ANALYSIS TECHNIQUES	18
1. Principle Components	19
2. Spectral Mixture Analysis	20
3. Low Probability of Detection (LPD)	21
4. Constrained Energy Minimization (CEM)	22
III. EXPERIMENT DESCRIPTION	23
A. OPERATION DESERT RADIANCE	23
1. Experiment/Objective Breakdown	24
a. Airborne Data Collection Objectives	24
(1) Experiment A	24
(2) Experiment B	25
b. Tower-Based Data Collect Objectives	25
2. White Sands Missile Range (WSMR)	26
3. Target Descriptions	26

a. Fabric and Painted Panels	26
b. Optical Target	29
4. Ground Truth Measurements	30
5. Sensor Characteristics	31
a. Advanced Airborne Hyperspectral Imaging System (AAHIS)	31
b. GER Digital Airborne Imaging Spectrometer (DAIS)	32
IV. EXPERIMENT OBSERVATIONS	35
A. WHITE SANDS MISSILE RANGE OBSERVATIONS	35
1. OPERATION DESERT RADIANCE	35
2. Site Layout	36
3. Weather Conditions	36
4. Targets	37
a. Materials	37
b. Construction	38
c. Care and Maintenance	38
d. Deployment/Retrieval	39
5. Experiment Sites	39
a. General Soil and Vegetation Make-up	39
b. Preparation	39
6. Ground Truth Measurements	40
7. Sensor Platform Performance	40
a. Pilot Proficiency	41
b. Airspace Coordination	41
c. Sensor Reliability	42
B. HYPERSPECTRAL OBSERVATIONS	42
1. Hardware and Software Configuration	42
a. HYDICE Starter Kit	43
b. ENVI	43
2. Hyperspectral Image Data	44
a. AAHIS Data	45
b. GER (DAIS) Data	45

V. DATA ANALYSIS	47
A. SPATIAL ANALYSIS OF THE SCENE	47
B. SPECTRAL ANALYSIS	48
1. Data Conversion	49
2. Data Preparation	49
3. Target Spectra Selection	50
4. LPD Analysis	51
a. LPD Results (TANK Target)	51
b. LPD Results (TAN BROWN Target)	52
5. Principle Components Analysis	53
a. Principle Component Results	53
VI. CONCLUSIONS	55
APPENDIX. FIGURES	57
LIST OF REFERENCES	99
INITIAL DISTRIBUTION LIST	103

ACKNOWLEDGMENT

The author would like to thank the following members of the HYDICE Program Office for their great support provided during this research: Pete Mitchell, Greg Pavlin, Rod Buntzen, Dave Pope, Dave Aldridge, Joe Deaver, Debbie Davidson and Shelley Seburn. Special thanks to William Farrand of Analytical Imaging and Geophysics, John Colwell, Mary Kappas and Bill Stoner of Science Applications International Corporation, and Joe Harsanyi and Joe Heijl of Applied Signals Technology Incorporated, for sharing their expertise in the hyperspectral arena with the author. Financial support provided by the Program Office to Professor Olsen is gratefully acknowledged.

I. INTRODUCTION

The field of imaging spectrometry, also known as hyperspectral imaging, has slowly emerged over the past two decades. Hyperspectral imaging refers to remote sensing based collection of temporally-registered imagery over a large number of discrete, contiguous bands whereby a complete reflectance spectrum is obtained. With parallel advances in optics, microelectronics and image processing software, hyperspectral imaging has matured and can provide detailed information concerning the earth's environment and the warfighter's battlespace.

Electromagnetic energy is the most abundant energy form available for remote sensing applications. Within the electromagnetic spectrum, the visual and solar reflected infrared regions can reveal specific reflective and emissive spectral signatures of the imaged object. The value of hyperspectral imaging systems is their ability to acquire complete reflectance spectrum for each picture element (pixel) in the image. Many materials have definitive absorption features that are 20-40 nanometers wide and thus are undetectable by the current broadband multispectral sensor systems. Hyperspectral sensors nominally acquire data in 10 nm bands providing sufficient spectral resolution for direct identification of those materials.

Military applications for hyperspectral sensors are just beginning to be evaluated. In the past, manual analysis of stereo images by image interpreters has been used for determining the shape, size and arrangement of specific targets and their features. Examples include targets such as roads, airports, dams, vehicles, structures and urban areas. The location, identification and assessment of military significant targets within the battlefield can be enhanced with the use of hyperspectral sensor systems. By applying hyperspectral imaging techniques and analysis, other differences, not based on shape and size, such as color, spectral reflectance and spectral emittance (temperature) can be identified within the image. Specific camouflage types, including paint and fabric, soil composition, downed pilot taggants, stressed vegetation, thermal plumes, nuclear,

biological and chemical agents are a few among a list of many possible candidates for detection/identification by hyperspectral sensor systems.

The data obtained for military use by hyperspectral sensors will most likely fall within the field of measurement and signature intelligence (MASINT). Imagery interpretation (II) and imagery intelligence (IMINT) products have been the traditional methods for evaluating and disseminating information relating to the description of objects, activities and terrain within the battlespace. Literal exploitation of imagery deals with the extraction of information from imagery by a human interpreter. MASINT, on the other hand, deals with the nonliteral exploitation of imagery. A hybrid definition of nonliteral imagery exploitation can be found in Joint Pub 1-02:

The process of extracting non-spatial information from image data, automatically or semi-automatically, using non-traditional, advanced processing techniques, employing models, measurements, signatures (spectral, textural, temporal, polarization), or other features to detect, locate, classify, discriminate, characterize, identify (material, unit, function), quantify (material, time, physical), track, predict, target, or assess objects, emissions, activities, of events represented in the imagery.

The Hyperspectral MASINT Support to Military Operations (HYMSMO) program grew out of military requirements for Operational Measurement and Signature Intelligence (OpMASINT) support and is sponsored by the Central MASINT Technology Coordination Office (CMTO). It is designed to demonstrate and advocate the utility of imaging hyperspectral spectroradiometers as true MASINT resources (as opposed to conventional IMINT assets). In addition, the HYMSMO program will examine the nontraditional, time-sensitive, MASINT application termed support to military operations (SMO).

The Hyperspectral Digital Imagery Collection Experiment (HYDICE) is a Congressionally funded "dual-use" initiative that has developed an airborne, imaging hyperspectral spectroradiometer, offering high spectral fidelity, spatial resolution, and performance. HYDICE, as the sensor is called, is an integral part of the HYMSMO program and will be utilized for data collection experiments in the spring of 1995. Data

collection experiments using non-HYDICE sensors have been completed and will continue throughout the program lifetime. The purpose of these experiments is to begin to evaluate the use of hyperspectral sensors in the detection and classification of military significant targets. One such experiment, Operation DESERT RADIANCE, took place at the White Sands Missile Test Range in New Mexico. The purpose of this experiment was to demonstrate the potential for using hyperspectral remote sensing to differentiate among natural and man-made materials.

The thesis is broken down into five chapters and two appendices. Chapter I, the Introduction is followed by Chapter II, Background, which addresses the history and accomplishments of hyperspectral imagery along with a brief explanation of the most current hyperspectral image processing and analysis algorithms dealing with material detection. Chapter III, Experiment Description, discusses the Operation Desert Radiance experiment where the data analyzed in this thesis was collected. Chapter IV, Experiment Observations, highlights significant observations made during the author's participation in the experiment. Chapter V, Data Analysis, describes the methods used in the detection of an actual tactical target by use of its spectral signature and the results attained. Chapter VI, Conclusions is followed by the Appendix which includes all figures identified in the thesis.

II. BACKGROUND

Hyperspectral imaging is one of the many forms of remote sensing available today for extracting information relating to the earth and its surroundings. Because all materials reflect, absorb, or emit photons in ways characteristic of their molecular makeup, a high resolution trace of the intensity of the transmitted, reflected, emitted or luminesced radiation versus wavelength forms a graphical record unique to a given material. (Rinker, 1990). Figure 2.1 is a plot of the percent reflectance vs. wavelength of two fabrics and a green leaf. The water absorption features at 1.4 and 1.9 micrometers are clearly visible and the plot shows a close similarity between fabric A and green leaf B. Fabric C is closely matched in spectral shape out to about 1.1 micrometers but at approximately 1.8 micrometers where it begins to deviate significantly. These differences provide the means to identify materials and detect man-made objects in large "natural" scenes. Hyperspectral imaging refers to the imaging of an area or "scene" over a large number of discrete, contiguous spectral bands such that a complete reflectance spectrum can be obtained for the area being imaged. The field of hyperspectral imaging has evolved over the last 2 decades primarily due to efforts by the National Aeronautics and Space Administration (NASA), the Department of Defense (DOD) and recently, private industry research and development.

A. HISTORY OF HYPERSPECTRAL IMAGING

1. Concept

Terrestrial remote sensing from aircraft and space was developed to provide specific information about the makeup of the earth's surface which was not readily obtainable from direct observation on the surface. Panchromatic sensors provide information in parts of the visible portion of the electromagnetic (EM) spectrum only. The level of detail within the image is dependent on the sensitivity of the sensor's detectors to differences in signal strength as it records the radiant flux reflected or emitted

from the object being sensed. For example, the French SPOT (System Pour l'Observation de le Terre) Panchromatic sensor uses 6 bit, Differential Pulse Code Modulation (DPCM) which provides the capability to represent the image scene in 64 different levels of gray. While this provides adequate detail for most human analysis techniques, it focuses only in the visible portion of the EM spectrum and does not exploit the differences in the reflectivity, as a function of wavelength, that can be represented by multispectral sensors.

The LANDSAT Thematic Mapper (TM) is a multispectral sensor capable of imaging in 7 bands of the visible, near infrared (NIR), shortwave infrared (SWIR) and the thermal infrared portions of the EM spectrum. Figure 2.2 shows the location, in wavelength, of the TM bands. Note the coarse resolution and the gap from 0.9 to 1.5 microns. Data from several bands can be combined to produce an image that contains information from each bandpass selected. A false-color composite image can be constructed by the assignment of one of the three primary colors to each of the selected bands. This image can, in many instances, provide additional information beyond that of a panchromatic image alone.

The main limitations associated with multispectral sensor designs is their inability to acquire the information necessary to identify the composition of surface materials, because of the poor spectral resolution of the sensors. The spectral reflectance and emittance characteristics for surface materials, which are determined by electronic and vibrational energy states within the materials, are usually too highly structured to be observed at coarse spectral resolutions (Vane, 1985). Figure 2.2 shows characteristic spectra from various minerals, along with the bandpass ranges of the LANDSAT TM. Different causes of absorption can be identified in the mineral spectra. Absorption due to electronic transitions can be detected at 0.92 micrometers. Vibrational absorption features due to bound and unbound water become more important in the determination of the target material at around 1.0 micrometers. These features may however be masked due to the presence of strong atmospheric water bands at 1.4 and 1.9 micrometers. Many materials and minerals exhibit distinctive absorption features in the region from 2.1 to 2.4

micrometers. This is due primarily to the combination bending-stretching overtones of the OH vibration. Laboratory work in the field of spectroscopy demonstrated the wealth of information contained in the reflectance spectra of various minerals and vegetation types thereby motivating the development of imaging spectrometry (Vane and Goetz, 1993). A graphical depiction of the hyperspectral imaging concept is shown in Figure 2.3. Images taken simultaneously in 100-200 spectral bands form an image cube, with each layer of the cube representing a different wavelength. Each pixel will have an continuous spectrum that can be used to uniquely identify surface materials.

2. Evolution

Laboratory and field experiments conducted in the 1960's and 1970's confirmed the possibility that solar reflectance measurements by airborne sensors could permit the identification of the mineral makeup of rocks, soils and vegetation. However, the spectral resolution for specific identification would have to be on the order of 10 to 20 nanometers covering the spectral region of 400 to 2500 nanometers. These results motivated the development of airborne and spaceborne hyperspectral imagers in the late 1970's. Curiously, one of the first systems flew on an early Shuttle flight.

The Shuttle Multispectral Infrared Radiometer (SMIRR) was flown on STS-2 in 1981. SMIRR measured spectral reflectance in 10 spectral bands with a spatial resolution of 100 meters. Investigation of the data by A.F.H. Goetz and L.C. Rowan concluded that the SMIRR had detected a previously unmapped mineral deposit containing specific clay and carbonite minerals (Taranik et al, 1993).

In 1980, the Jet Propulsion Laboratory (JPL) began the development of the Thermal Infrared Multispectral Scanner (TIMS). Imaging in the 8 to 12 micrometer range with a spatial resolution of 20-30 meters, depending on flight altitude, TIMS first flew over Cuprite, Nevada gathering thermal emission spectra of the various mineral deposits. In August 1994 TIMS was flown on board a NASA C-130 aircraft over the McDowell

Mountains and urban areas of Scottsdale, Arizona to collect data that will be used by the city in the development of its Geographic Information System (GIS) (Constance, 1994).

a. Airborne Imaging Spectrometer (AIS I/II)

JPL began development of the AIS in the early 1980's after the successful flight of SMIRR on the shuttle. A critical area of sensor development had been that of the detector which is the device that converts the energy of the incoming photons to an electrical signal. Early multispectral sensors, the LANDSAT Multispectral Scanner and the Thematic Mapper, incorporated discrete detector elements which were scanned across the earth's surface as the spacecraft moved along its orbital path. The main limitation to these early designs was the short residence time of the detector in each instantaneous field of view (IFOV) thereby reducing the signal to noise ratio (SNR) of each detector element (Vane and Goetz, 1988). The use of multiple line arrays has been demonstrated by the French SPOT (System Probatoire Pour l'Observation de la Terre) satellite. An area array design was first utilized with AIS I. Designed as a testbed for the future development of space based, infrared imaging spectrometers, AIS I incorporated a 32 x 32 element, mercury cadmium telluride (HgCdTe) array. The AIS I sensor used a grating spectrometer to separate the incoming signal into 128 contiguous bands in the spectral region from 1.2 to 2.4 micrometers with a spectral resolution of 9.3 nanometers. AIS II was configured with a larger, 64 x 64 element, HgCdTe array and covered the region from 0.8 to 2.4 micrometers at a spectral resolution of 10.6 nanometers. Figure 2.4 depicts the evolution of different image acquisition techniques.

Kruse, 1987, utilized data sets acquired by both the AIS I and AIS II in an analysis of hydrothermally altered rocks in the northern Grapevine Mountains, of Nevada and California. By calculating the band position, band depth and bandwidth of the strongest absorption features of each spectrum and mapping these parameters into a hue, saturation, intensity (HSI) coded image, he was able to rapidly identify different mineral groups, as shown in Figure 2.5. Individual spectra from the images were

compared with laboratory spectra obtained from on-site samples. Positive identification of sericite, montmorillonite, calcite and dolomite was accomplished using the AIS data. As shown in Figure 2.6, the distinct absorption features at varying bandpasses provide a means to uniquely identify a specific mineral.

Some limitations in the use of the AIS II were found in a study conducted by Riggs and Running (1990). While studying Norway Spruce and White Pine plots, they determined that high spectral resolution imagers provided only limited information concerning water stress in conifers at the landscape scale. Figure 2.7 shows the relative reflectance plots of stressed and control White Pines. The plots clearly show that there is not a notable increase in the reflectance of the stressed group even though the group had been stressed for approximately 3 weeks. The weakness in the use of hyperspectral data for this purpose does not appear to have been sensor related. The problem appears to be that the apparent reflectances of the vegetation do not change appreciably with deprivation of soil water over extended periods. Only trees approaching lethally, low water content levels will be distinguishable.

Forest canopy characteristics and nitrogen cycling were analyzed using AIS data acquired over a series of Wisconsin forest ecosystems. Analysis revealed that the canopy lignin or a closely associated property was influential in canopy reflectance within the 1.2 to 1.6 micrometer spectral region. These results prove that further study of forest canopy chemistry with remote sensing should be conducted (Wessman, et al, 1987).

b. Airborne Visible/Infrared Imaging Spectrometer (AVIRIS)

The next major step in the evolution of imaging spectrometers was the Airborne Visible/Infrared Imaging Spectrometer (AVIRIS). First proposed to NASA in 1983, AVIRIS first flew engineering evaluation flights in 1987 and became operational in 1989. AVIRIS was originally designed for the airborne collection of spectral images that would provide data necessary for the development of hyperspectral information extraction methods. The sensor is flown on a NASA ER-2 aircraft and can image in 224 contiguous

spectral channels at a spectral resolution of 10 nanometers while covering the spectral region from 0.4 to 2.5 micrometers. Figure 2.8 shows the design layout of the AVIRIS sensor.

Initial results from AVIRIS were promising. Image geometry, uniformity, signal-to noise ratio and spatial resolution were just as expected. The use of AVIRIS showed that valid spectral and radiometric calibration of radiance measuring instruments is required for physically based analysis of the measured data and for quantitative comparison of data acquired at different sites, and times. Figure 2.9 shows an early example of the spectral quality delivered by the AVIRIS sensor. This spectra was derived from averaging the individual spectra extracted from a 5 x 5 pixel region of an image acquired over the Cuprite Mining District in Nevada. It is interesting to note the agreement between the characteristic atmospheric absorption features that are observed with AVIRIS, (solid line) and the LOWTRAN atmospheric model predictions in parentheses. AVIRIS requirements initially specified a spectral calibration accuracy of ± 5 nanometers. In-flight calibration of the spectral and radiometric characteristics of the sensor by Green et al, (1990) showed that a significant radiometric error could be introduced with as little as ± 1 nanometer error in the wavelength calibration. The AVIRIS sensor has been continually upgraded since its inception by improving the radiometric calibration and in-flight stability, increasing the signal-to-noise ratio, enhancing the scanner performance for geometric image fidelity and increasing the overall instrument reliability.

Calibration experiments with the instrument have continued with each flight season. These periodic experiments combine AVIRIS overflights with *in-situ* measurements of the surface and atmospheric conditions present during the overflight. The measurements are used to constrain the radiative transfer modeling algorithm which predicts the upwelling radiance incident upon the sensor. The actual radiance measured by AVIRIS and the model predicted radiance are compared in order to validate the spectral and radiometric characteristics of AVIRIS in flight. Figure 2.10 shows a

comparison of the MODTRAN predicted radiance and the AVIRIS measured radiance acquired during a calibration/validation experiment over Ivanpah Playa, California on 7 March 1991. Figure 2.11 shows the Ivanpah calibration/validation signal-to-noise performance of the AVIRIS along with the design requirements for the sensor. Table 2.1 highlights the current AVIRIS characteristics along with past collection operations.

SPECTRAL	Wavelength range	400 to 2500 nm
	Sampling	≤ 10 nm
	Spectral response (fwhm)	10 nm nominal
	Calibration	≤ 1 nm
RADIOMETRIC	Radiometric range	0 to maximum lambertian
	Sampling	~ 1 dn noise rms
	Absolute calibration	$\leq 7\%$
	Intraflight calibration	$\leq 2\%$
	Precision/noise	exceeding NE Δ L/SNR requirement
GEOMETRIC	Field of view (FOV)	30 degrees (11 km)
	Instantaneous FOV	1.0 mrad (20 m)
	Calibration	≤ 0.2 mrad
	Flight line length	Up to ten 100 km flight lines

SENSOR	Imager type	Whisk-broom scanner
	Cross track samples	614 elements
	Scan rate	12 scans/second
	Dispersion	Four grating spectrometers (A,B,C,D)
	Detectors	224 detectors (32,64,64,64) Si & InSb
	Digitization	10 bits (12 bits planned for 1995)
	Data rate	2.125 Mwords/second
	Spectrum rate	7300 spectra/second
	Data capacity	>10 gigabytes ($>10,000$ km ²)
	Onboard calibration	Radiometric and spectral
	Position & pointing	Lat, lon, alt, and roll, pitch, yaw
	Launches	~ 30 per year

AVIRIS DATA FACILITY (ADF)	Performance monitoring	48 hours from acquisition
	Archiving	One week from acquisition
	Quick-look distribution	One week from acquisition via Internet (anon ftp)
	Calibration	Two weeks from request
	Quality monitoring	Prior to distribution
	Distribution	Two weeks from request
Engineering analysis	Priority as high as required	

Months of operations	8	7	8
Aircraft bases	4	4	4
Principal investigators supported	32	35	24
Investigator sites flown	172	211	382
Launches	34	38	53
Inflight calibration experiments	3	3	3
Square kilometers flown	114,300	138,400	250,000
Flight scenes	1143	1384	2500
Gigabytes processed	317	363	>600
Data scenes calibrated/distributed	1120	1212	2000
Approximate data turnaround	2.5	1	1

Table 2.1 (AVIRIS Instrument Characteristics, Sarture et al, 1995)

Numerous geological, botanical and atmospheric studies have been conducted using the AVIRIS instrument. The use of AVIRIS for the detection of changes in vegetation communities between seasons has shown dramatic spectral differences within various vegetative communities (Miller, et al, 1990). Figure 2.12 shows the representative reflectance curves attained for various vegetation communities on April 13, 1989, June 2, 1989 and August 31, 1989. The plots show distinctive changes in the red-edge reflectance during the April to June period and again from the June to August period.

Hyperspectral imagers have been used for the measurement of primary productivity in small lakes. This activity is commonly derived by measuring the quantity of photosynthesizing material (e.g. phytoplankton). AVIRIS images acquired over Mono Lake in 1989 provided reflectance spectra indicative of chlorophyll a, (Figure 2.13). An attempt was made to calculate the amount of Chlorophyll contained in the lake by using a chlorophyll concentration algorithm developed for the Coastal Zone Color Scanner (CZCS), carried on the Nimbus series satellites. The amount of chlorophyll calculated was half that determined by on-site sampling. The discrepancy was determined to be in the algorithm itself since it was designed for much smaller concentrations normally found in oceanic waters. Further development is underway on an algorithm that can be applied to inland water bodies of this size (Melack and Pilorz, 1990).

Total column water vapor determinations can enhance studies in the fields of meteorology, climatology and high precision geodesy using the global positioning system. Gao and Goetz (1990), were very successful in their determinations of column water vapor estimations using AVIRIS data. By using spectral curve fitting of AVIRIS acquired spectra and simulated spectra along with band ratioing techniques, Figure 2.14. and Figure 2.15, they were able to estimate the column water vapor amounts to within 5% of those determined by a radiosonde.

c. Geophysical Environment Corporation Imaging Spectrometer (GERIS)

One of the major commercial sources for spectrometers is GER. One of their primary systems is GERIS, a 63 channel spectrometer that utilizes three spectrometers. The optics scanning mirror scans an area of 512 pixels covering out to 45 degrees either side of the nadir crosstrack position. The incoming signal is then split and sent to the three spectrometers, each of which has its own line array. Spectrometer I records signals in 31 channels between 0.47 to 0.84 micrometers at a spectral resolution of 12.3 nanometers. Spectrometer II records 4 channels in the 1.40 to 1.90 micrometer range at a resolution of 120 nanometers. The SWIR region, 2.0 to 2.45 micrometers, is covered by spectrometer 3 at a resolution of 16.2 nanometers or 28 channels.

GERIS was utilized in a study of a corn stand that overlaid a former waste deposit site in Germany. The study was part of the European Imaging Spectrometry Campaign (EISAC). The waste site had opened in 1899 and was a depository for industrial and household refuse until its closure in 1949 when it was covered with humus and converted to agricultural land use. Figure 2.16 shows the average spectra from three different locations on the study site. In the visible and near-infrared regions, (top plot), differences in relative reflectance are 2% and 5% respectively. In the SWIR region the differences are smaller and discontinuous. Lehmann, et al, (1990), determined that the relative differences were most probably caused by heavy minerals which caused a stress situation to occur in the vegetation cover.

d. Fluorescence Line Imager (FLI)

The Canadian Department of Fisheries and Oceans operates the Fluorescence Line Imager (FLI). The instrument was built by Moniteq Ltd and can be operated in one of two separate modes. In the spatial mode the sensor operates as a pushbroom, multispectral scanner. In the spectral mode, the sensor operates as an imaging spectrometer, imaging in 288 contiguous bands in the region from 0.4 to 0.8 micrometers. Each spectral band is spaced at 1.3 nanometer intervals which provides a spectral

resolution of 2.6 nanometers. The sensor is normally flown on an Ontario Centre for Remote Sensing aircraft at an altitude of 1000 to 1800 meters. Rock, et al, (1990), utilized the FLI while studying coniferous forest damage on Whiteface Mountain, NY. On-site, red edge (660nm-800nm) spectral samples of birch leaves and Balsam Fir needles were acquired at the time of the experiment. First derivative curves were calculated and the mean, +/- the standard deviation was plotted as shown in Figure 2.17. The FLI was then flown over the site. After calibration of the data from instrument received radiance to ground reflectance values, both the reflectance and first derivative curves for the Birch and Fir spectra were plotted as shown in Figure 2.18. Comparison of the in-situ spectra and the FLI acquired spectra indicates a remarkable similarity in the red-edge region.

e. Hyperspectral Digital Imagery Collection Experiment (HYDICE)

HYDICE was initiated in 1991 as a classified study to determine the utility of using hyperspectral imaging technology for intelligence applications. The effort was expanded in 1992 to include the procurement of a research quality sensor system with civil agency participation under the Congressionally-funded, Dual Use Initiative.

Hughes Danbury Optical Systems (HDOS) has produced a highly calibrated, imaging prism spectrometer of the nadir, push-broom type. HYDICE measures reflected solar energy along a 1 km ground swath at a flight altitude of 6000 meters. The instrument's spectral range is from 400 to 2500 nanometers, with a nominal spectral resolution of 10 nanometers. Ground sampling distance is dependent on sensor flight altitude and ranges from 1 to 4 meters.

As of winter 1995 HYDICE was being fitted into a Convair-580 aircraft for initial aircraft compatibility checks prior to the initiation of the 1995 data collection experiments. Figure 2.19 is a physical view of the HYDICE instrument. Signal-to-noise ratio is an important requirement for earth remote sensing. Since the entire spectral range of the instrument is incident on the same focal plane array, HYDICE incorporates a

multiplexer to accommodate the large dynamic range required by the focal plane. As Figure 2.20 indicates, the dynamic range is broken down into three regions, A, B and C. The multiplexer is also divided into three regions to accommodate the maximum expected signal. This design effectively optimizes the signal-to-noise ratio together with the dynamic range.

A spaceborne derivative of the HYDICE concept has been investigated. (Silvergate, et al, 1994). By using telescope type foreoptics the HYDICE concept could be adapted to a spaceborne configuration, see Figure 2.21.

f. Shuttle Imaging Spectrometer Experiment (SISEX)

Designed as a demonstrator of technologies relating to imaging spectrometers, SISEX would image in 128 separate spectral channels from 0.4 to 2.5 micrometers, provide a ground instantaneous field of view (GIFOV) of 30 m at a Shuttle altitude of approximately 250 km, and produce a swath width of 12 km. Spectral resolution in the early stages of the design was set at 20 nanometers but was sharpened to 10 nanometers after field work and analysis in support of the AVIRIS concept determined the latter as more beneficial (Herring, 1987). After the design process began, the Earth Observation System (EOS) was conceived. Initial EOS plans called for a High Resolution Imaging Spectrometer (HIRIS) to be deployed with the system. In an effort to conserve dollars, NASA began to develop SISEX as a test bed for the HIRIS design and planned to utilize SISEX components on HIRIS in order to reduce costs. The Challenger accident caused NASA to restrict any future use of the shuttle for advanced instrumentation testing and in 1987 the Jet Propulsion Laboratory canceled SISEX in favor of HIRIS (Taranik, et al, 1993).

HIRIS development continued and in 1988 the Jet Propulsion Laboratory proposed to fly HIRIS on a polar orbiting platform. HIRIS was to image in 196 spectral channels in the range from 0.4 to 2.5 micrometers. However, the declining NASA budget caused an indefinite postponement of the HIRIS program in 1992.

g. Moderate Resolution Imaging Spectrometer (MODIS)

MODIS is an Earth Observing System (EOS) instrument that is slated for flight on board the EOS-AM and EOS-PM satellite series. MODIS will be employed to enable a better understanding of the global earth system to include the interaction between land, ocean and atmospheric processes (Thompson, 1990) The instrument is an imaging radiometer incorporating a traditional, cross-track, scan mirror, coupled with linear detector arrays. There are four focal planes that contain the detector arrays and each incorporates spectral interference filters.

MODIS will image in 36 spectral bands in the range from 0.4 to 15 micrometers. Spatial resolution will be between 250 meters and 1 kilometer at nadir.

3. Evolution Summary

The following table summarizes the evolution of hyperspectral imaging sensors. The Landsat Thematic Mapper is included to enable the reader to compare the attributes of current multispectral sensors with those of the hyperspectral breed:

System	No. of Bands	Spectral Range (Micrometers)	Bandwidth (Nanometers)	GIFOV (Meters)
Landsat TM	7	0.45-0.52 0.52-0.60 0.63-0.69 0.76-0.90 1.55-1.76 2.08-2.35 10.40-12.50	70	30
TIMS	6	8.2-8.6 8.6-9.0 9.0-9.4 9.4-10.2 10.2-11.2 11.2-12.2	400 400 400 800 1000 1000	20-30
AIS I	128	1.2-2.4	9.3	11.4
AIS II	128	0.8-2.4	10.6	12.3
AVIRIS	224	0.4-2.5	10	20
SISEX	128	0.4-2.5	10	30
GERIS	63	0.4-2.5	12.3/120/16.2	
FLI	288	0.4-0.8	2.6	
HYDICE	210	0.4-2.5	10	1-4
MODIS	36	0.4-15	varied	250/500/1km

Table 2.2 (Bandwidth characteristics of multispectral and hyperspectral systems)

B. ANALYSIS TECHNIQUES

Multispectral image analysis techniques can further exploit information contained in multispectral images. Visual classification can be achieved by assigning three of the primary colors (red, green, blue) to each of the three sensor bands selected and viewing the image. The information content represented by this false-color image will depend on the spectral bandpasses utilized.

Land cover categorization, more commonly known as Terrain Categorization (TERCAT) involves categorizing the image pixels into land coverages utilizing spectral pattern recognition. Figure 2.22 shows a 3-dimensional space defined by the axes which represent the intensities of the selected bands, in this case, 3 bands from the LANDSAT Multispectral Scanner (MSS). A point can be defined within this space for each pixel in the image. In an ideal case, each class or category of land cover would be represented by the same point. In reality, the category will be represented by a clustering of pixel values. The different clusters may be distinct and widely separated from each other and can be identified with a specific land cover type. This generally requires that a study of the area in question has been done to determine the predominant land cover types present. Otherwise, simple operator experience can be used as a basis. By using selected pixels from the scene, commonly referred to as "training data" or "sites", high levels of classification accuracy can be achieved. A number of techniques have evolved which constitute rotations in wavelength (color) space.

1. Principle Components

Principle components or the Karhunen-Loeve transformation grew out of the statistical treatment of psychological problems (Cracknell and Hayes, 1991). Principle components is a special data transformation which transforms the information content of the original measurement set (e.g., multispectral bands) into a coordinate system which is orthogonal in it's new coordinates. This orthogonality is determined by a rotation that leaves the data uncorrelated in the new coordinates. In some instances, these new principle component bands may be more easily categorized than the original image.

Principle components analysis has the following advantages in the analyses of multispectral and hyperspectral data:

- 1) Most of the radiance in the multispectral data is relegated to one or two principle component bands.
- 2) Noise relegated to less-correlated principle component bands.

- 3) Spectral differences between different surface materials become more apparent in the principle component bands than in the original multispectral bands.

Application of principle component transforms to hyperspectral data has only recently become practical. It will help in categorization, and reduction of the dimensionality of the data sets. The number of principle component images generated will be equal to the number of spectral bands that make up the image cube. The majority of the information within the scene will most likely be described by the first few (generally 10 or less) principle components. Principle components will reduce the data volume of the hyperspectral set but will de-emphasize individual spectra or target signatures. This is due to the fact that the majority of the spectral signatures within a hyperspectral scene are highly correlated not orthogonal, and the principle component images contain information that is a linear combination of several spectral classes (Harsanyi and Chang, 1994).

Sub-pixel targets can only be identified by utilizing data reduction techniques that model the spectral contributions of the target and background materials (Farrand and Harsanyi, 1995). Spectral mixture analysis techniques and low probability of detection algorithms based on orthogonal subspace projection show the greatest promise for detection and classification.

2. Spectral Mixture Analysis

Spectral mixture analysis is based on the assumption that the majority of the spectral variation in a multi or hyperspectral data set can be accounted for by a relatively small number of endmember spectra. Endmembers define the vertices of the mixing space. The first step in the spectral mixture analysis process is to determine the number and identity of the spectral endmembers. Image analysis software such as the Spectral Image Processing System (SIPS), developed by the Center for the Study of Earth from Space (CSES), utilize programs written in Interactive Data Language (IDL) format for

linear spectral unmixing. During the process, a spectral endmember library is formed using an iterative process and then decomposed using Singular Value Decomposition (SVD). This allows for determination of the degeneracy of the library or the number of eigenvectors that make the largest contribution to the variance spanned by all the endmembers. One method of determination has been the noise-adjusted, Principle Components Transform. If the results of the degeneracy indicate that the normalized singular values of the endmembers are unique (spectrally separable and orthogonal), then the user can continue on to the next phase of the unmixing process. However, if all but one of the singular values is zero, the user must reselect new endmembers prior to proceeding. The endmember spectra can then be extracted directly from the Principle Component images and will define areas on the ground that are spectrally unique and which correspond to specific materials. Laboratory or field measured spectral reflectances can then be used in the spectral mixture analysis program as "reference endmembers". The user can then run the unmixing program whose output is another image data cube. The cube contains one image for each endmember showing the derived spatial patterns of abundance for that endmember. Additionally, two additional images are generated that can be used to assess the uncertainty in the unmixing results.

3. Low Probability of Detection (LPD)

LPD is based on the concept of orthogonal subspace projection (OSP) which is a result from least squares theory (Harsanyi and Chang, 1994). The technique basically involves a two step process. The first step is the determination of a matrix operator that eliminates undesired or interfering signatures. Basically, this is an optimal interference rejection process in the least squares sense. Secondly, it is necessary to develop a vector operator that maximizes the residual desired signature signal-to-noise ratio. Both of these operators are then combined into an overall orthogonal subspace projection classification operator which reduces the non-Gaussian detection and classification problem presented by pixels containing mixed spectra to the solved problem of detecting an unknown

constant in white noise. The LPD algorithm does not require the user to have prior knowledge of the background signatures present in the image. In a simulation conducted by Harsanyi and Chang, 100 mixed pixels were simulated using reflectance spectra for red soil and dry grass and creosote leaves, as shown in Figure 2.23. Pixels 20, 40, 60 and 80 contained the creosote leaves reflectance spectrum at abundances of 20, 15, 10 and 5% respectively. Figure 2.24, illustrates the detection and classification problem associated with spectrum of similar shape. In this case, pixels 18-22 are shown on the plot. Pixel 20, which contained the creosote leaves reflectance spectrum at 20% abundance is included in the plot but is not readily distinguishable from the other pixels. The OSP operator was then formed using the creosote leaves spectrum as the reflectance signature of interest. The operator was then applied to each pixel. Figure 2.25 indicates that the pixels containing the creosote leaves spectrum were selected by the algorithm.

The application of this technique to hyperspectral images with mixed pixels has shown that signatures of interest can be detected at abundance levels as low as a few percent at signal-to-noise ratios of less than or equal to 50:1 (Harsanyi and Chang, 1994).

4. Constrained Energy Minimization (CEM)

CEM is an additional analysis technique that is similar to LPD. However, the CEM operator does not depend on the signature of interest occurring with a low probability. It is less stringent than the LPD approach identified above and like LPD, does not require prior knowledge of the undesired background signatures. In basic terms, a linear operator is used that minimizes the total energy in a hyperspectral image sequence with the constraint that the energy associated with the signature of interest is maintained. In this case, CEM works well in the detection of sub-pixel targets that occur over a large number of pixels. The CEM technique is particularly useful for geologic and environmental research as demonstrated by Harsanyi et al, (1994).

III. EXPERIMENT DESCRIPTION

The data utilized in this thesis is the result of airborne hyperspectral remote sensing collections conducted at White Sands, New Mexico in October 1994. The name of the experiment was Operation DESERT RADIANCE.

The HYMSMO program sponsored a comprehensive survey of military operational and intelligence needs. The needs are currently under evaluation by the Unified Commands for prioritization based on time-sensitivity and information criticality. In addition, the Defense Intelligence Agency (DIA), sponsored a study that determined the information needs of military commanders based on operational user definitions. These "levels of information" (LOI's) show common areas that can be used to effectively reduce the HYMSMO needs to a common set of experiments. These experiments are based on target classes recognized by the Joint Chiefs of Staff (JCS): objects (mobile and fixed), emissions, activities and events.

A. OPERATION DESERT RADIANCE

The DIA sponsored, Assured Support to Operational Commanders (ASOC) study, identified LOI's which include: characterization (target spectral "signatures"), detection classification, discrimination and identification (material, function and unit). Each of these LOI's relate to the set of target classes previously identified.

The DESERT RADIANCE experiment sought to concentrate it's efforts in the LOI's concerned with exposed objects (mobile and fixed) and cultural features. The main reasoning for this was the necessity to gain experience and knowledge from exposed object signatures in order to properly evaluate the degradation of LOI content as the target becomes obscured or camouflaged. The underlying principle being that the ability to characterize the spatial, spectral (textural, temporal and other) signature of a target is necessary for detection and satisfaction of the LOI's. DESERT RADIANCE's highest priority was to determine the ability to remotely detect and identify the material

properties of a target at the sublitteral and/or subpixel level, given proper spectral characterization. Abundance estimation or the quantification of a target material type at the subpixel level and evaluating the effect of spectral taggants were additional objectives. To further define the target class of exposed mobile and fixed objects utilized for this experiment, one must consider that mobile objects are generally those that are less than or equal to a few pixels in the spatial dimension which would be adequate for a literal imagery analyst to perform detection and geolocation based on spatial characteristics alone. The fixed objects and/or cultural features are those that occupy more than a few pixels and are termed "multi-pixel" targets.

1. Experiment/Objective Breakdown

The DESERT RADIANCE operation involved objectives relating to the airborne collection of target signatures and objectives relating to the tower-based collection of target signatures.

a. Airborne Data Collection Objectives

Two experiments involved airborne data collection. Experiment A dealt with exposed mobile objects located at test sites A and B. Experiment B examined exposed fixed objects, cultural features located at White Sands and Las Cruces, N.M. The following is a list, by experiment, of the objectives:

(1) Experiment A

- ♦ Remote spectral characterization of materials associated with exposed mobile objects.
- ♦ Remote sublitteral/subpixel detection of separate categories of materials associated with exposed mobile objects.
- ♦ Remote identification of materials associated with exposed mobile objects, at both the literal and sublitteral level of spatial resolution.

- ♦ Remote detection and functional identification of exposed mobile objects, at both the literal and sublitteral level of spatial resolution, through the use of spectral taggants.

(2) Experiment B

- ♦ Remote spectral characterization of materials associated with exposed fixed objects.
- ♦ Remote identification of materials associated with exposed fixed objects, at both the literal and sublitteral level of spatial resolution.
- ♦ Remote detection, classification and discrimination of separate categories of materials used in exposed fixed objects and/ or cultural features.
- ♦ Quantification of the aerial extent and relative abundances (subpixel fraction) of materials used in exposed fixed objects and/or cultural features.
- ♦ Remote detection and functional identification of exposed fixed objects, at both the literal and sublitteral level of spatial resolution, through the use of spectral taggants.

b. Tower-Based Data Collect Objectives

The tower-based data collect concentrated on the spectral characterization of exposed mobile objects and desert backgrounds. The objectives are as follows:

- 1) Assess the variation in spectral signatures as a function of solar angle:
 - * Complex target, full pixel
 - * Simple target, partial pixel
 - * Complex target, partial pixel

- 2) Remote spectral characterization of desert backgrounds.
- 3) Remote spectral characterization of exposed mobile objects at long range.

2. White Sands Missile Range (WSMR)

The WSMR is located 40 miles north of El Paso, Texas in southern New Mexico. Figure 3.1 depicts the relative location of the WSMR. The main test area is approximately 40 by 100 NM in size and is generally utilized by the Army to evaluate missile and rocket systems.

The primary site of interest at WSMR for the operation was the Electro Optical (EO) Range. Located within the range is a 100' tower, experiment test site A and experiment test site B. The two experiment test sites were developed to take advantage of different vegetative backgrounds associated with each site. Each test site was combined with the 100' tower location to form separate flight tracks followed by the airborne sensors. In addition, Condran Airfield, located to the south of the tower was used as an additional calibration/visual checkpoint for experiment site A. Figure 3.2 depicts the actual flight patterns flown for the data collections on 27 and 28 October 1994.

3. Target Descriptions

a. Fabric and Painted Panels

The Topographic Engineering Center (TEC) supplied the fabric and painted materials to facilitate the construction of target panels. These panels were grouped in some cases to form target panel arrays that simulated exposed mobile object dimensions. Panel dimensions were varied in size to allow some panels to either completely fill pixels or be subpixel depending on sensor altitude. These dimensions are based on the expected ground sample distance (GSD) calculations as well as the along-track and lateral instantaneous fields of view of the sensors. In addition, panels of similar material were

placed close together to allow for spectral mixing when viewed from high altitudes. Extreme care was taken with the target panels. Each night, all panels were removed from the experiment test sites and covered to prevent any moisture/dust contamination when not in use. WSMR personnel supplied two camouflaged nets that were used to conceal vehicles and desert background materials. Table 3.1 lists the fabric materials and Table 3.2 lists the painted panels that were deployed during the DESERT RADIANCE exercise.

Target Designation / Priority	Target Description	Target Size (ft)	Target Mix Pattern ³
F1 / 1	Plain weave 100% cotton; Green 483	12 x 7.5	c1
F2 a / 1 F2 b	Temporary tenting, coated; Nylon cotton; Green 483	12 x 10 9.5 x 10	c1 c1
F3 / 1	Desert 3 color ¹ ; 50/50 cotton twill	12 x 8	c2
F4 a / 1 F4 b F4 c	BDU woodland ² ; 50/50 cotton/nylon	12 x 9.5	c3 c3
F5 / 1	Temporary tenting, tan 459, with/without blackout	9.5 x 9.5	c2
F6 a / 1 F6 b	Light tan 379, 50/50 cotton/nylon twill	9.5 x 7.5 9.5 x 7.5	c2 c2
F7 a / 1 F7 b F7 c	Woodland poncho, 100 % nylon, coated	12 x 9.5	c3 c3
F8 a / 1 F8 b	BDU woodland, Nomex/Kevlar	17 x 9.5 12 x 9.5	c3 c3
F9 / 1	Desert camouflage, radar scattering (NSN 1080-00-103-1211)	30 x 12 (estimated)	
F10 / 1	Woodland camouflage, radar scattering (NSN 1080-00-103-1246)	30 x 12 (estimated)	
F12 a / 1	Parachute, light olive	24 x 12	
F12 b / 1	Parachute, light olive	12 x 12	
F12 c / 1	Parachute, light olive	12 x 6	
F12 d / 1	Parachute, light olive	6 x 6	
F13 a / 2	Parachute, dark olive	24 x 12	
F13 b / 2	Parachute, dark olive	12 x 12	
F13 c / 2	Parachute, dark olive	12 x 6	
F13 d / 2	Parachute, dark olive	6 x 6	

1) 3 color desert - Lt. tan, 44; lt. brown, 9; lt. khaki, 47 %; 2) Woodland - lt. green, 20; dk. brown, 30; brown, 34; black 16 %; 3) c1, c2, c3 denote adjacent grouping of the panels on one of the data collection days.

Table 3.1 (Fabric Materials Deployed, Operation Desert Radiance, Anderson, 1995a)

Target Designation/ Priority	Target Description	Target Size (ft)	Target Mix Pattern
P1 / 1	Black	10 x 6	c4
P2 / 1	Brown	10 x 6	c4
P3 / 1	Tan	10 x 6	c5
P4 / 1	Tan Taggant (SpectIR)	10 x 6	c5
P5 / 1	Green	10 x 6	c4
P9 / 1	Lt Tan Taggant Surface Optics)	10 x 6	c5
P10 / 1	Lt Tan Reference(Surface Optics)	10 x 6	c5

Table 3.2 (Painted Panel Deployed, Operation Desert Radiance, Anderson, 1995a)

The WSMR provided a limited number of military vehicles and equipment to support the experiments. Table 3.3 lists the vehicle designations and descriptions.

Target Designation / Priority	Target Description	Target Size (ft)	Target Deployment
V1 / 1	M-60 tank, desert camouflage	9 x 20 x 8	With/without F9
V2 / 1	M-60 tank, woodland camouflage	9 x 20 x 8	With/without F10
V5 / 1	Bronco, woodland	5 x 8 x 4	Open and near bushes
V6 / 1	Bronco, woodland	5 x 8 x 4	Open and near bushes
V7 / 1	Bronco, woodland	5 x 8 x 4	Open and near bushes
V8 / 1	Bronco, woodland	5 x 8 x 4	Open and near bushes
V9 / 2	HMMWV decoy	7 x 15 x 6	Open and near bushes
V10 / 1	CHAPARRAL	8 x 15 x 8	In tower experiment

Table 3.3 (Tactical Vehicles Deployed, Operation Desert Radiance, Anderson, 1995a)

Calibration targets were deployed by EG&G, Incorporated. The targets were used to provide reflectance and absolute radiance references for the airborne data. Table 3.4 lists the calibration targets and their associated reflectance percentages. Note that the 60% reflectance target was not deployed due to the likelihood that it would saturate the AAHIS airborne sensor. Figure 3.3 depicts the Site B target layout for 27 October 1994.

Target Designation/ Priority	Target Description	Target Size (ft)	Comments
C1 / 1	Reflectance panel, 2%	20 x 20	
C2 / 1	Reflectance panel, 12%	20 x 20	
C3 / 1	Reflectance panel, 24%	20 x 20	
C5 / 1	Reflectance panel, 36%	20 x 20	
C5 / 1	Reflectance panel, 48%	20 x 20	Tower, experiment
C6 / 1	Reflectance panel, 60%	20 x 20	Not deployed
C7 / 1	Condron Airport asphalt, TBD %	50 x 50	West end runway 090
C10 / 2	Large white parachute material		Backup calibration for the DAIS Sensor

Table 3.4 (Calibration Targets Deployed, Operation Desert Radiance, Anderson, 1995a)

b. Optical Target

An optical test target was deployed during the collection runs. It's design was based on a concept developed by Dr. William Stoner, Science Applications International Corporation (SAIC). Dr. Stoner proposed that the exposure of small reflective gratings to sunlight will produce diffracted light at discrete wavelengths depending on the orientation of the gratings (Stoner, 1994).

Figure 3.4 depicts the geometry of the sun, grating and airborne sensor. The grating grooves are perpendicular to the plane of the sun, grating and sensor flight path. This configuration presents the possibility that discrete line spectra can be produced and detected by the sensor. Figure 3.5 shows the grating rotated from the perpendicular to the sun, grating and sensor flight path. By comparing the two figures one can see that the reflected light rays are unaffected by the rotation, but the diffracted rays are rotated within the plane of the sun equal to the rotation of the grating. The diffracted ray that is "up and normal" to the grating would be detectable by the airborne sensor flying within the same plane. Rotation of the grating will cause a cone to be formed by the diffracted rays about the reflected ray, see Figure 3.6.

Dr. Stoner proposed that circular gratings in the form of compact discs (CD's) would provide the necessary grating geometry to produce a nearly continuous cone of

diffracted rays about the reflected rays and accommodate uncertainties in the knowledge of the sun's position.

The solar spectrum is fairly smooth at the 10 nanometer scale. The collected wavelength spikes are however more narrowband in nature. This is due to the fact that the geometry of the sun, grating and sensor functions like a grating monochrometer. The frequency of the wavelength spikes will be dependent on the sun's zenith angle and azimuth which can be derived for specific locations given the time of day.

The total spectrum collected by the sensor will be a combination of three components:

- 1) Line spectrum from deffracted sunlight.
- 2) Skylight reflected specularly by the gratings.
- 3) Light reflected from the natural background in the remaining portion of the ground-spot that is not taken up by the gratings.

Relative radiances were calculated to determine an optimum number of CD's for the experiment. Four CD's were utilized and placed on a self-leveling platform elevated 10 degrees. Each CD was then placed on the platform at 0, 2, 4 and 6 degrees elevation respectively to provide varying orientations with respect to the sun. This set-up was necessary to provide four separate wavelength spikes during the sensor overflight. Wavelength spikes can be determined by using a Mathcad program developed by Dr. Stoner and observations of sun zenith angle and elevation taken at the site starting at 1000 (L) through 1600 (L), 27 October 1994.

4. Ground Truth Measurements

The Topographic Engineering Center (TEC) was responsible for formulating the Ground Truth Protocol for the operation. The Protocol defined the standard operating procedures for collecting ground truth measurements in the field. The purpose of the ground truth collection during the airborne collection operations was to provide a means to relate the reflectance of the surface to the energy recorded by the imaging sensor. The

energy reaching the sensor is dependent on the incident irradiance at the surface, the physical properties of the surface, emission of the surface and the effects of atmospheric absorption and scattering on the incident and reflected energy. In addition to TEC's in situ spectroradiometric measurements of the target materials and background, EG&G provided ground truth measurements of the calibration target panels. The spectral data was compiled and made available as an ascii file to facilitate any spectral comparison of the target/background/calibration materials with image derived spectra.

5. Sensor Characteristics

The DESERT RADIANCE experiment set forth specific requirements for sensor performance. Availability and cost were the initial drivers for the selection process. However, due to the nature of the experiment (detection/discrimination of targets from their background), and it's hyperspectral orientation, several key sensor performance characteristics needed to be met. The following characteristics were considered in the final selection: signal-to-noise ratio, number and width of the spectral channels, overall spectral coverage range and adequate spatial resolution. As a result of a technical assessment of the available sensors, two sensors were selected for the DESERT RADIANCE experiment. The SETS Technology, Advanced Airborne Hyperspectral Imaging System (AAHIS) and the Geophysical and Environmental Research (GER) Corporation's, 63 channel, Digital Airborne Imaging Spectrometer (DAIS).

a. Advanced Airborne Hyperspectral Imaging System (AAHIS)

The AAHIS sensor is a second generation sensor that was originally developed by Science Applications International Corporation (SAIC), San Diego, California. The sensor was upgraded in a cooperative effort with SETS Technology INC., Honolulu, Hawaii and is utilized by the state of Hawaii for maritime applications. The basic block diagram depicting the AAHIS major components is shown in Figure 3.7. The AAHIS sensor was designed for high signal-to-noise ratio performance based on it's intended use in maritime applications which involve low reflectance environments (e.g. 5%

reflectance). Table 3.5 lists the AAHIS performance characteristics. The table also lists the sensor's signal-to-noise ratio performance over a land-based (20% reflectance) environment. Figure 3.8 shows the signal-to-noise ratio performance in both environments over the full wavelength span of the sensor. The sensor was calibrated at the Naval Command, Control and Ocean Surveillance Center, Research and Development Division (NRaD), using a 1 meter integrating sphere and subsequently installed into a Piper Aztec, twin engine, aircraft for flight operations at WSMR.

Sensor Parameters	Nominal Value
Signal-to-Noise (5 % reflectance target) • 50 Hz frame rate	200-400
Signal-to-Noise (20 % target) • 50 Hz frame rate	500-850
Useful spectral range (nm)	440-870
Number of spectral channels	72
Nominal bandwidth (nm) • 4 channels summed on chip • 2 channels summed in software	12.4
Cross track IFOV (mradians) • 2 channels summed in software	1.1
Along track IFOV (mradians)	1.0
Spatial pixel number	190
Frame rate (maximum) (Hz)	55
Swath width (degrees)	11.4
Data record length/tape at 55 Hz (seconds)	30
Digitizer (Bits)	12

Table 3.5 (AAHIS Sensor Characteristics, Anderson, 1995a)

b. GER Digital Airborne Imaging Spectrometer (DAIS)

The GER sensor was selected to compensate for the lack of a short-wave infrared (SWIR) capability in the AAHIS sensor. Many unique spectral features manifest themselves in the SWIR domain in narrow spectral bands thereby validating the need for a sensor such as the GER DAIS. Figure 3.9 depicts the sensor configuration and optics layout. The DAIS employs 3 different detector arrays, Silicon for the VIS/NIR, Lead

Sulfide (PbS) for the SWIR and Mercury Cadmium Telluride (HgCdTe) for the thermal IR. The sensor's low scan rates can affect the spatial resolution at low altitudes and cause subsequent undersampling of the scenes in this regime. However, the sensor can still provide high spectral resolution in the same context. Table 3.6 lists the sensor characteristics. Calibration of the DAIS sensor is not possible due to the wide scanner aperture and the lack of a calibration facility, therefore a 50' x 50' area of the Condron Airfield runway approach end was used as a calibration site. The selection of this site was based on its relative uniformity with respect to background. Ground truth data of the calibration site was taken by TEC.

Sensor Parameter	Nominal Value
Signal-to-Noise (5 % reflectance target)	Not available
Signal-to-Noise (50 % reflectance target) • 9 Hz frame rate	100-300, VIS/NIR 20 - 70, 2.0-2.4 μ m SWIR 0.2 ° C NEAT
Useful spectral range	460-1000 nm VIS/NIR 2.0-2.4 μ m SWIR 8.0-12.5 μ m Thermal IR
Number of spectral channels	28 VIS/NIR 29 SWIR 6 TIR
Nominal bandwidth	25 nm VIS/NIR 18 nm SWIR 750 nm TIR
Cross track IFOV (mradians)	3.3
Along track IFOV (mradians)	5.0
Spatial pixel number	512
Frame rate (maximum) (Hz)	9 SWIR-limited 20 Recorder-limited
Swath width (degrees)	45
Data record length/tape at 55 Hz (seconds)	Not available
Digitizer (Bits)	8

Table 3.6 (GER 63 DAIS Sensor Characteristics, Anderson, 1995a)

IV. EXPERIMENT OBSERVATIONS

Observations of the experiment conducted by the HYDICE office and exploitation team is presented below. This chapter is broken down into two main sections. The first presents the observations made by the author of the experiment test sites, target preparation and handling, and sensor platform performance during the set-up and conduct of Operation Desert Radiance at White Sands Missile Range (WSMR) from 24-25 October 1994. The second section is the observations of the hyperspectral data sets produced by each of the collection platforms.

A. WHITE SANDS MISSILE RANGE OBSERVATIONS

The White Sands Missile Range was selected for the experiment based on the spectral consistency of the desert background present, the predictability of weather conditions along with low humidity, tower access and general capability of the Missile range complex to accommodate and facilitate an exercise of this type. The facility is located at an altitude of approximately 4000' and lies in a relatively flat valley on the eastern side of the Organ Mountains in southeastern New Mexico. The valley is oriented N-NE to S-SW with a gradual elevation increase as one travels northeast.

1. OPERATION DESERT RADIANCE

The DESERT RADIANCE experiments were to focus on overtly exposed mobile and fixed targets, to include cultural features and backgrounds. The author observed experiment set-up and participated in the preparation of targets and target placement sites on 24-25 October 1994. The actual collection flights occurred after the author's departure, on 26, 27 and 28 October 1994. Therefore, the author does not have first-hand observations relevant to these collection periods. Minor adjustments to portions of the experiment set-up occurred during these two periods, but they do not appear to have affected the outcome of the experiments.

The experiment effort was planned to take advantage of the exploitation team's manpower. Separate groups were formed within the exploitation team to facilitate target construction, experiment site preparation and other specific technical duties such as ground truth data collections.

2. Site Layout

The White Sands Missile Range is uniquely suited to accommodate an experiment of this type. Its isolation from major urban areas and overlying restricted airspace provide a controlled environment within which airborne sensor platforms can maneuver and the desert environment provides a spectrally uniform environment that can enhance the contrast between target and background.

Within the range complex is the Electro Optical (EO) Range that contains a 100' tower, clear dirt pad areas and well maintained, dirt/gravel access roads. The composition of the roads enhances the production of dust clouds whenever a vehicle passes but the two experiment sites appeared to be at a sufficient distance from this contamination source.

The two experiment sites, A and B, are within the EO Range and can be observed easily from the tower. Site A appears to run N-NE from the tower and tower access road on the southern end to an access road running NW-SE on the northern end. Site B is approximately 1/4 mile NW of the tower and contains a 50' wide (approx.) dry wash and is bounded by an access road on the NE side.

The tower itself has large landings every twelve feet with 360 degree look capability. The top of the tower incorporates a covered structure which contains electrical outlets, tables and a small, accessible balcony for equipment mounting.

3. Weather Conditions

The southeastern portion of New Mexico provides a benign weather environment in which to conduct experiments. The latitude of the site provides for a relatively high sun angle, with very little influence from frontal activity year round. The overhead

conditions on 24 October 1994 ranged from clear skies to a high percentage cloud coverage, with altocumulus and altocirrus cloud types present. The first flight day, 25 October, held marginal weather conditions consisting of cumulus clouds with bottoms at 5000' above ground level (AGL). Temperatures varied from the 40's overnight to the mid 70's during the daytime. Relative humidity was low, but the low overnight temperatures caused dew to form on the landscape. Wind was usually calm in the morning hours but began to pick up slightly in the early afternoon.

4. Targets

The targets utilized in OPERATION DESERT RADIANCE were detailed in Chapter III. The WSMR provided workshop facilities for the construction of target frames and the mounting of target materials. Upon arrival at the target construction site, the author observed numerous targets in various stages of completion. Distinct target sizes were observed and closely approximated the target dimensions identified in the previous chapter. Tactical vehicles with various paint schemes were utilized. As these vehicles were moved along the dirt/gravel roads, dust was thrown up. No apparent attempt was made to clean the dust collected on the vehicles prior to any overhead collect.

a. Materials

Materials for the targets were provided by the Topographic Engineering Center (TEC) and brought to the experiment site. The fabrics appeared to be those used in military clothing, tenting, parachutes and camouflage. (e.g. Nomex, desert camouflage material, woodland camouflage material and green nylon parachute material). The color make-up of the fabrics included dark/light greens, tans, tan/browns and black. The parachutes were not homogeneous in color but instead, were made up of triangular segments with varying shades of Olive Drab (OD) green. The common thread was that all the fabrics were designed to inhibit detection by blending in with surrounding

background materials. TEC also supplied 2' x 2' Aluminum panels painted with various types and colors of paint.

b. Construction

Each target panel was constructed with 1" x 4" Pine boards with each connection secured with wood screws. A hole was drilled into each corner of the panel frame to accommodate 10-12" spikes used for anchoring purposes. The individual fabric types were then cut to dimension and stapled onto the frames. The size of the frames and the composition of the fabrics limited the amount that the material could be stretched across the frames without tearing. This caused the fabric to dip slightly as it layed across the frame. In addition, some warping of the wood frames was observed. Similar frames were constructed for the painted panels which were placed inside the frame structures to form 6' x 10' target arrays. The individual panel corners were not secured and some of the panels were observed to warp while laying inside the frames.

Parachute material was used to cover a 4' x 4' x 4' box target and was folded to form various sized panels (without frames) and staked to the ground. The color of the parachute material stretched over the box was not homogeneous and was fairly transparent. A similar condition occurred with the parachutes folded and staked to the ground. The edges of the panels, which contained most of the folded material, appeared darker than the material towards the center of the panel. The parachute material could be stretched but was susceptible to tearing at the staked corners. In addition, the thinness of the material allowed for a small amount of material flapping during windy conditions.

c. Care and Maintenance

The exploitation team was provided with a large flatbed tractor trailer to facilitate the transportation of the target frames to and from the experiment sites. Care was taken in the loading/off-loading of the targets to eliminate tearing and minimize dust/dirt contamination. Due to the probability of moisture formation on the targets during the night and the possibility of particle contamination during transport, large

plastic sheets were secured over the top of the targets after they were stacked aboard the flatbed.

d. Deployment/Retrieval

Prior to each day's collection event, the target panels were deployed to the designated experiment site, A or B. Exploitation team members were formed into working groups to deploy/retrieve the targets from the sites. WSMR personnel were utilized in the movement of tactical vehicles to designated locations and the erection of camouflage netting.

5. Experiment Sites

Two experiment sites were utilized for the DESERT RADIANCE operation. Both sites were in close proximity to the observation tower and initially looked no different from one another. Closer inspection reveals that the sites provide separate background types.

a. General Soil and Vegetation Make-up

Site A contains a large number of Mesquite and Creosote shrubs ranging in size from 1 to 5 feet. The soil conditions are a loose sand and dirt mixture with small areas of hard-packed soil. The large quantity of shrubs enable targets to be placed adjacent to the shrubs thereby providing some coverage and spectral mixing. Site B contains much less vegetation and a dry wash on the southern end. Very loose sand makes up the wash and its adjacent banks while more hard-packed dirt and sand encompass the remaining portion of the site.

b. Preparation

Extensive preparation of the two experiment sites was performed prior to target placement. Each placement location was marked out to the approximate dimensions of the target to be placed there. The area within the target dimensions was cleared of all

low-lying shrubs, grasses and debris and the soil leveled to ensure that once the target was placed, it presented a relatively level surface to the sensors. Care was taken to ensure that a minimal amount of soil was disturbed beyond the boundaries of the targets.

6. Ground Truth Measurements

Ground truth measurements were taken on a variety of objects both natural and man-made. Prior to the deployment of man-made target materials, ground truth measurements were collected on the surrounding desert vegetation and soils. In addition, the TEC teams used cherry pickers to collect spectra from the M-60 tanks and other tactical vehicles. The man-made material spectra were acquired by positioning the tripod of the portable field spectrometer adjacent to a target panel. The spectrometer was swung over the target material which positioned the instrument aperture approximately 10-12" from the edge of the target frame. The composition of the different fabric materials restricted the amount of stretch that could be applied without tearing. This fact caused, in certain instances, the material within the field of view of the spectrometer not to be perpendicular to the sensor. Observations of the calibration panels staked out by EG&G from the tower showed significant deformations in the panel surfaces. The ground truth data was recorded on portable PC's from the spectrometers and copied in a DOS format to 3.5" floppy disks. The number of spectra taken in the 0.4-2.5 micron range varied for each target of interest.

7. Sensor Platform Performance

The author observed one day of sensor overflights on 25 October, 1994. A flight planning session was conducted separately each night after the overall planning meeting to address issues or procedural problems that had arisen during the previous days flights. Collection altitudes were discussed and chosen based on the frame rates of the sensors and the desired GIFOV. It appeared that the flights at the higher altitudes of 4, 6 and 8000' (AGL) would be affected by the pilot's inability to reference the flightline markers

layed out at either end of the track. The GER pilot visited the experiment sites and used a hand-held Global Positioning System (GPS) receiver to record navigational waypoints.

a. Pilot Proficiency

It became apparent during the first meeting on 23 October, 1994, that both pilots were relatively inexperienced. The author has no knowledge of the number of flight hours possessed by each pilot or their experience level in relation to remote sensing overflights. The pilots were concerned about the restricted area course rules, check-in/check-out procedures, experiment flightline orientations, flight altitudes, high altitude aircraft performance and bad weather flight determinations (weather calls). Concerns about the presence of two aircraft within the operating airspace of the experiments at the same time were alleviated after discussions with the experiment coordinators.

Both aircraft attempted to fly the pre-briefed flight tracks on 25 October 1995 but they did not orient themselves properly. Both aircraft ran patterns from north to south instead of from south to north as briefed. The effect of crosswinds was very evident from the ground perspective. The ground track of the sensor platforms progressively moved east/southeast within the experiment area boundaries. This caused lateral displacement from the run-in course line, poor sensor-target geometry or a complete miss of the target area.

b. Airspace Coordination

Prior coordination with the WSMR range control was made during advance trips and prior to the actual flights. The initial check-in and entry into the restricted area did not go smoothly and some course rules were not briefed to the experiment team by WSMR personnel. Radio problems with one of the aircraft, frequency assignments and proper execution of course rules were some of the problem areas. No face-to-face briefs were conducted between range personnel and the sensor platform pilots.

c. Sensor Reliability

The AAHIS sensor developed inverter problems during the first overflight on 25 October, 1994. The aircraft returned to the Las Cruces airport and the part was ordered and replaced prior to the 26 October collections over Las Cruces. Saturation of the detector array at high altitudes was a concern of the experiment team.

There had been concern expressed regarding the frame rate of the DAIS sensor prior to the operation. GER stated that the sensor would provide a frame rate of 12 Hz. During the first coordination meeting on the evening of 23 October, 1994, the GER team stated that the sensor could only provide a frame rate of 8.5 Hz. This caused a concern over the fact that scenes imaged at the lower altitudes would be undersampled due to the aircraft speed over the ground.

The GER aircraft experienced mechanical difficulties after the 25 October flight and was not utilized again until 28 October, 1994.

B. HYPERSPECTRAL OBSERVATIONS

Data from both sensors was provided to the author by the HYDICE Office through Dr. Linda Kalman, The Aerospace Corporation. In all, seven Exabyte tapes were received. Due to the limited disc space and the large volume of data contained on the tapes, a decision was made to load only certain files that had been found by the exploitation team to be of sufficient quality to be used in analysis work. An initial viewing of the AAHIS collected, 27 October data 8 file was conducted during late January and February 1995. Subsequent analysis was conducted at the HYDICE Program Office. The HYDICE exploitation team helped/directed the analysis, and as a result, the time to analyze the data was reduced significantly.

1. Hardware and Software Configuration

The hardware configuration at the HYDICE office consisted of a UNIX based, Sun workstation with approximately 4 Gigabytes of storage capacity. The software utilized

for observation of the data sets consisted of two software packages: The HYDICE Starter Kit, (an extension of) the Spectral Image Processing System (SIPS) and the Environment for Visualizing Images (ENVI). Both SIPS and ENVI provide graphical interfaces that utilize the Interactive Data Language (IDL) to perform spectral image processing functions. The HYDICE Starter Kit incorporates advanced detection algorithms not currently found in SIPS or ENVI. Similar equipment and software were used in the analyses done at The Naval Postgraduate School.

a. HYDICE Starter Kit

The author found that the HYDICE Starter Kit was extremely sensitive to the type of inputs or commands and many times would abort to the IDL prompt. This required exiting from IDL and rebooting the software each time. This could have been attributed to the author's unfamiliarity with software operation, however, other members of the exploitation team have encountered the same problems. The SIPS_View module of the Starter Kit can be utilized to visualize and perform limited analysis on large imaging spectrometer data sets. Color composite images are relatively easy to produce and extraction of individual spectra from pixels or selected groups of pixels is straightforward. Extracted spectra can be compared to previously collected laboratory or field spectra stored in a spectral library. The spectral library function allows the user to display and manipulate single/multiple spectra and to save the results for output.

The Starter Kit incorporates advanced detection algorithms not currently carried as a part of SIPS, these are: Orthogonal Subspace Projection, Low Probability of Detection and Constrained Energy Minimization along with Principle Components.

b. ENVI

The author found the ENVI software package very easy to use and more forgiving of anomalous inputs. Image file information is easily displayed and ENVI allows multiple windows to be opened, thereby facilitating the comparison of selected

images. Plotting and annotation of spectra is straightforward and the software provides the capability to save the plots in a variety of output formats.

2. Hyperspectral Image Data

Hyperspectral data was collected over two areas. The first was the experiment area within the White Sands Missile Range complex and the second was over the urban and agricultural areas of Las Cruces, New Mexico. The objective of the data analysis was to determine if the detection algorithms would provide reliable indications of a target's presence, in this case, the V1 tank underlying the F9 radar scattering camouflage. The collections over the Las Cruces urban area were not examined because locations of potential military related targets could not be confirmed and subsequently compared to detection images. In order to perform these analyses the experiment environment should be as controlled as possible. With this in mind, initial observations of the data sets were done to examine various aspects of the images.

- The spatial quality of the images was sufficient to resolve features within the field of view.
- The target in question was included in the image.
- The inclusion of calibration targets within the same field of view as the target in question.
- The spectral quality of the image.
- The target/sensor geometry.

The optical target described in Chapter IV was placed in the experiment area of Site B on 27 October, 1994. Each image was examined to see if the area in which the target was placed was in fact imaged by the sensors.

a. AAHIS Data

Each hyperspectral data set was loaded and examined utilizing the HYDICE Starter Kit, for the above characteristics. In total, 29 sets of data were examined. Only one data set was found that met the above criteria. This set, the 27 October, 1994, Data set #8, was collected over site B at 2000" (AGL) and approximately 1250:51 hrs (MST). As shown in Figure 4.1, this scene includes the V1 Tank target as well as the calibration panels.

One data set was found that could possibly contain the optical target. The target's exact location was not known, however, an approximate location was determined after discussion with the experiment coordinator. The 28 October 1994 data set #13, as shown in Figure 4.2, showed potential for covering the target location. Spectral examination of the scene however showed that the AAHIS detector became saturated between approximately band 33 (.6129 microns) and band 53 (.7236 microns). This saturation made the image unusable for this analysis.

b. GER (DAIS) Data

The GER data sets were examined using the HYDICE Starter Kit. The images over the Site B area, collected on 28 October 1994 (data sets 11-14), were found to be severely undersampled. The undersampling, due to low sensor frame rates in relation to sensor platform velocity over the ground. As seen in Figure 4.3, this causes the image to take on an appearance that the scene is squashed and severely restricts any spatial resolution and hence, identification of potential targets. However, this fact does not effect the spectral quality of the image itself. It was possible to define some relatively linear features such as roads provided they were vertically presented in the image. These images were not considered in the analysis of the V1 tank spectra because the spatial location of the tank target could not be identified.

The optical target may have been sampled in the GER images, the problem was that the extremely poor spatial coverage of the site would not allow for verification of

potential detections in the general area of the target location. In addition, any false alarms, or false detections, would be difficult to isolate.

V. DATA ANALYSIS

The objective of the analysis was to determine if an exposed target could be detected by using the Low Probability of Detection (LPD) or Constrained Energy Minimization (CEM) algorithms. In addition, a Principle Components (PC) transformation was conducted on the entire scene to examine any similarities that may exist between the LPD component image and any of the PC images. As described in Chapter IV, the 27 October 1994 AAHIS data set 8 was the only scene with the required spatial and spectral qualities to be utilized in the analysis. The specific object of interest was the M-60 tank, cataloged as vehicle V1, in Table 3.3. At the Site B set-up for 27 October the V1 tank target was covered with a radar scattering, desert camouflage net cataloged as F9, in Table 3.1.

The analysis focused on whether the V1 tank spectra could be detected through the camouflage. Since the openings in the camouflage were much less than the pixel size, the V1 spectra would most probably be subpixel in nature and be mixed with the camouflage spectra in addition to any contaminant spectra from the vehicle. Note that in all the figures presented here, wavelength values are in microns and reflectance values are in percent reflectance.

A. SPATIAL ANALYSIS OF THE SCENE

The 27 October, data 8 scene is shown in Figure 4.1. The size of the scene is 192 samples x 512 lines x 70 wavelength bands. For the scene presented, information for band 6 was arbitrarily selected (0.46207 microns).

The general layout of the target area can be seen. Spatial resolution computed for the scene based on the 2000' (609 m) flight altitude and an IFOV of approximately 1.0 milliradians, is 0.67 meters². Visual quality of the image is good although there is some blurring present. The target area is bordered by the dirt road that cuts through the top right half of the scene and what looks like a burm located in the lower left portion of the

scene. The large (20' x 20') calibration panels are visible. The remaining target panels are located to the left of the calibration panels. Exact locations can be verified with the Site B target layout presented in Figure 3.3.

The V1 tank which is covered by the F9 camouflage is clearly visible in a blow-up of the scene as shown in Figure 5.1a. Figure 5.1b will be discussed later in this chapter. Heavy shadows are present on the north side of the tank indicating a midday sun position at collection time. However, it is not clear whether the shadow is caused by the tank body which is approximately 3 meters in height by 7 meters long or the covering camouflage. The tank presents a surface area of approximately 24 meters² on the top surface and 20 meters² along the north side while the camouflage has a total surface area of approximately 104 meters². Very prominent tank tracks are visible along a path from the tank's location to the dirt road. Vegetation is sparse although there are a large number of Mesquite bushes located throughout the scene.

B. SPECTRAL ANALYSIS

The 27 October 1994, data 8 scene was loaded into the Hydice Starter Kit for initial analysis. The approach taken for the analysis was to assume that the nature and make-up of the prevailing background signatures present within the scene were unknown. In addition, the objective of the analysis was to detect a man-made target signature (V1 tank spectra) that was situated within a naturally occurring background. Since the area of the exposed surfaces was small in relation to the overall scene, the V1 tank spectra would most probably occur in relatively few pixels within the scene and not be statistically significant. For these reasons, the LPD algorithm was chosen for its robustness in detecting sub-pixel targets given the above conditions. The CEM algorithm was not applied to the data because the V1 Tank spectra did not constitute a sub-pixel target that occurred in a relatively large number of pixels within the scene.

1. Data Conversion

The ground truth data provided by TEC was sampled from 400-2500 nanometers with values represented in percent reflectance. Each target spectra was then resampled utilizing the AAHIS wavelength file to produce spectral plots of the target spectra within the AAHIS sensor range.

Two files were created in ENVI utilizing the Empirical Line Method described by Farrand et al, (1994). The first was the gains file which incorporates the atmospheric transmittance and instrument factors and the second was the offsets file which takes into account the atmospheric path radiance. Both files were applied to the target spectra in order to convert them from surface leaving reflectance percentages to AAHIS sensor perceived radiance. Figures 5.2 and 5.3 show the gains and offsets plots. Both files were derived from samples taken from the calibration panels located at the middle right hand portion of Figure 5.1. Both files were constructed by Dr. William Farrand, a member of the HYDICE exploitation team.

2. Data Preparation

The methods described in paragraph B1 were applied to the selected target spectra. The next objective was to prepare the spectra for use with the LPD algorithm. The algorithm assumes that sensor noise and the combined at-sensor radiance of unmodeled components in the scene are Gaussian in nature, and are independent and identically distributed (iid). (Farrand and Harsanyi, 1995). When a data cube is converted to surface reflectance by application of gains and offsets files, the noise statistics of the image will be effected and the assumption that the noise is iid would not be true. For this reason, the target spectral signatures and the pixel values of the image should be represented in sensor perceived radiance.

The ground truth spectra were converted to sensor perceived radiance by utilizing the spectral math capability of the Starter Kit. To convert each spectra, each ground truth data file was multiplied by the gains file and the product added to the offsets file. Figures

5.4 through 5.9 depict the original target spectral plots and the new target spectral plots after conversion to sensor perceived radiance utilizing the gains and offsets files. One should note the distinct similarities in the overall shapes of the spectral plots and the fact that the TANK spectra is an exact match to the V1 TAN spectra. Figure 5.10 depicts the Site B soil spectra which can be used to compare to the target spectra similarities. Similarities in overall spectral shape can be seen out to 0.6 microns but the soil spectra takes on a more linear slope beyond that point out to the end of the sensor range. The target spectra all show distinct differences in the slope of their plots beyond the 0.6 micron wavelength range and therefore should be discernible from the background. Figure 5.11 depicts the F9 Camouflage spectra for later comparison.

3. Target Spectra Selection

The LPD algorithm requires a target spectrum that is run against the entire data cube. TEC sampled five areas on the V1 tank. The samples taken represented the brown, light tan, tan-brown painted areas of the tank along with the gray painted gun boot and a rusted area on the left rear of the tank. The plots of these various paint spectra along with an average of all the spectra collected over the tank is shown in Figure 5.12. Out of these spectral plots, three were chosen as representative of the V1 tank spectra, these were:

- ♦ The average V1 spectra sampled and represented as TANK
- ♦ The average V1 Tan spectra sampled and represented as V1 TAN
- ♦ The average V1 Tan Brown spectra sampled and represented as V1 TAN BROWN

To better compare the target spectra, Figure 5.13 has been provided. Due to the obvious similarity between the TANK spectra and the V1 TAN spectra, it was decided to use only the TANK and the V1 TAN BROWN spectra as target signatures when running LPD.

Figure 5.14 compares the spectral shapes of the TANK spectra and the F9 spectra. Spectral similarities appear out to approximately 0.74 microns where the two plots begin to diverge from each other. These characteristic differences should allow for discrimination of the TANK spectra from the F9 camouflage.

4. LPD Analysis

The LPD algorithm was run with the TANK and the V1 TAN BROWN spectra as target signatures. After selection of the scene and the target spectra, primary eigenvectors are computed and a correlation matrix constructed. In the context of the LPD algorithm, the primary eigenvectors characterize the majority of the spectral variability in the image and are used to form an operator that suppresses the undesirable background signatures. In the initial LPD runs, the first 11 primary eigenvectors were removed by the algorithm. It should be noted that if a certain material is present in an amount greater than the target spectra, but in a small enough quantity to be excluded among the primary eigenvectors, then it may show up as a false alarm in the LPD component image. One solution is to increase the number of eigenvectors to be removed, thereby increasing the amount of background that is eliminated. The LPD component image provides an assessment of the relative abundance of a particular material under the assumption that target and background spectra are linearly mixed.

a. LPD Results (TANK Target)

Figure 5.16 shows the results of the LPD run using the TANK spectra as the target signature. For this image, a 50% contrast stretch was applied. Figure 5.17 is the same LPD component image but with a histogram equalization applied. This is a special case of a contrast stretch, which enhances the detectability of the features within the image by mapping data values into display values such that a roughly uniform distribution of gray levels is presented. The V1 TANK spectra shows up as a bright spot in the upper left corner of the image. This position can be compared to the location of V1 Tank in Figure 5.1. Several false alarms occur within the image and are circled for

clarity. The brightest false alarm pixels indicating higher DN value assignment are evident in Figure 5.16 and come from the panels marked P3 (TAN CARC PAINT) and P4 (TAN TAGGANT). False hits also occurred on other panels such as the F2 (GREEN NYLON TENTING) and the F6 (TAN TWILL) and are more evident in Figure 5.17 after application of a Histogram equalization. This is most probably due to these spectra being included in the residuals but not included among the primary eigenvectors. Figure 5.18 is the same target signature run using 20 eigenvectors in order to eliminate more of the undesired background. The false alarms are more evident in this image due to contrast stretching that was applied to highlight the higher DN values. Overall, the LPD operator has performed well in suppressing the majority of the background in each of the component images.

b. LPD Results (TAN BROWN Target)

Figure 5.19 shows the results of the LPD run utilizing the TAN BROWN target spectra and 11 eigenvectors. The differences between this component image and the one shown in Figure 5.16 are not readily distinguishable. This fact holds true again when comparing Figure 5.20, the same LPD image except with a histogram equalization applied, with Figure 5.17. Figure 5.21 is the LPD component image run for this target spectra using 25 eigenvectors. In this image, the abundance of the target spectra shown in the location of F9/V1 appears less. In addition, some of the false alarms on certain panels disappear while others appear for the first time. This may be caused by the elimination of certain residuals by removing more eigenvectors and the utilization of a different target spectra. A histogram stretch is applied again to this image for uniformity. Again, the LPD operator did a good job of background suppression using 25 eigenvectors.

Figure 5.15 compares four different spectra that show up as false alarms in the LPD runs. The P3 (TAN CARC PAINT) spectra shows the most spectral variability

across the sensor range, while the remaining three spectra, P9, F6 and Desert Color BDU (TAN) exhibit only minor slope/shape differences.

5. Principle Components Analysis

The Principle Components Transformation produces a set of uncorrelated images equal to the number of spectral bands in the image. The images with the most information or largest variance make up the first Principle Component with each successive image containing less variance. In addition, each successive Principle Component image will be orthogonal to the previous one. Typically, the first 6 to 10 Principle Components will account for more than 99% of the total variance within a scene. Hyperspectral data, by nature, is highly correlated between each spectral band. This is due primarily to the fact that the spectrum of most materials vary slowly and in similar fashion. The main benefit in the use of the Principle Components Transformation with hyperspectral data sets has been in the area of data volume reduction. The approach taken for this analysis was to see if any of the Principle Component Images would closely resemble any LPD results and if so, what do the different components represent?

A Principle Component Transformation was run on the 27 October data 8 set to see if any similarities exist between any of the principle Component band images and the LPD Component images.

a. Principle Component Results

The Principle Components Transformation was conducted using the ENVI software package. Each component image was examined for similarities with the LPD results. Figures 5.22 and 5.23 show component images 1 and 2. Component 1, containing the most variance within the scene, looks very similar to Figure 4.1. Figure 5.1b is a blow-up of the V1 Tank target from Principle Component 1. It is clear that the Tank target representation in this figure is more detailed than that of Figure 5.1a. Principle component 2 is distinctly different but bears no resemblance to either of the LPD component images. Component 8 and 10 showed the greatest likeness to the LPD

component images. Component 9 did not show any meaningful data. Figure 5.24 shows component 8. The F9/V1 tank target and panels F2, P3, P4 and P9 show up clearly in the image. No direct correlation with either LPD component image was observed. The 10th component image shown in Figure 5.25, shows numerous target panels in addition to the F9/V1 tank target. A comparison with Figure 5.21, the LPD run using 25 eigenvalues, reveals a close match on all target hits. This component should represent less than 1% of the total scene variance. This would indicate that the target panels are spectrally similar in this range and comprise a very small portion of the total pixels in the image.

VI. CONCLUSIONS

Operation Desert Radiance was the preliminary attempt by the HYDICE Program Office in demonstrating the utility of hyperspectral imagers for detecting a tactical target based on its spectral characteristics alone. The author's participation in the collection experiment and analysis of the sensor data has highlighted the complexities associated with an experiment of this size.

The experiment was well designed but very ambitious. The use of the AAHIS sensor proved to be a good choice. However, the GER (DAIS) should not have been utilized based on its poor signal-to-noise ratio and low frame rates. The use of "budget" pilots by the sensor operators severely reduced the usefulness of the data collected.

Ground truth measurements during the experiment were performed by TEC and EG&G. The number of ground truth samples taken for each material appeared to be small. In addition, the samples were not well distributed over the entire surface of the tank and represented spectra of portions of the surface with various paint schemes. These spectra were averaged and may not be an accurate representation of the overall spectra from the tank. A more accurate method of collecting the ground truth would be to collect the entire spectra of the tank from an overhead position. It is understood, however, that the large number of materials to be sampled in such a short timeframe may have contributed to the small sample sizes.

Distortions appeared in some of the calibration panels sampled by EG&G and the parachute target materials were not homogeneous in color as they were folded into panels on the ground. In addition, some warping of the painted panels was also observed. These facts, coupled with the fact that the majority of the samples were taken over the corners of the target panels, probably resulted in the collection of spectra that were not representative of the entire panel.

The results of the data analysis clearly show that unique target detection is possible utilizing the LPD algorithm. A higher than expected number of false alarms occurred

even though a large majority of the background was suppressed. The similarity between the Principle Component 10 image and the 25 eigenvector, LPD component image was intriguing. Both results show that the majority of the targets contribute very little to the overall scene variance and are subsequently seen only in the higher order component.

The LPD algorithm performed well during the analysis but its capabilities to detect a specific target spectra were limited because it could not utilize the spectral variability associated with wavelengths beyond 1.0 micron. The use of the HYDICE sensor in future collections should correct this problem by imaging out to 2.5 microns.

The analysis shows that image processing algorithms for automatic target detection need more refinement to eliminate the high false alarm rate. Further target detection studies utilizing sensors that provide a greater degree of spectral resolution and which cover a broader spectral region will determine if the problems encountered in uniquely detecting a target are related to the spectral variability of the target material utilized in the algorithms.

APPENDIX. FIGURES

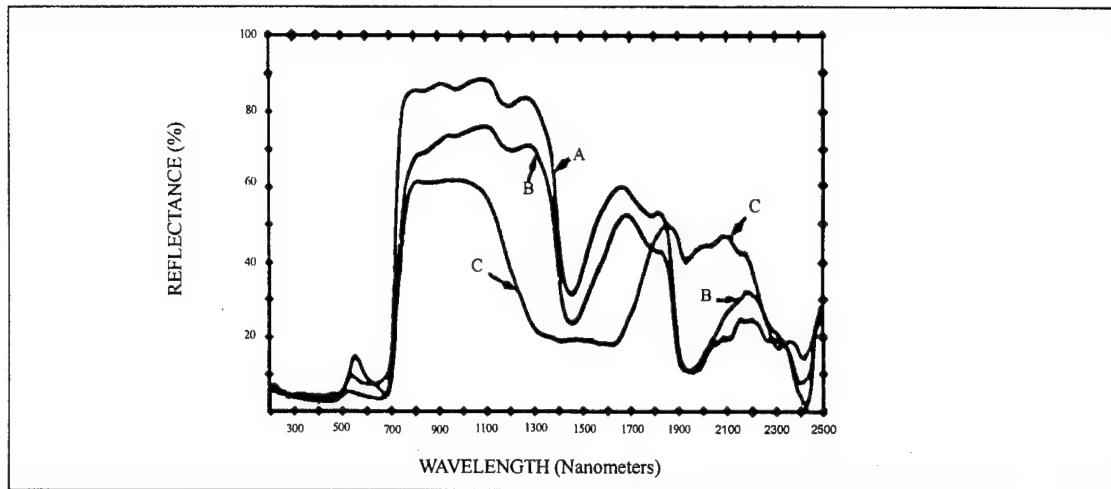


Figure 2.1 (Rinker, 1990)

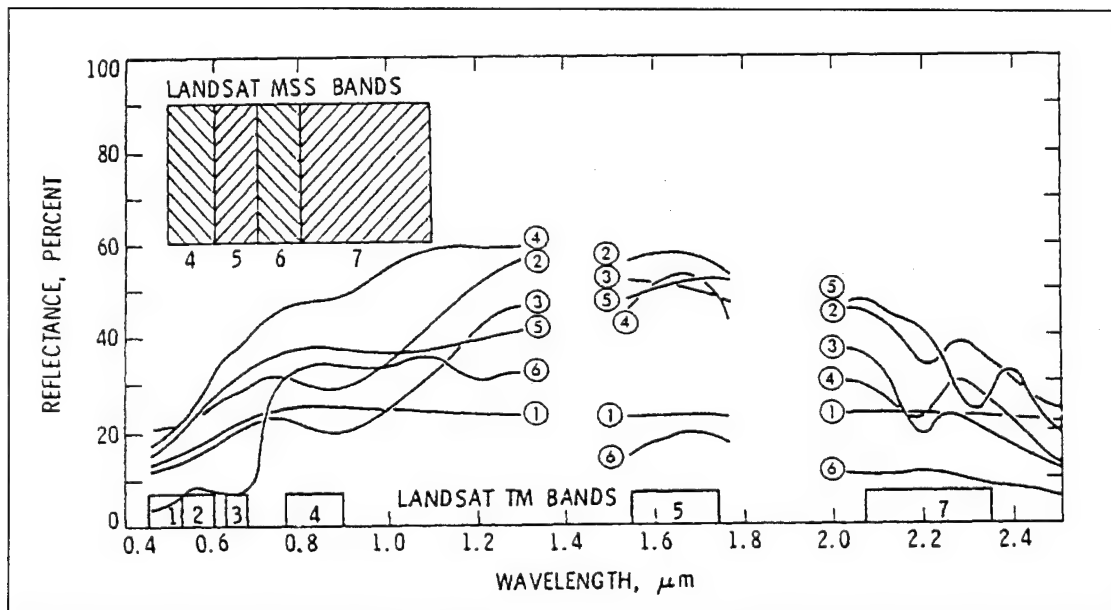


Figure 2.2 (Vane, Goetz, 1988)

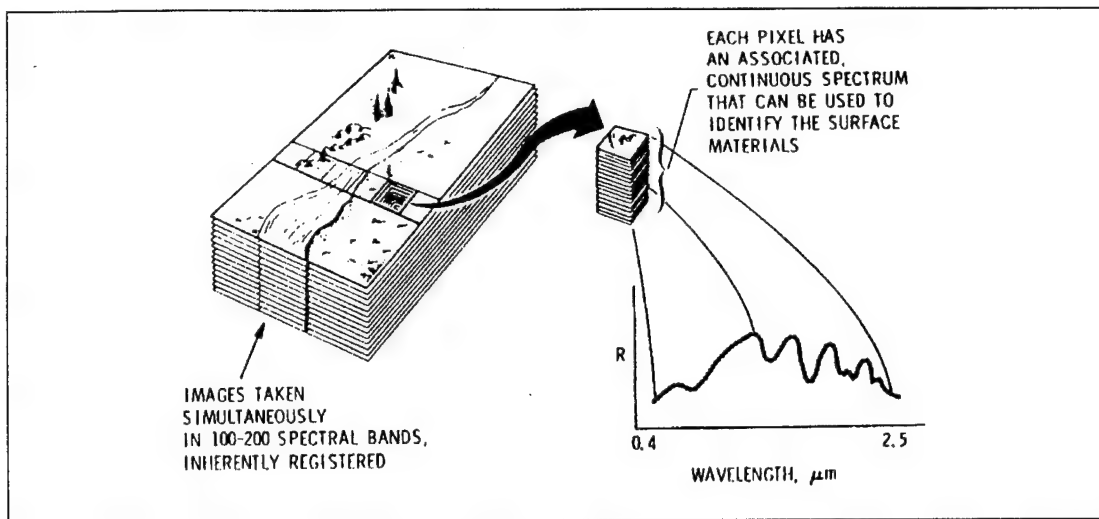


Figure 2.3 (Vane, Goetz, 1988)

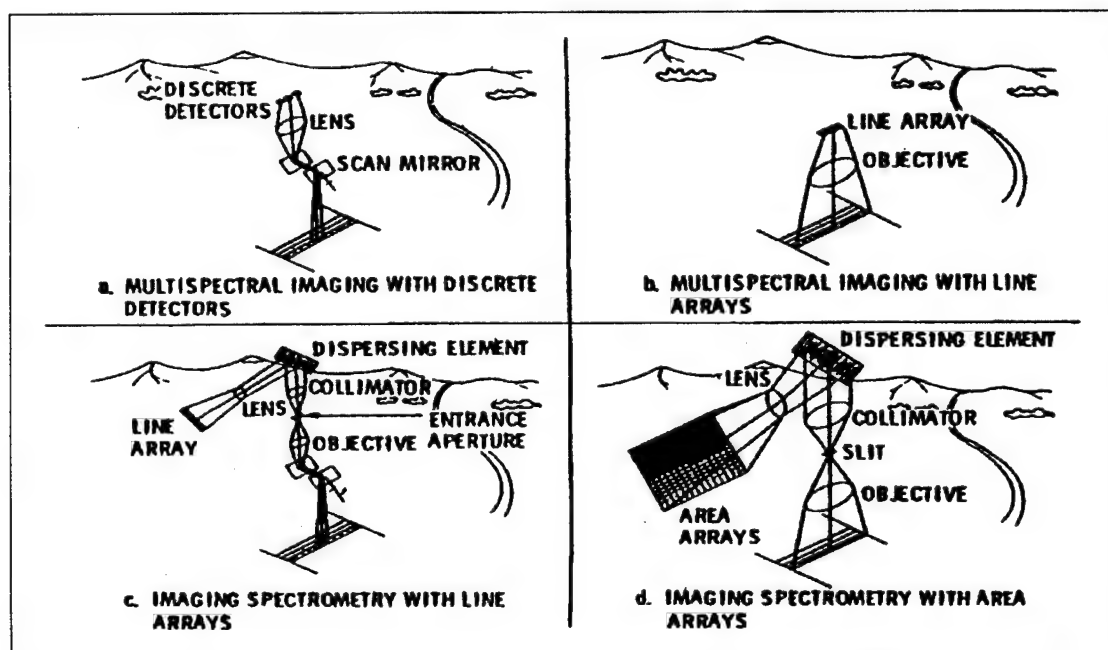


Figure 2.4 (Kruse, 1987)

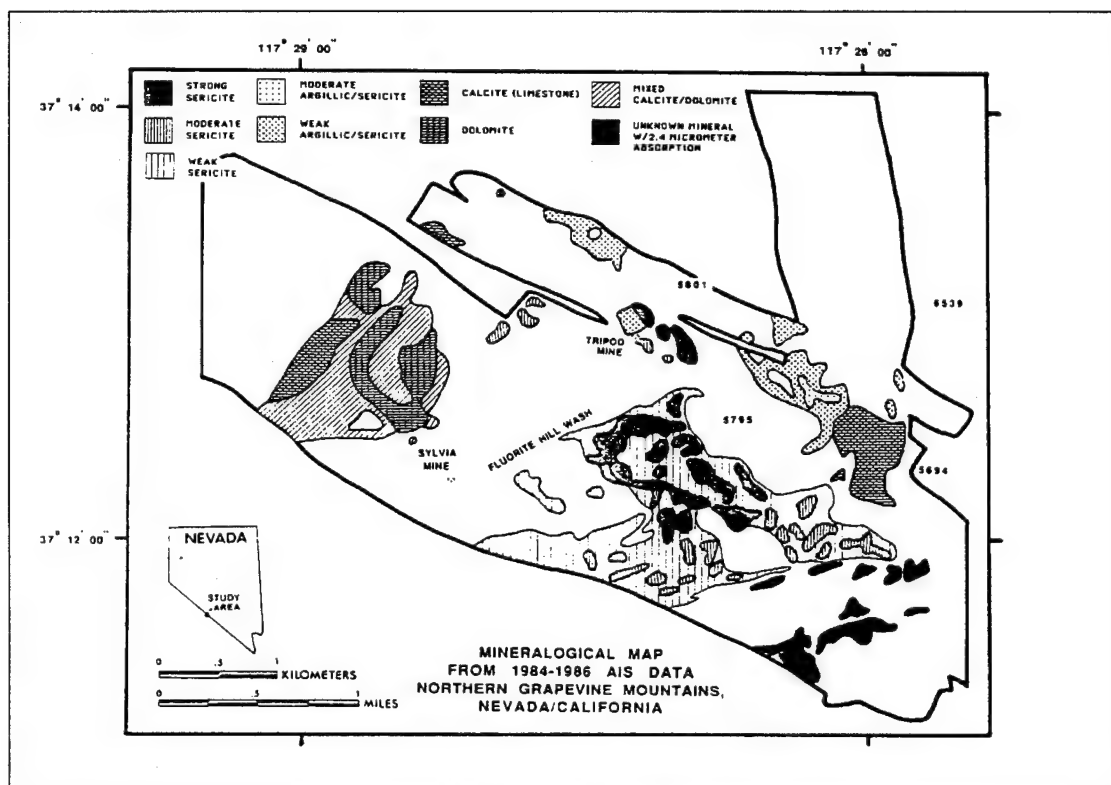


Figure 2.5 (Kruse, 1987)

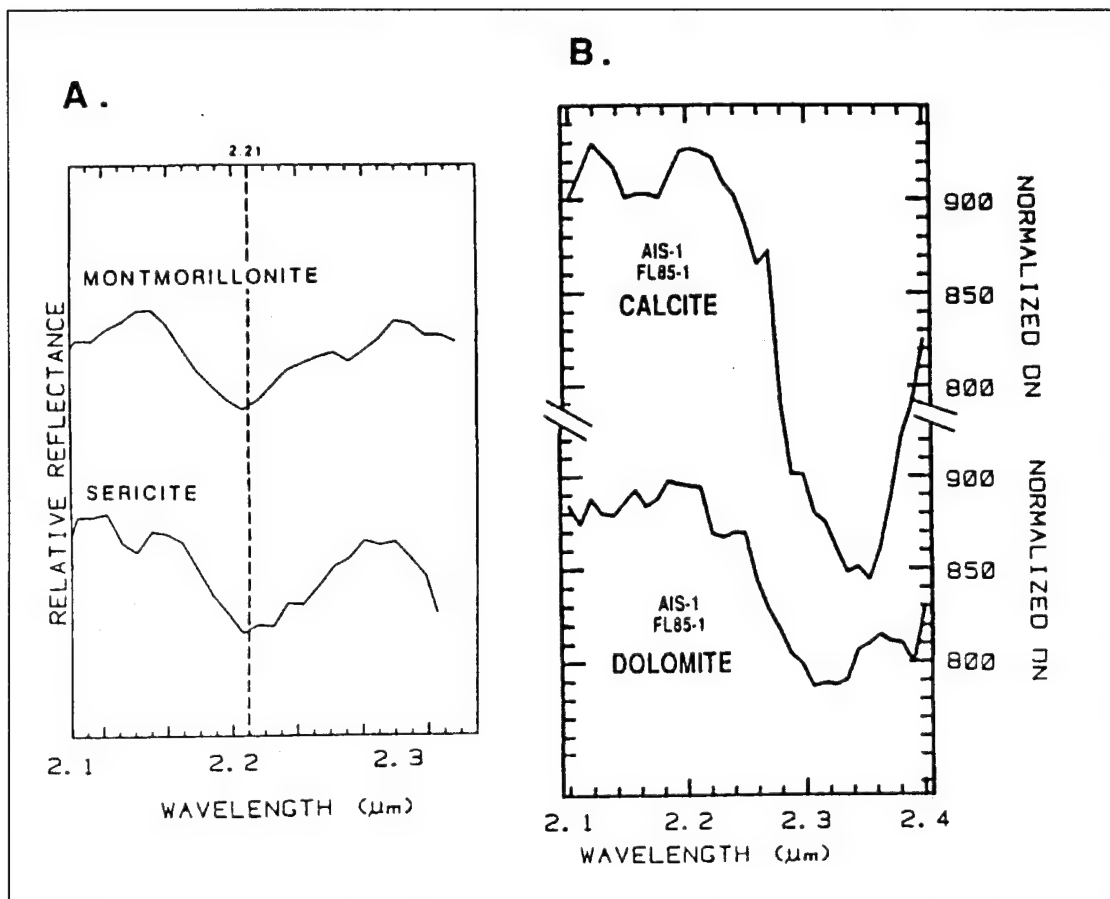


Figure 2.6 (Kruse, 1987)

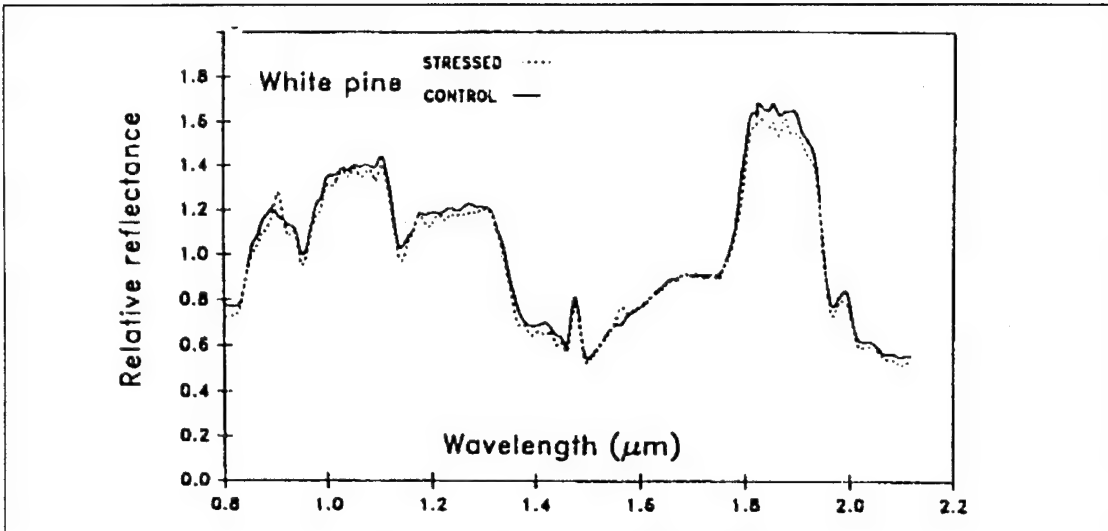


Figure 2.7 (Riggs, Running, 1990)

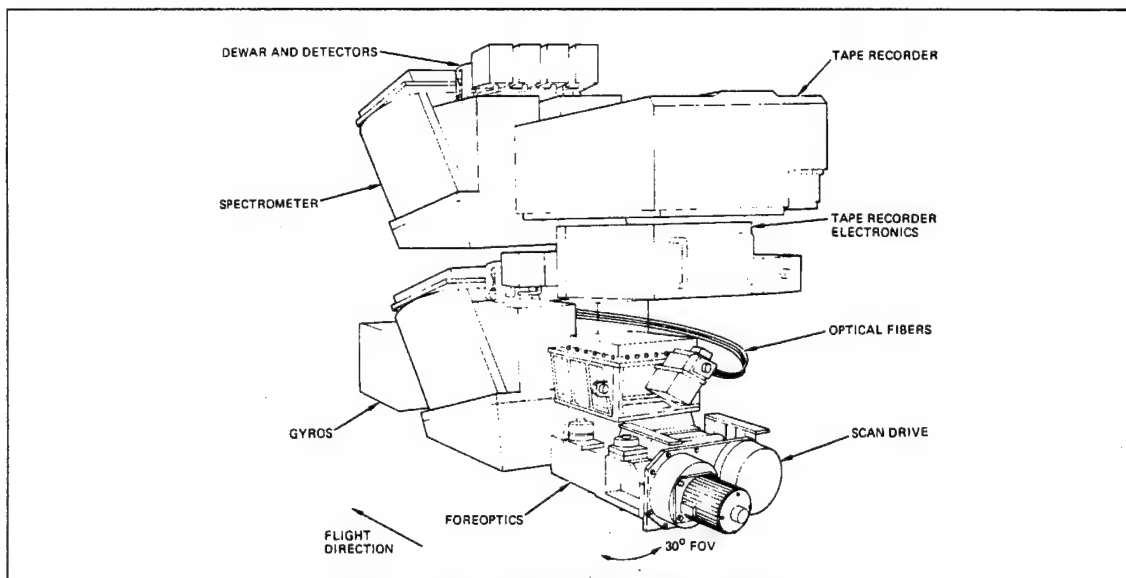


Figure 2.8 (AVIRIS Inst, Miller, 1991)

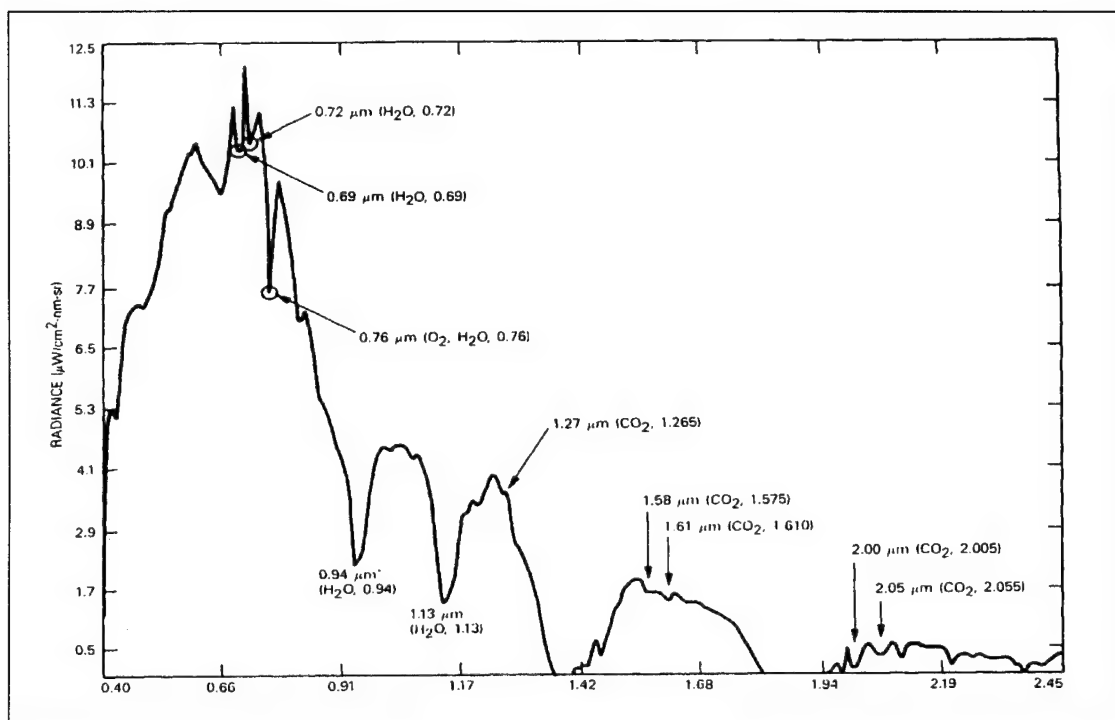


Figure 2.9 (Vane, 1987)

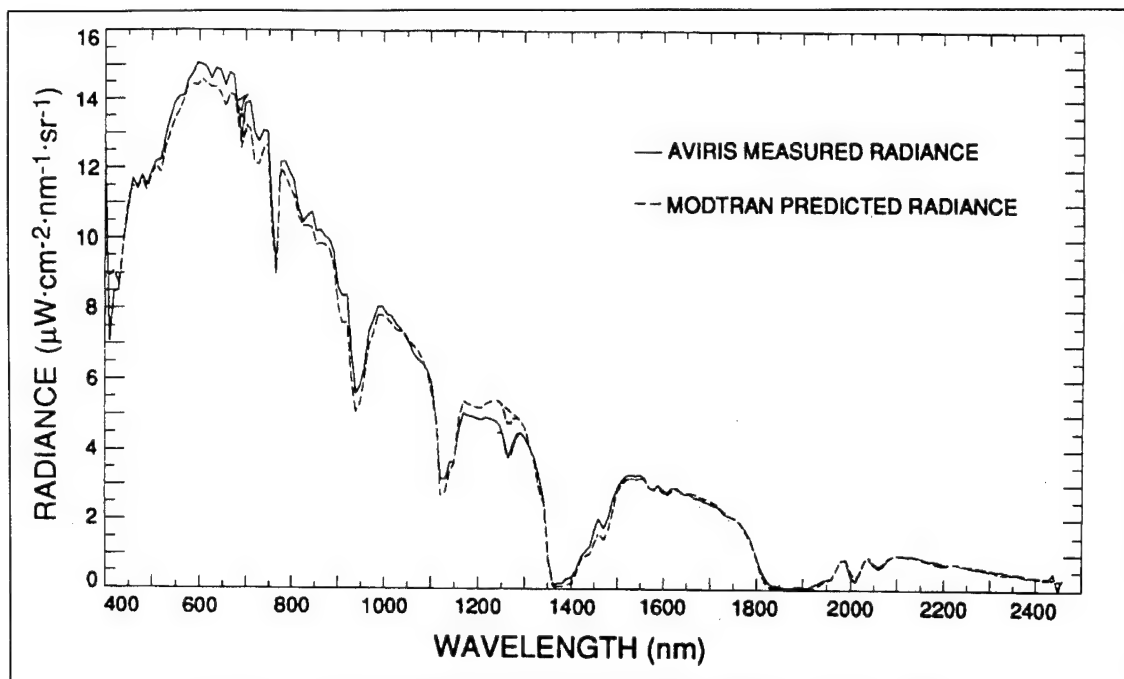


Figure 2.10 (AVIRIS Radiance/MODTRAN Radiance, Chrien, 1991)

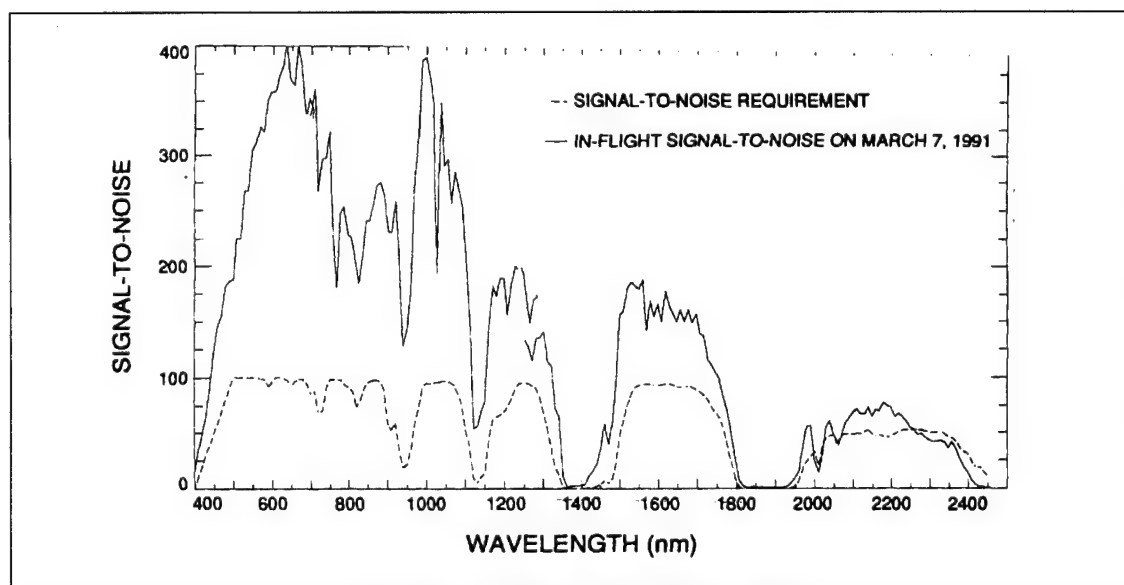


Figure 2.11 (AVIRIS SNR, Chrien, 1991)

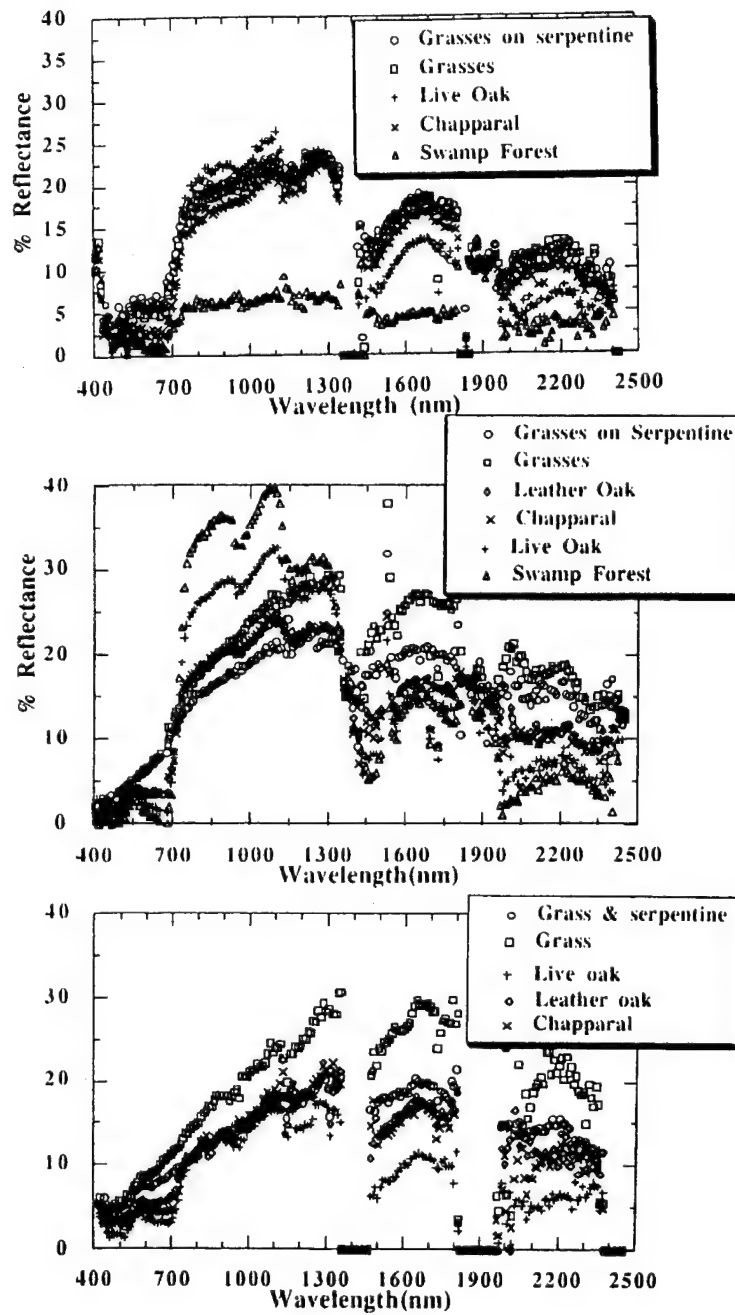


Figure 2.12 (Miller, et al, 1990)

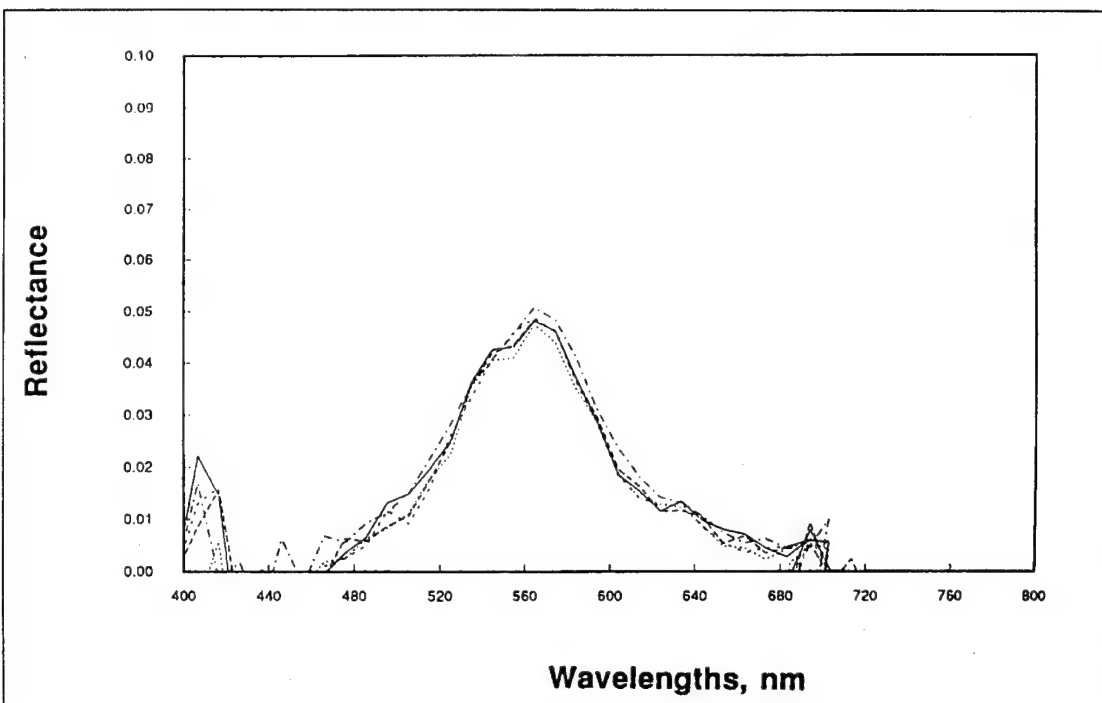


Figure 2.13 (Melack, Pilorz, 1990)

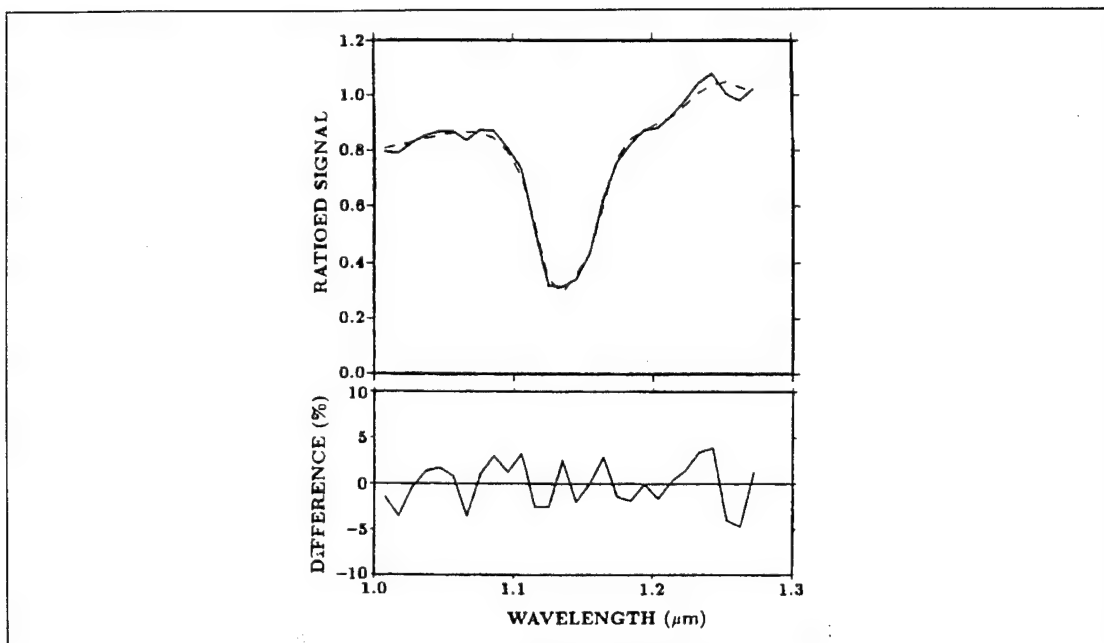


Figure 2.14 (Gao, Goetz, 1990)

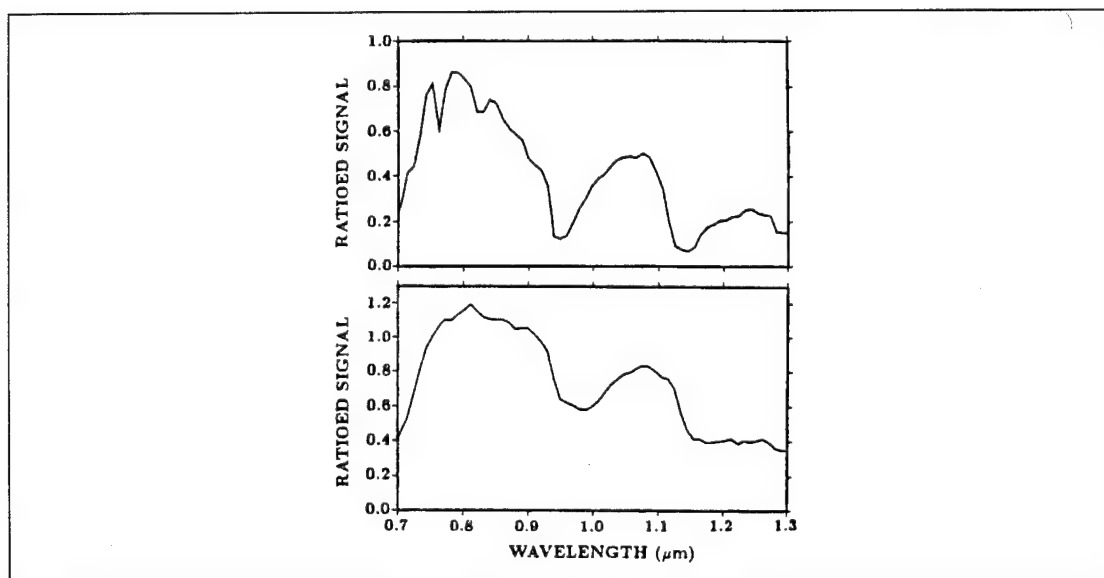


Figure 2.15 (Gao, Goetz, 1990)

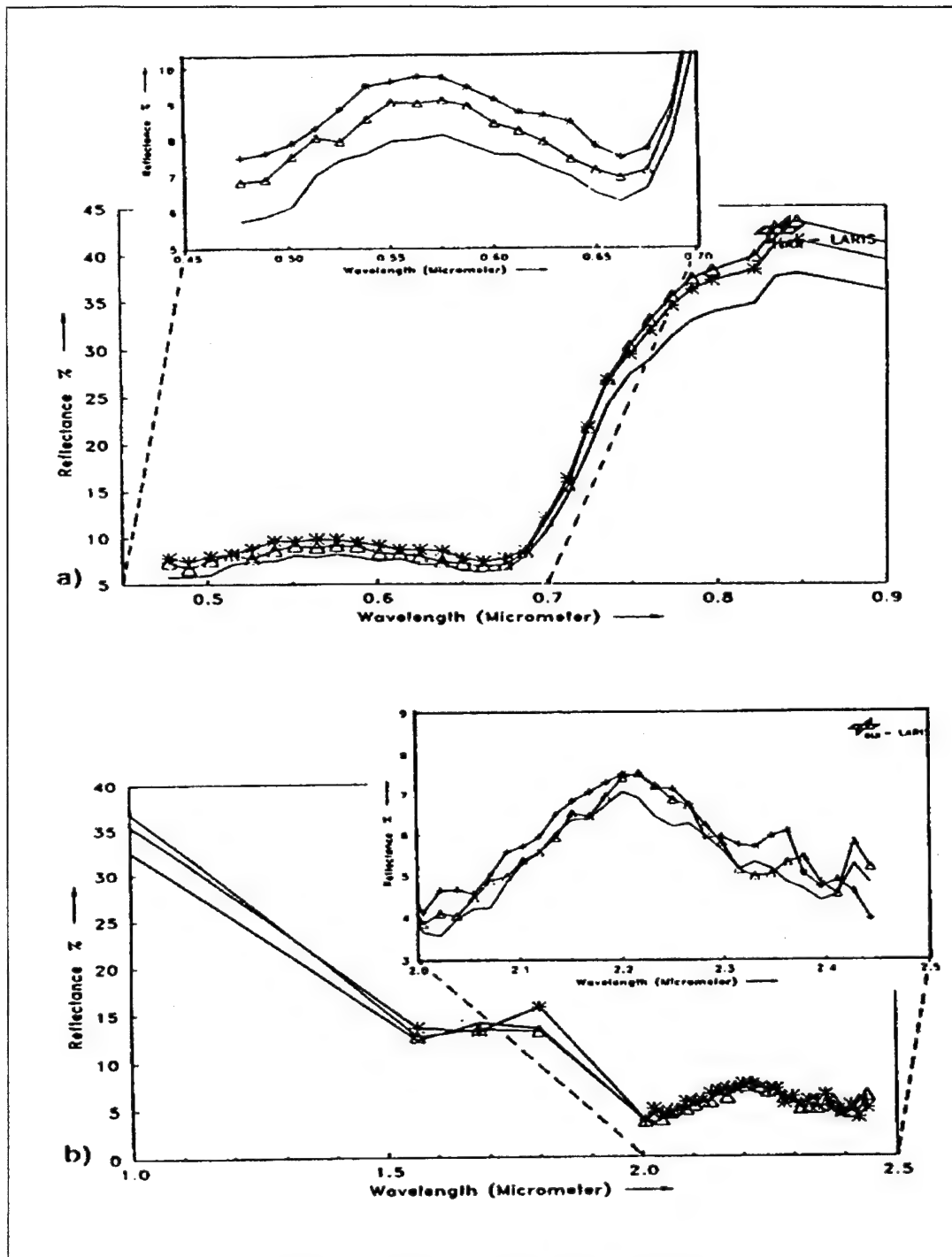


Figure 2.16 (Lehmann, et al, 1990)

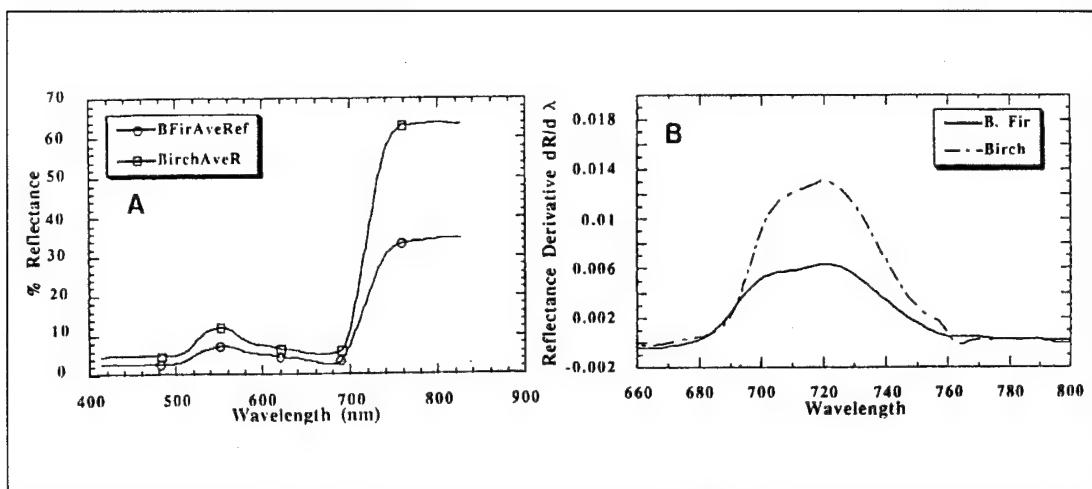


Figure 2.17 (Rock, et al, 1990)

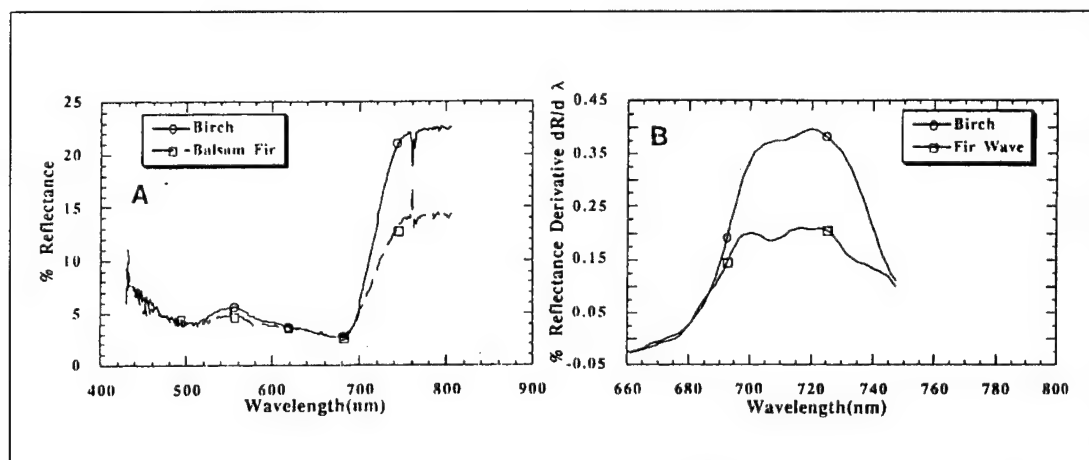


Figure 2.18 (Rock, et al, 1990)

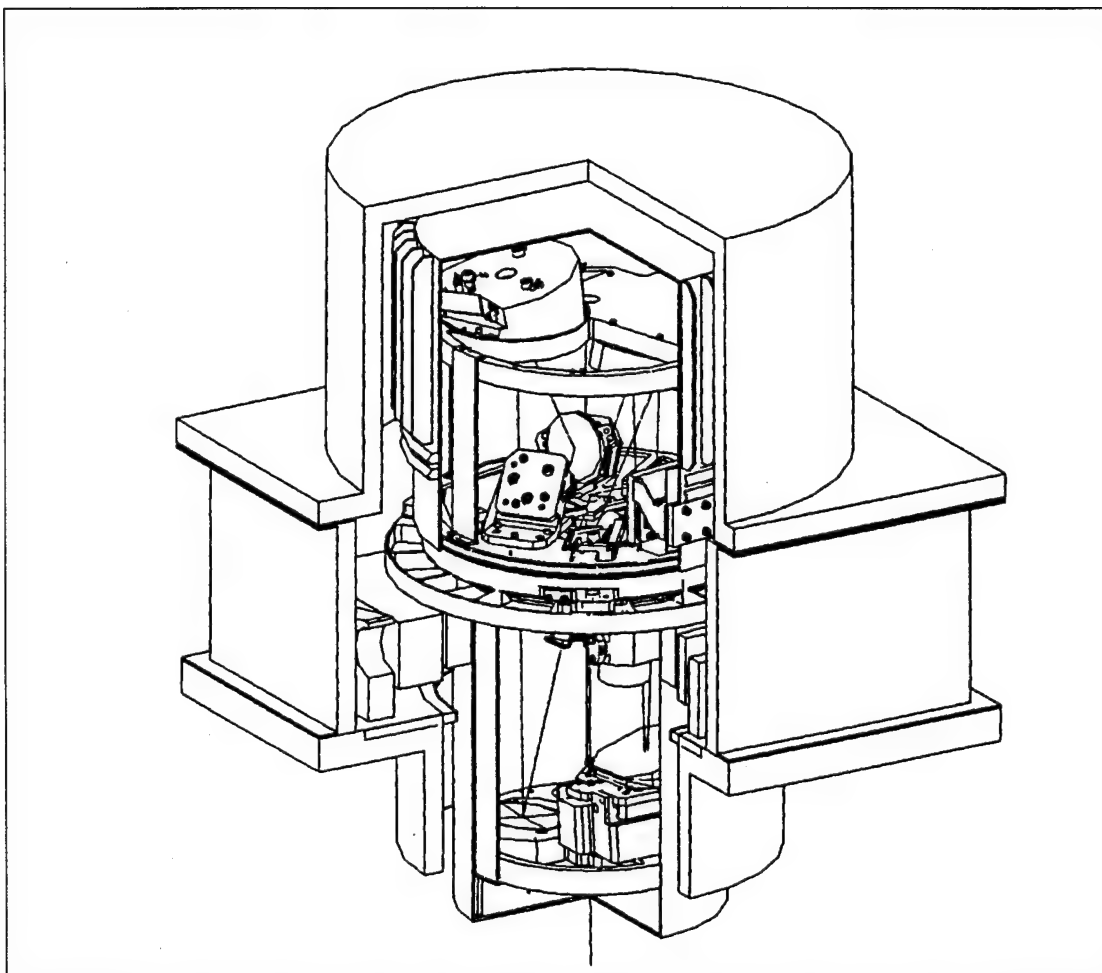


Figure 2.19 (HYDICE instrument, Hughes Danbury Optical Systems, 1993)

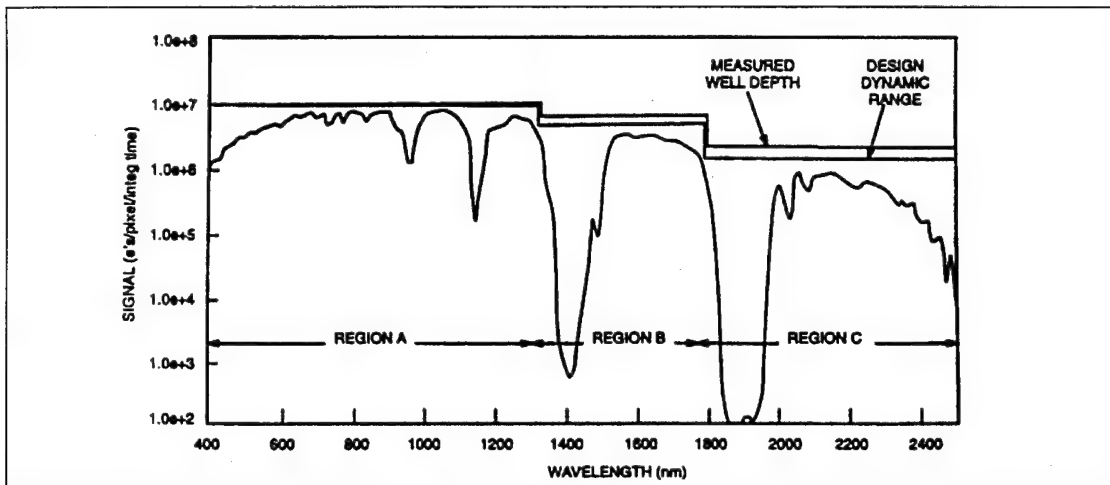


Figure 2.20 (Silvergate, et al, 1994)

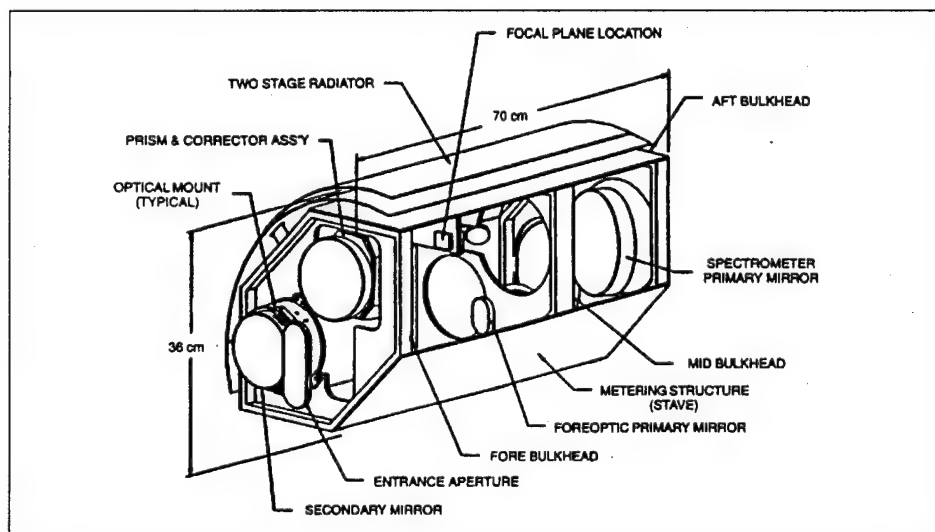


Figure 2.21 (HYDICE spaceborne concept, Silvergate, et al, 1994)

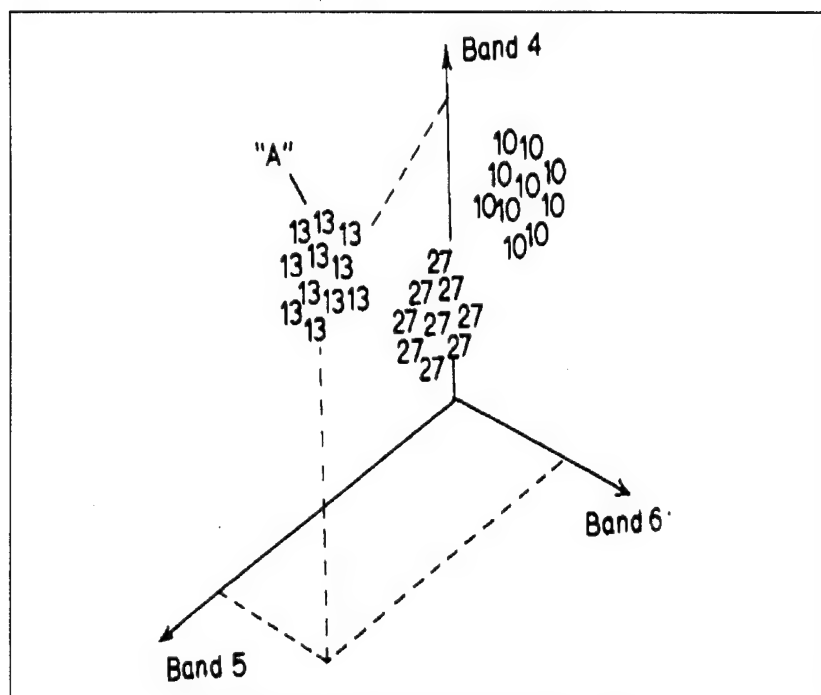


Figure 2.22 (Cracknell and Hayes, 1991)

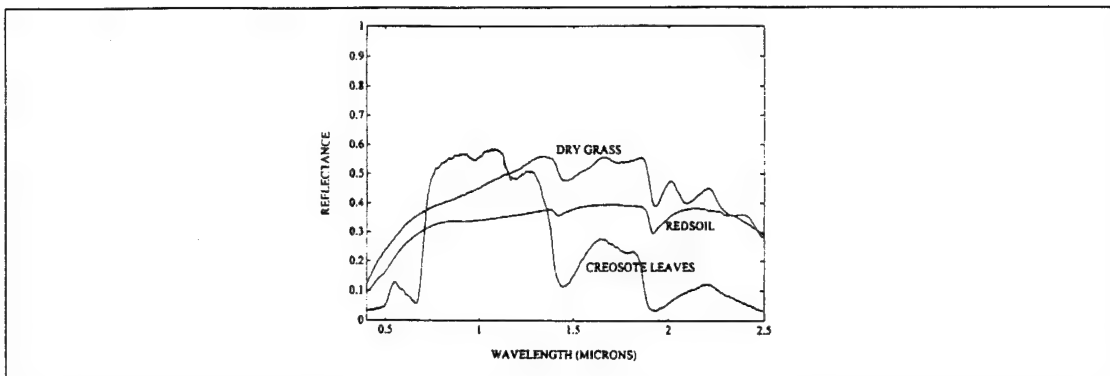


Figure 2.23 (Harsanyi and Chang, 1994)

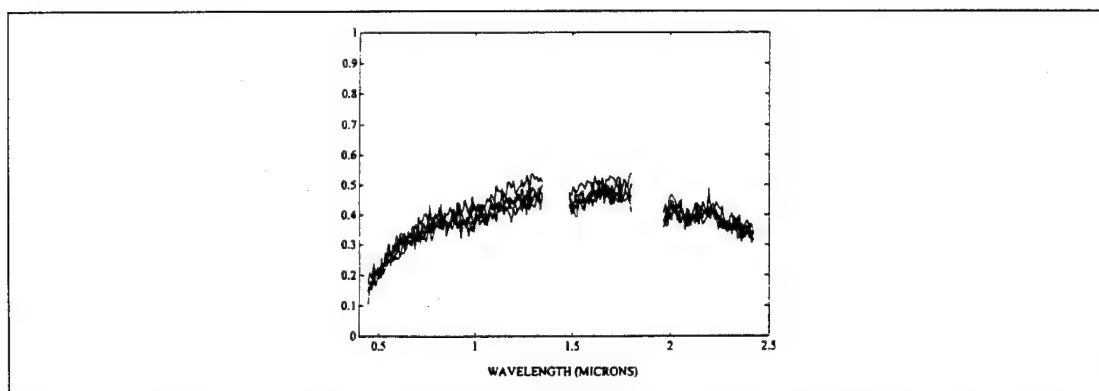


Figure 2.24 (Harsanyi and Chang, 1994)

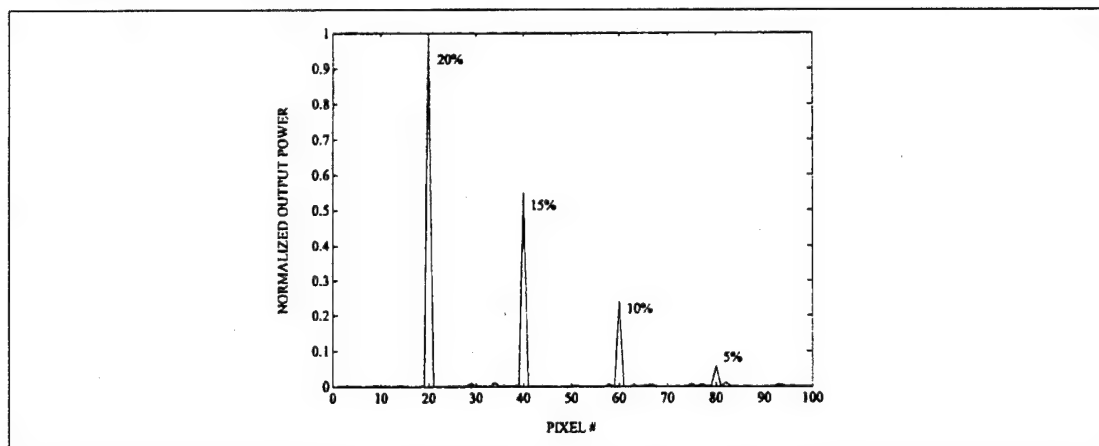


Figure 2.25 (Harsanyi and Chang, 1994)

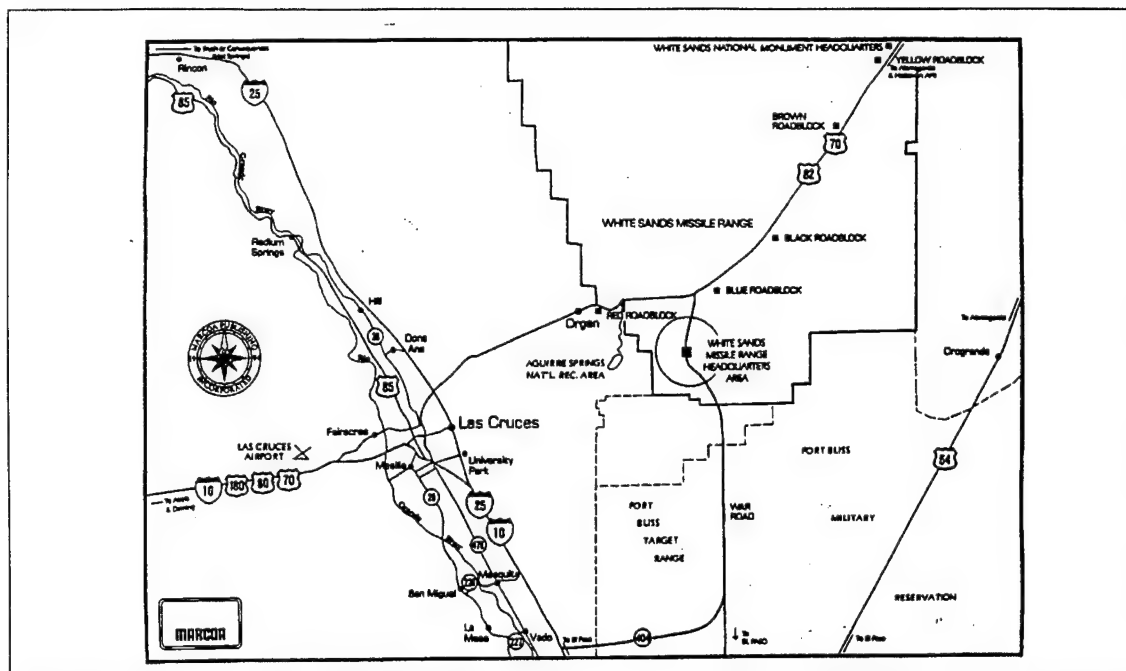


Figure 3.1 (WSMR/ Las Cruces, N.M., Anderson, 1995a)

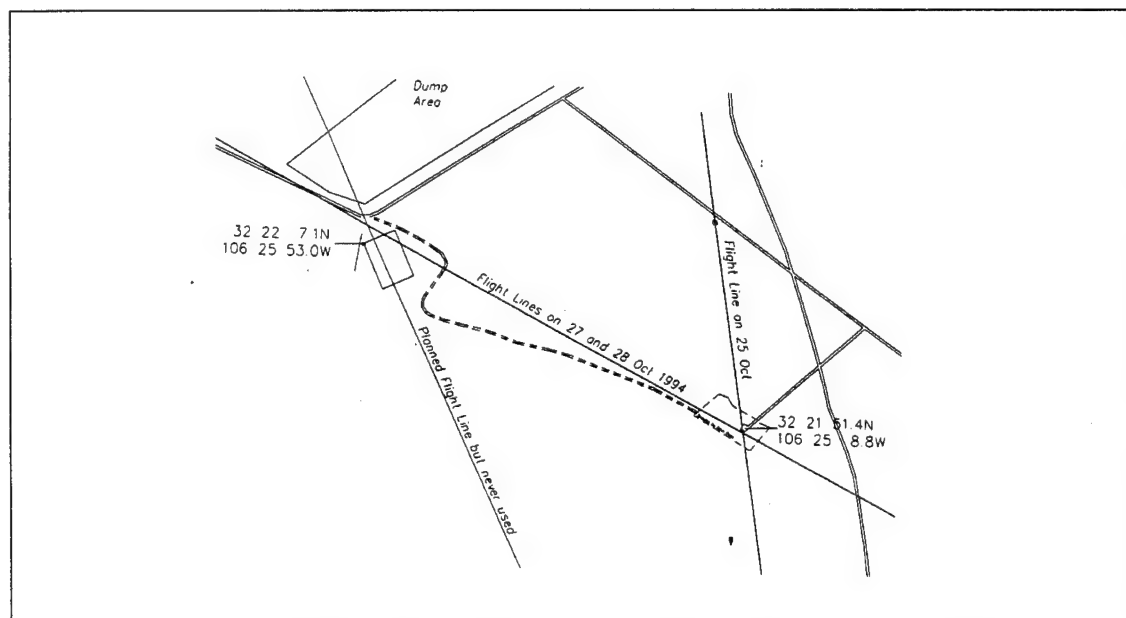


Figure 3.2 (WSMR, Desert Radiance-Actual Flight Lines, Anderson, 1995b)

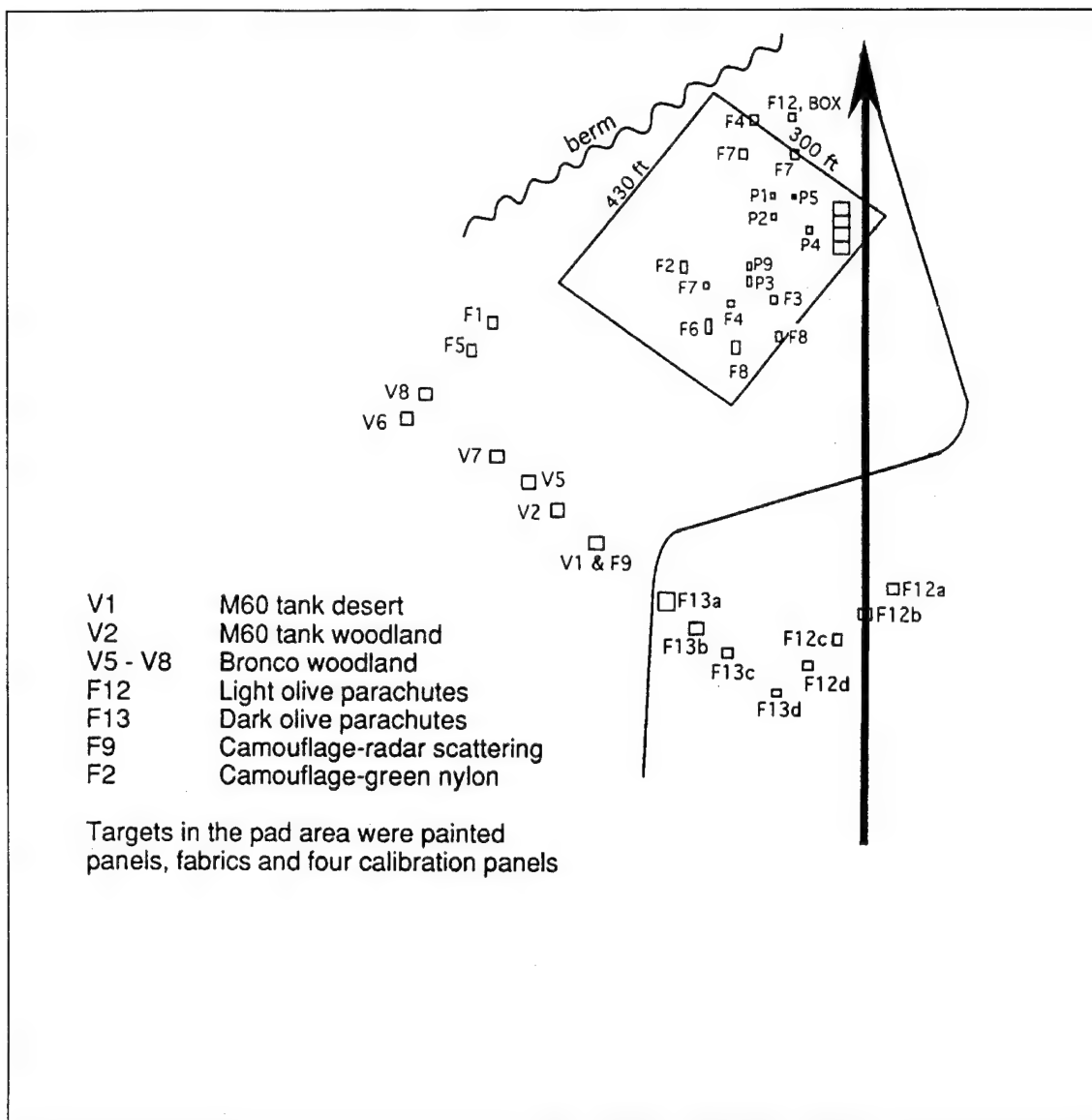


Figure 3.3 (Target Layout-27Oct 1994, Anderson, 1995b)

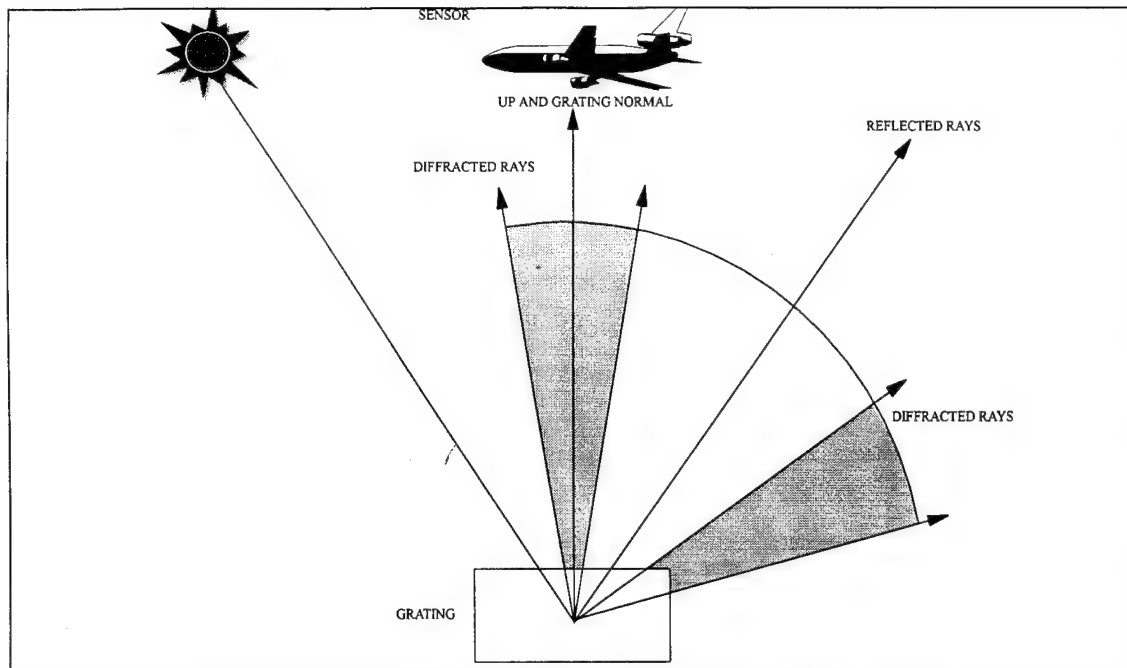


Figure 3.4 (Geometry of Diffraction-Flat Gratings, Stoner, 1994)

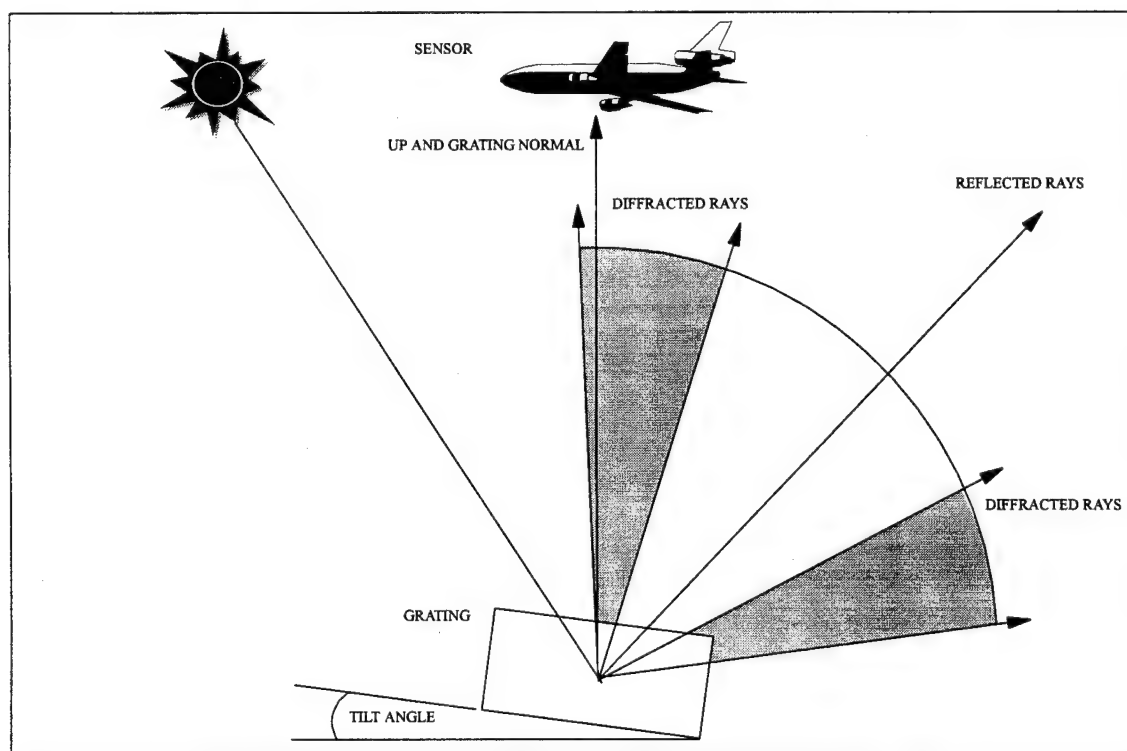


Figure 3.5 (Geometry of Diffraction-Tilted Gratings, Stoner, 1994)

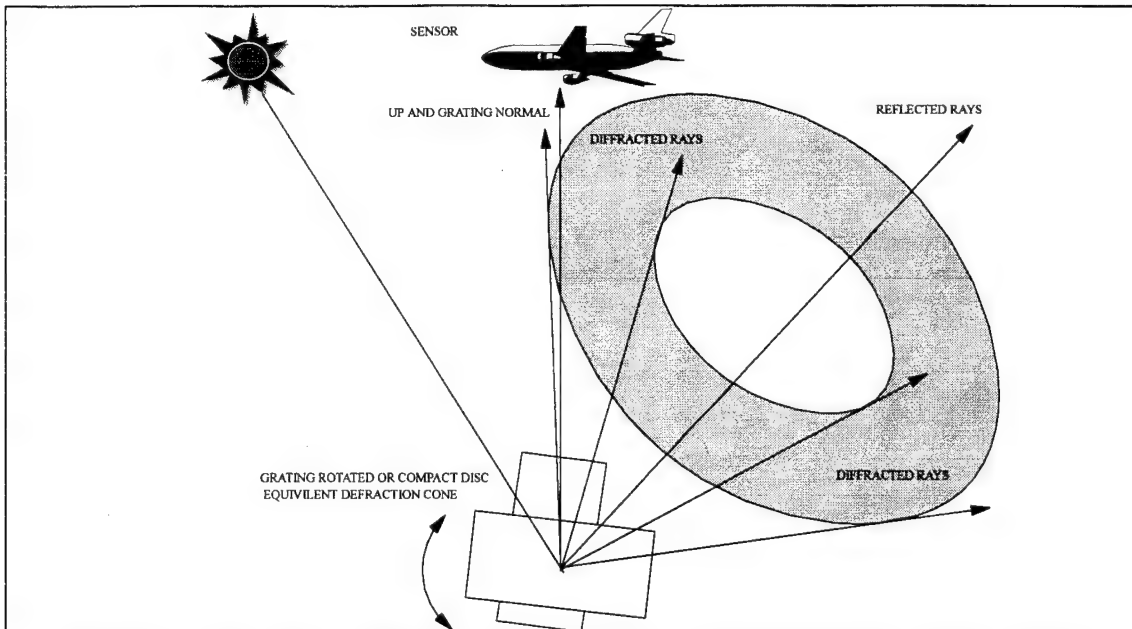


Figure 3.6 (Geometry of Diffraction Cone of Rotated or Circular Gratings, Stoner, 1994)

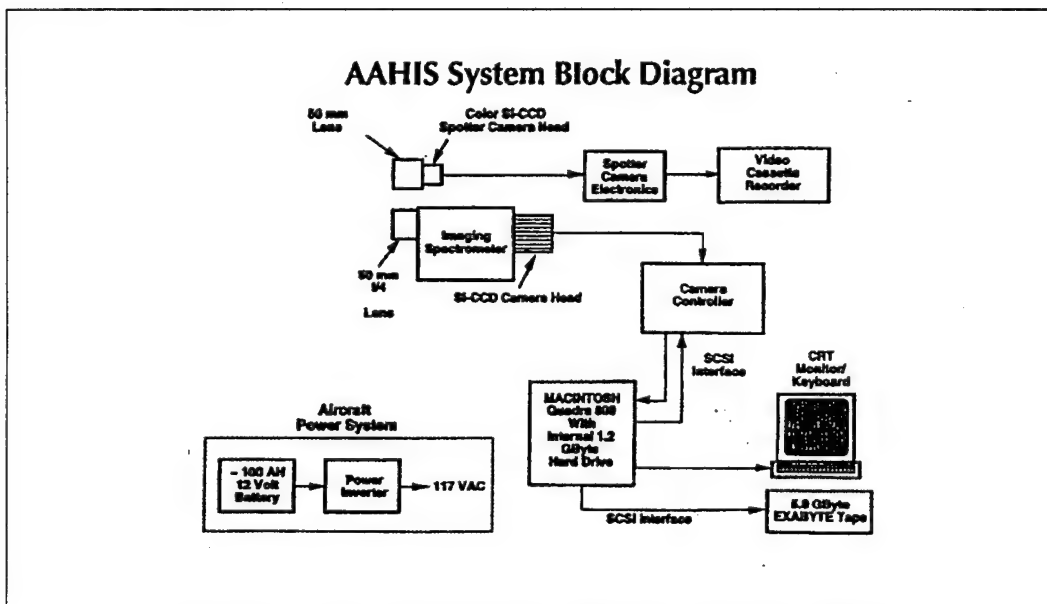


Figure 3.7 (AAHIS System Block Diagram, Anderson, 1995a)

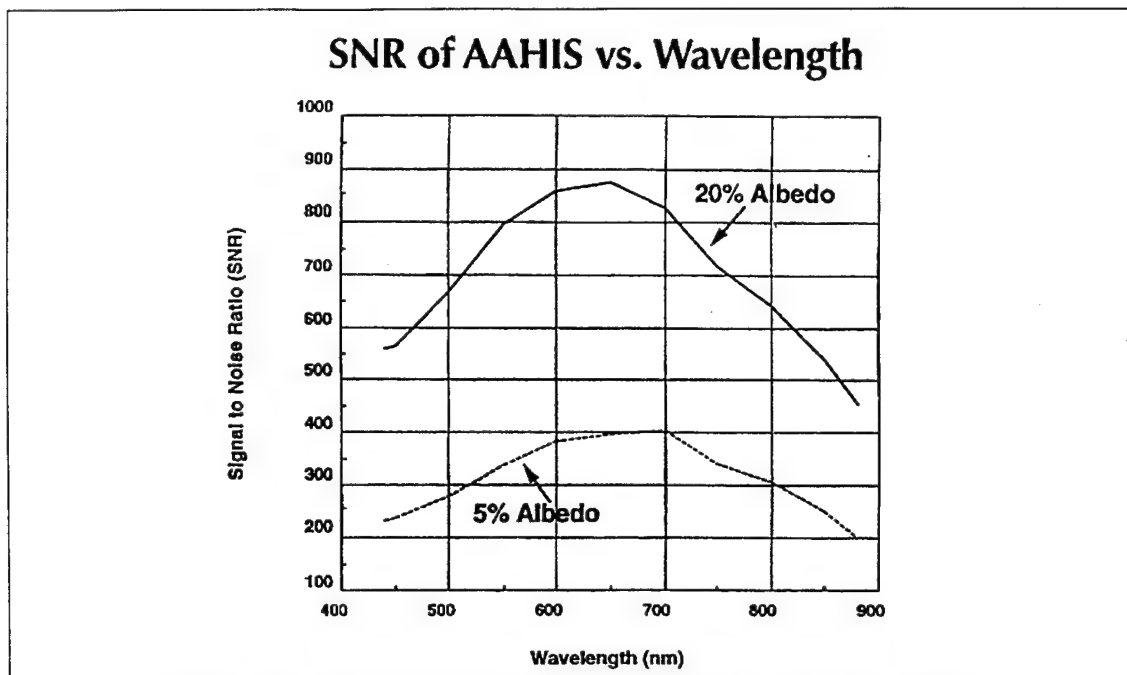


Figure 3.8 (AAHIS Signal-to-Noise vs. Wavelength, Anderson, 1995a)

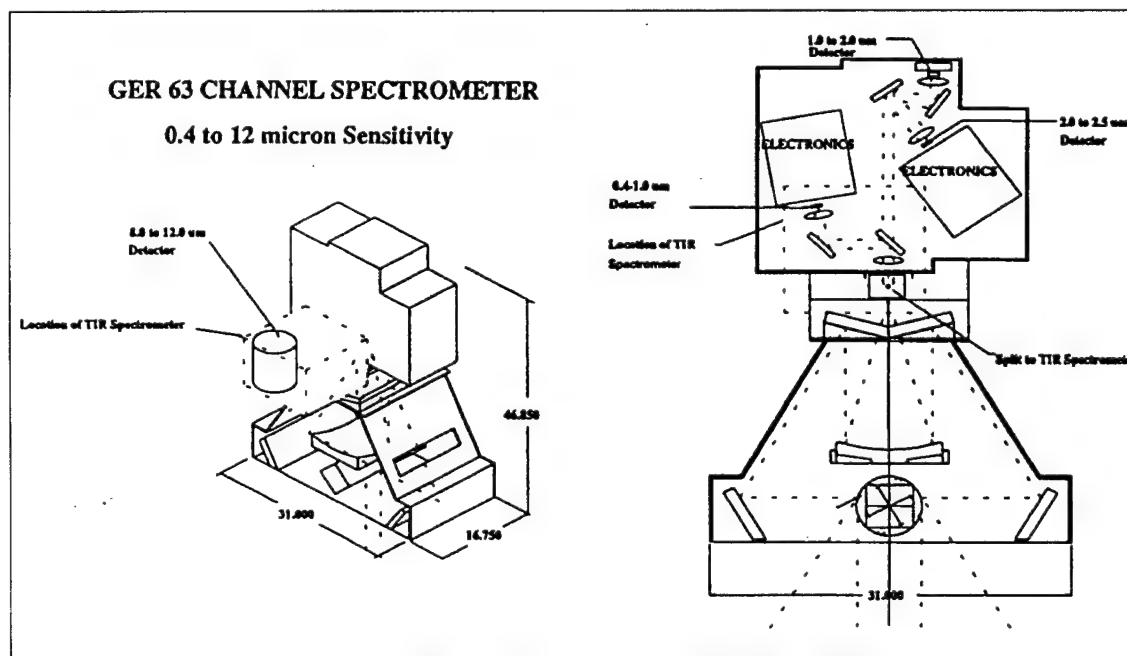


Figure 3.9 (GER 63 DAIS Schematic, Anderson, 1995a)

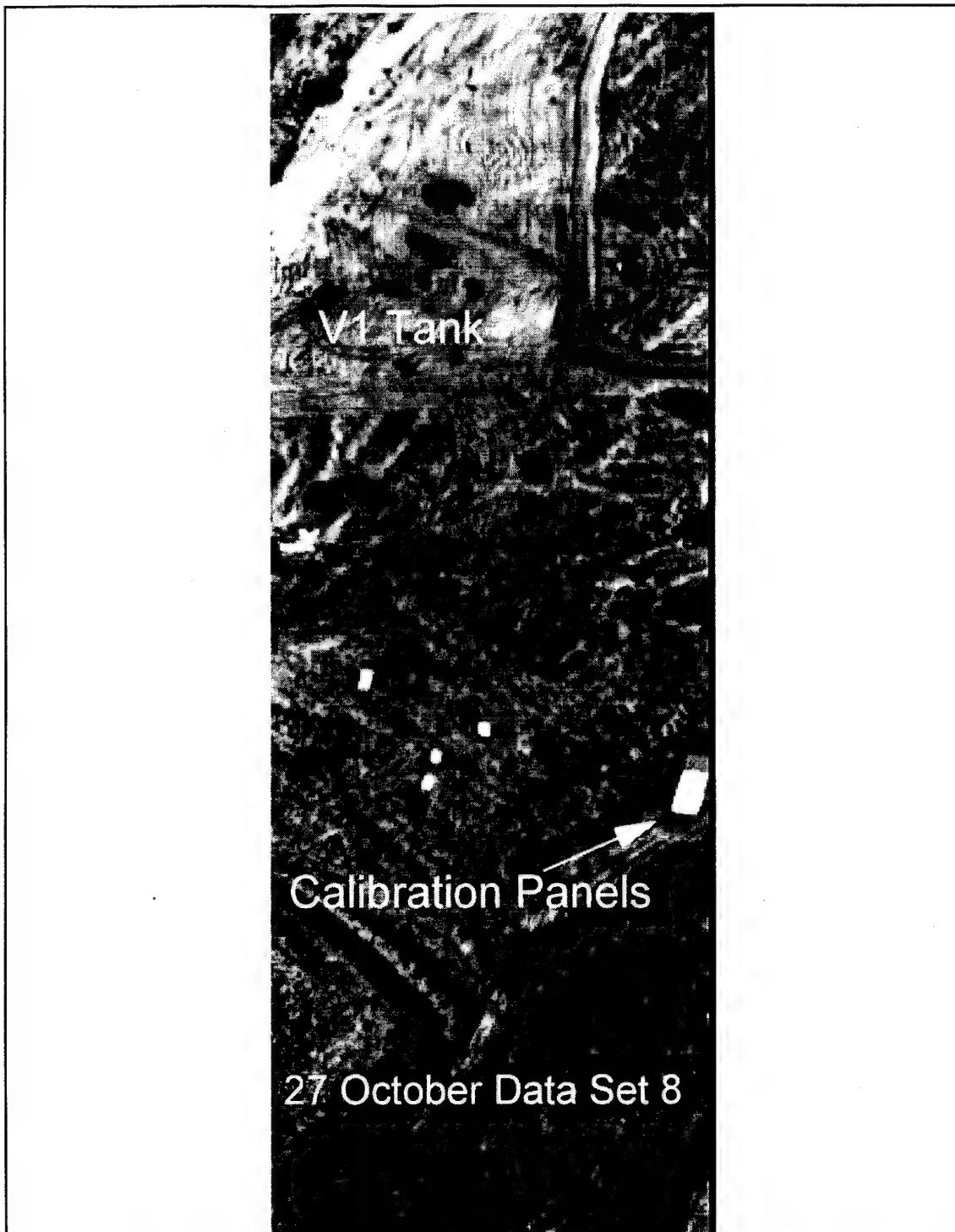


Figure 4.1 (27 October 1994 AAHIS Data Set 8)

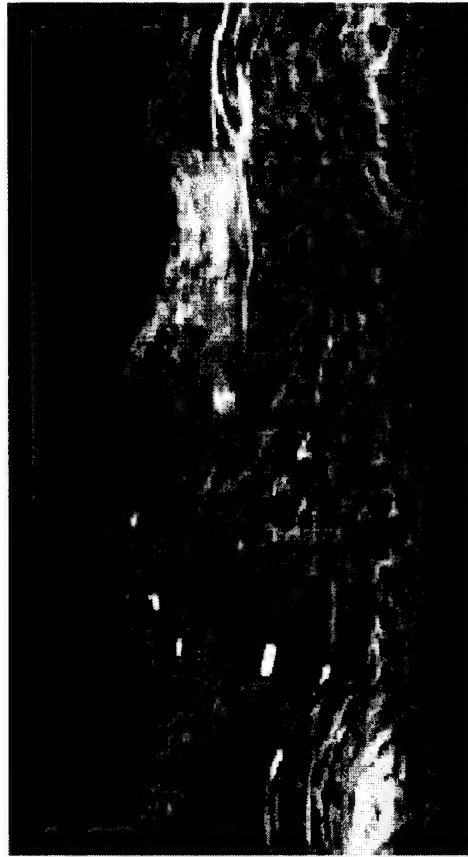


Figure 4.2 (AAHIS 28 October Data 13)

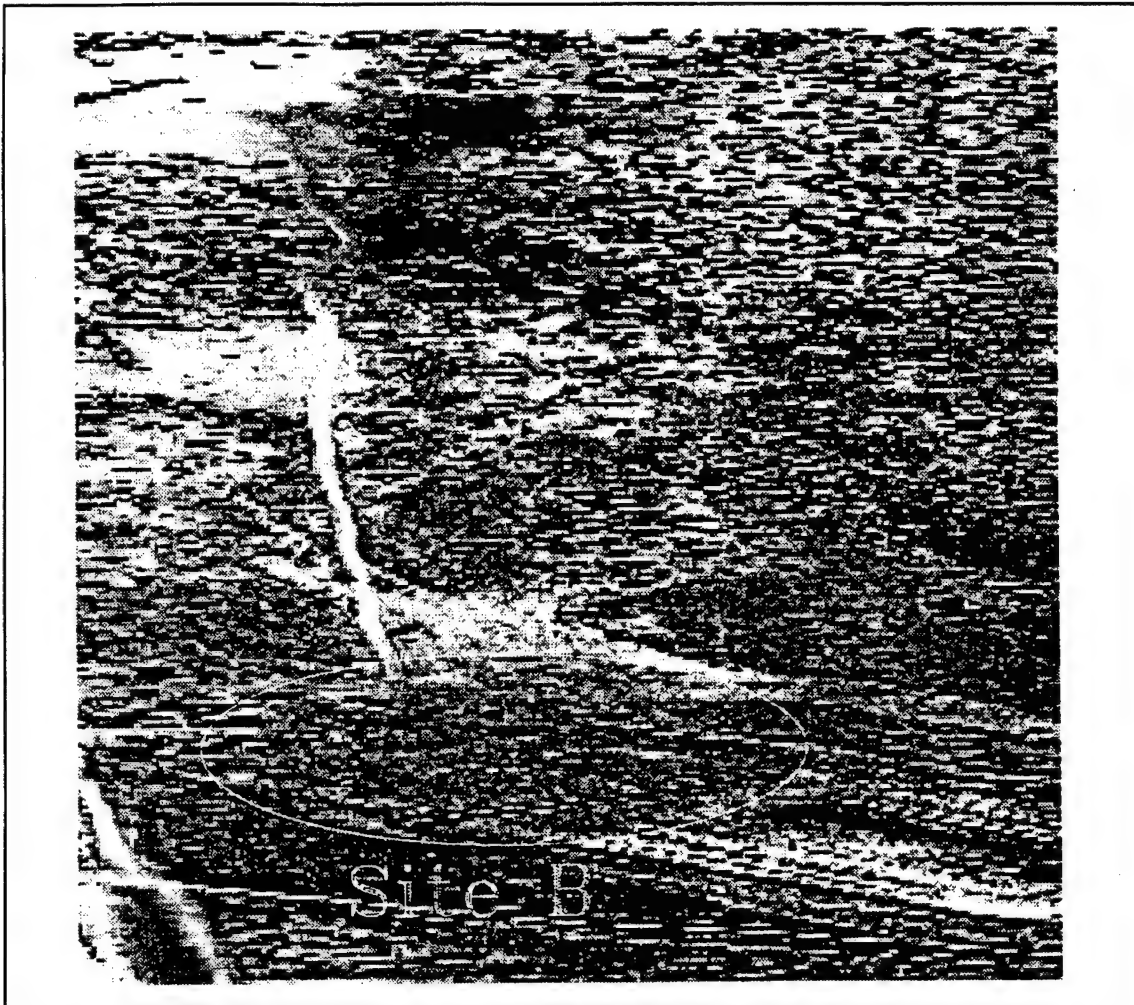


Figure 4.3 (GER 28 October Data 13)

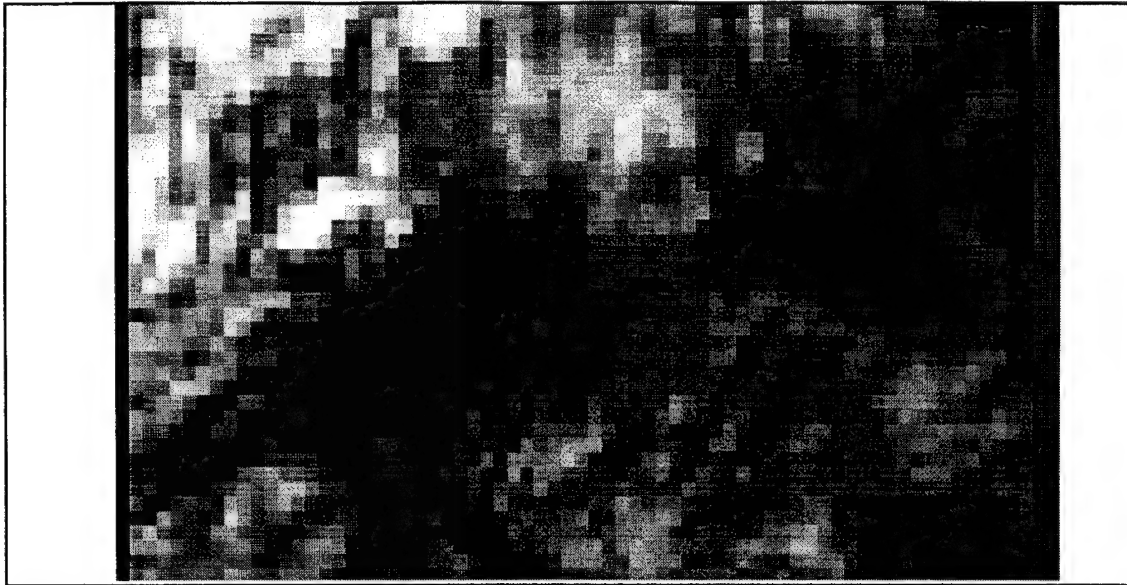


Figure 5.1a (V1 Tank Target--Pixel Blow-up--27 October Data 8)

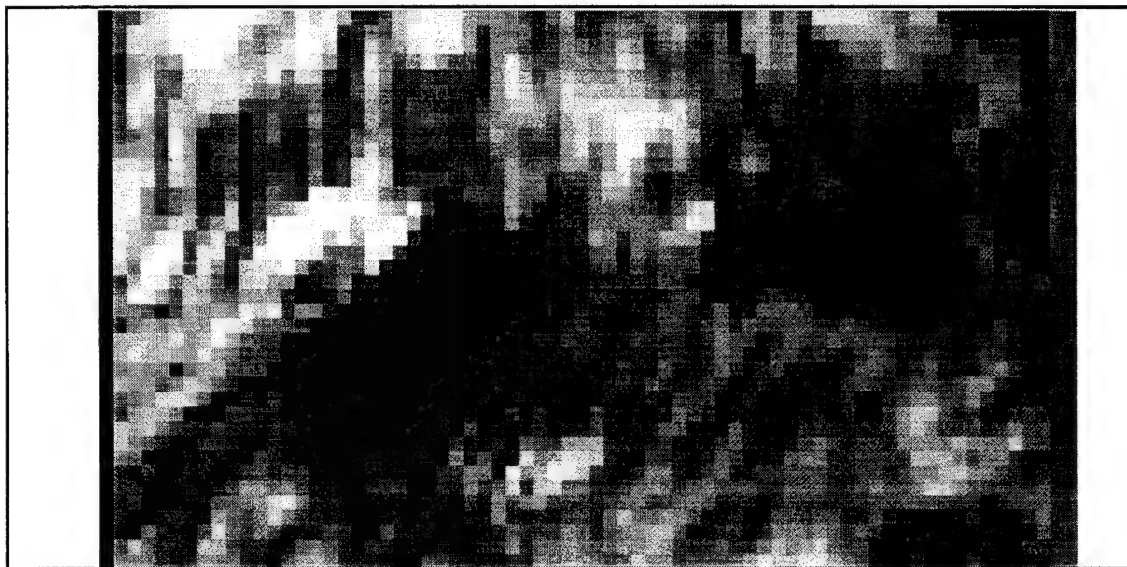


Figure 5.1b (V1 Tank--Pixel Blow-up--Principle Component 1)

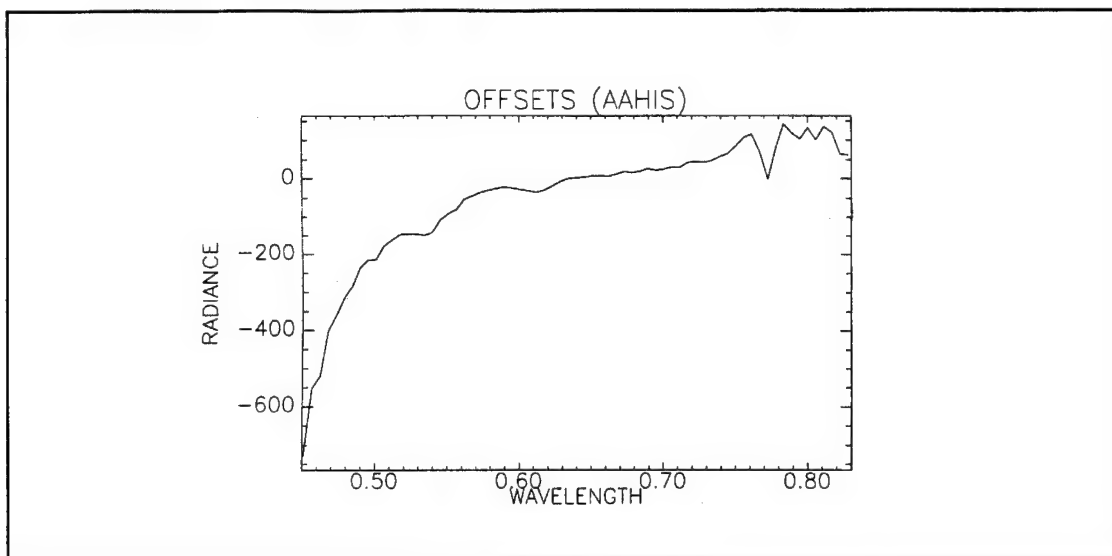


Figure 5.2 (AAHIS Offsets)

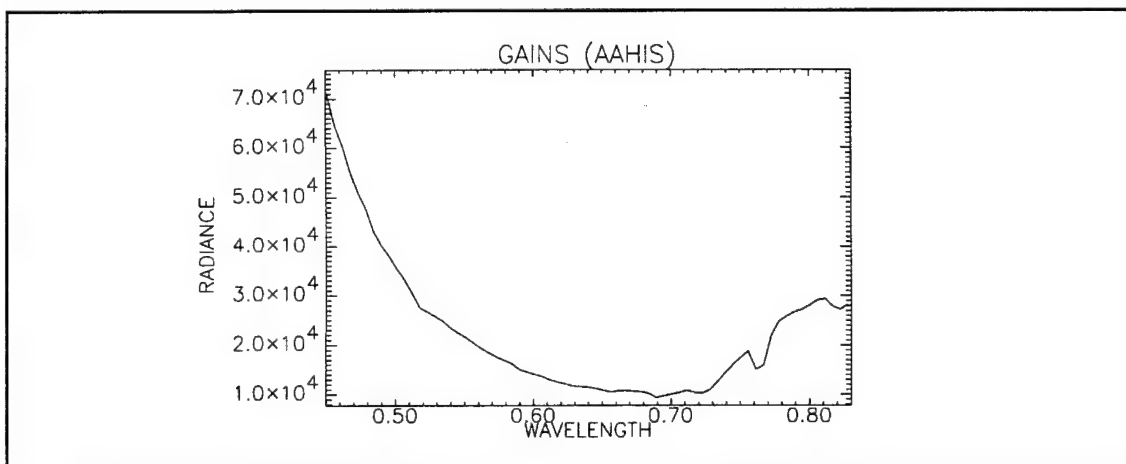


Figure 5.3 (AAHIS Gains)

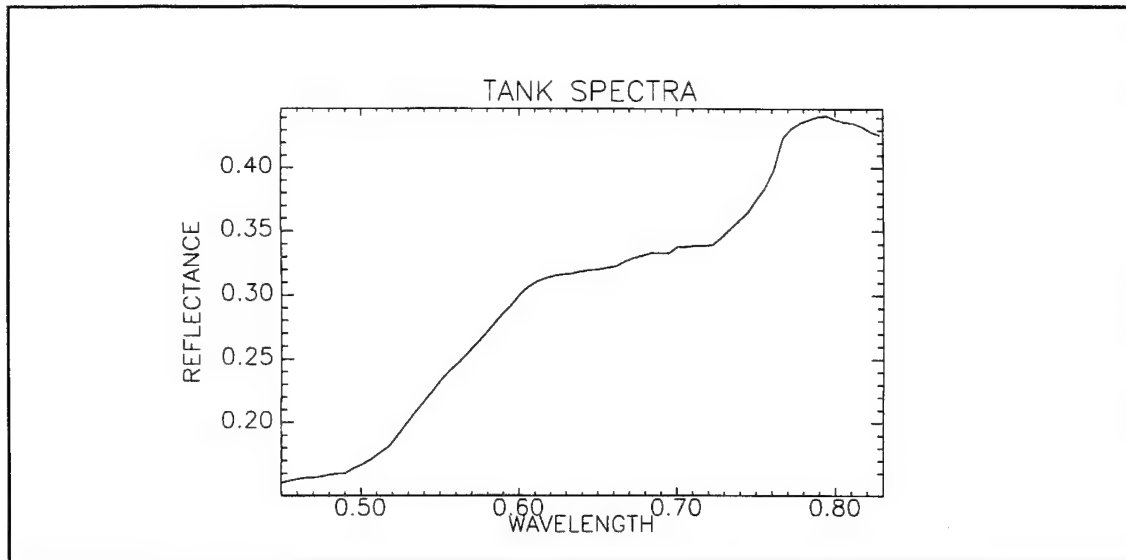


Figure 5.4 (Tank spectra from TEC ground truth ---AAHIS sensor range)

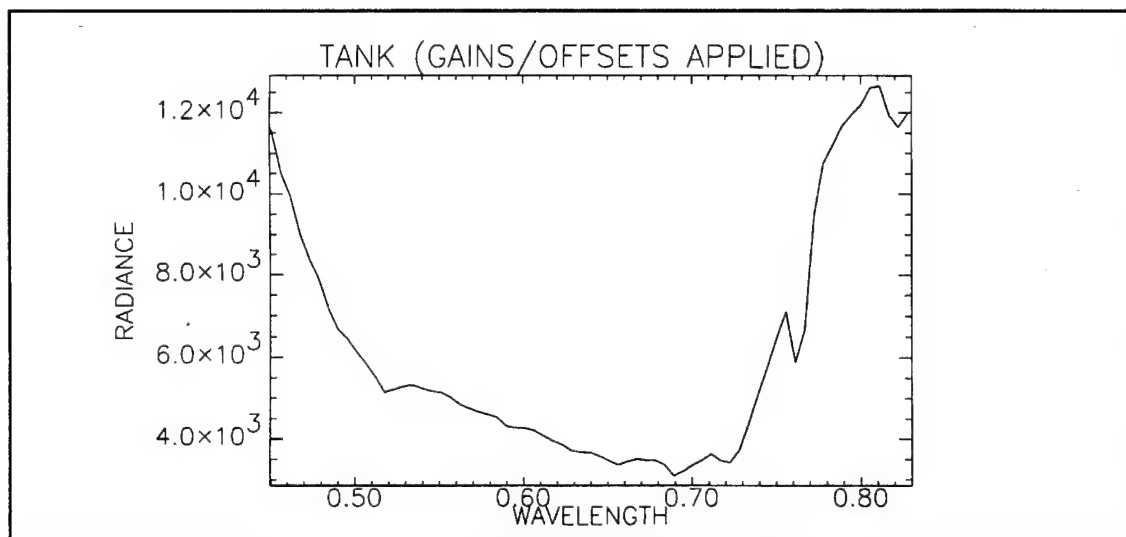


Figure 5.5 (Tank spectra with AAHIS Gains /Offsets applied)

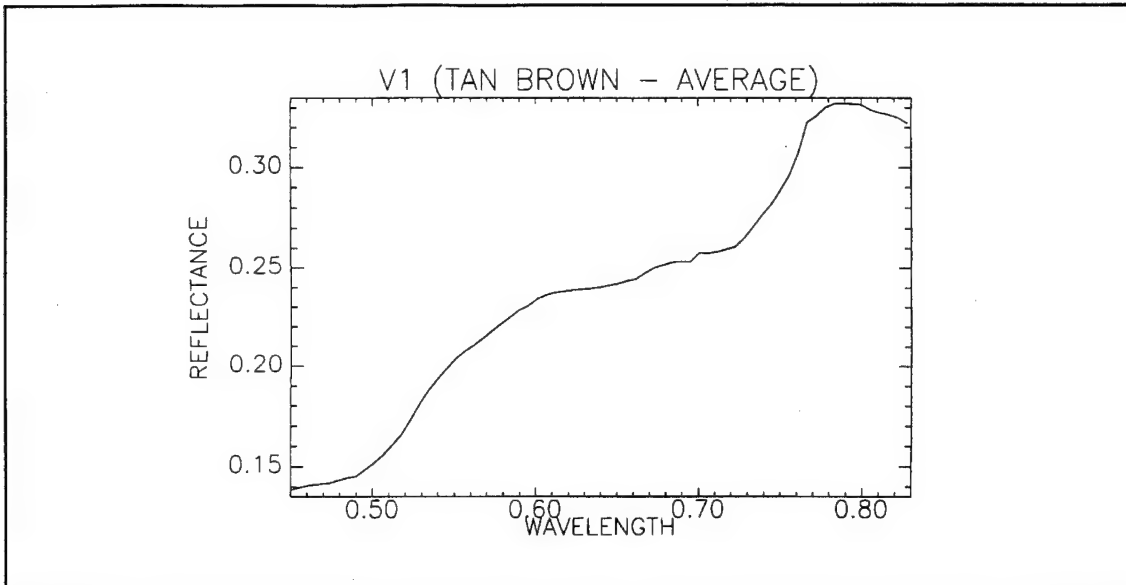


Figure 5.6 (V1 Tan Brown spectra from TEC ground truth --AAHIS sensor range)

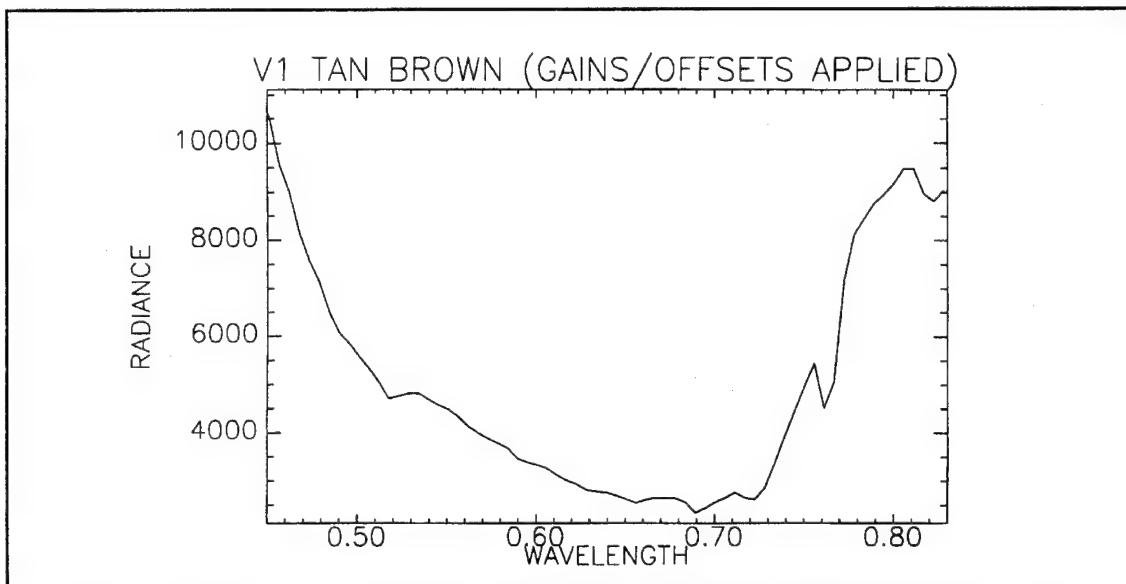


Figure 5.7 (V1 Tan Brown spectra with AAHIS Gains/Offsets applied)

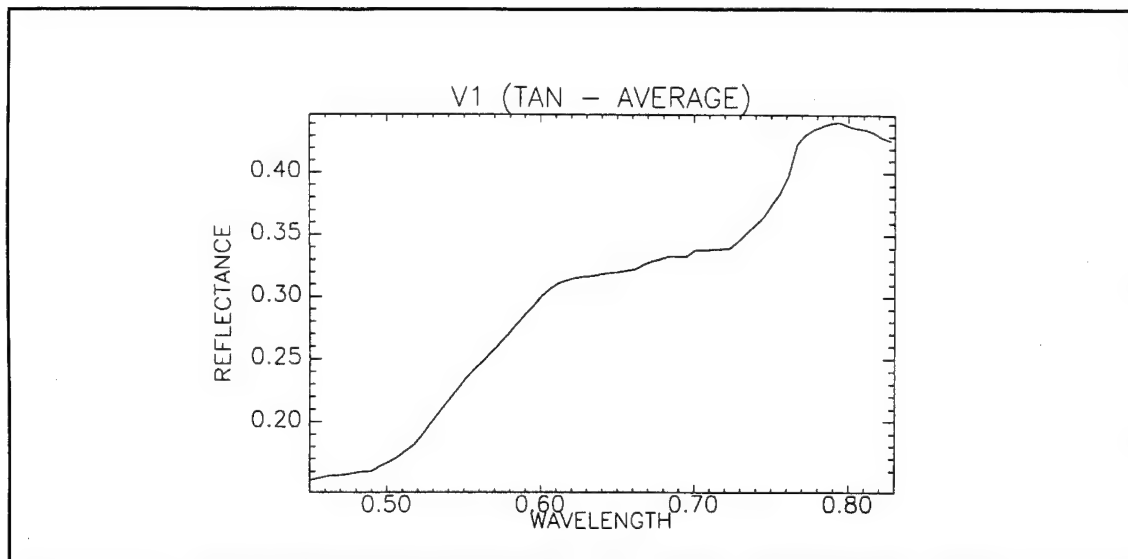


Figure 5.8 (V1 Tan spectra from TEC ground truth -- AAHIS sensor range)

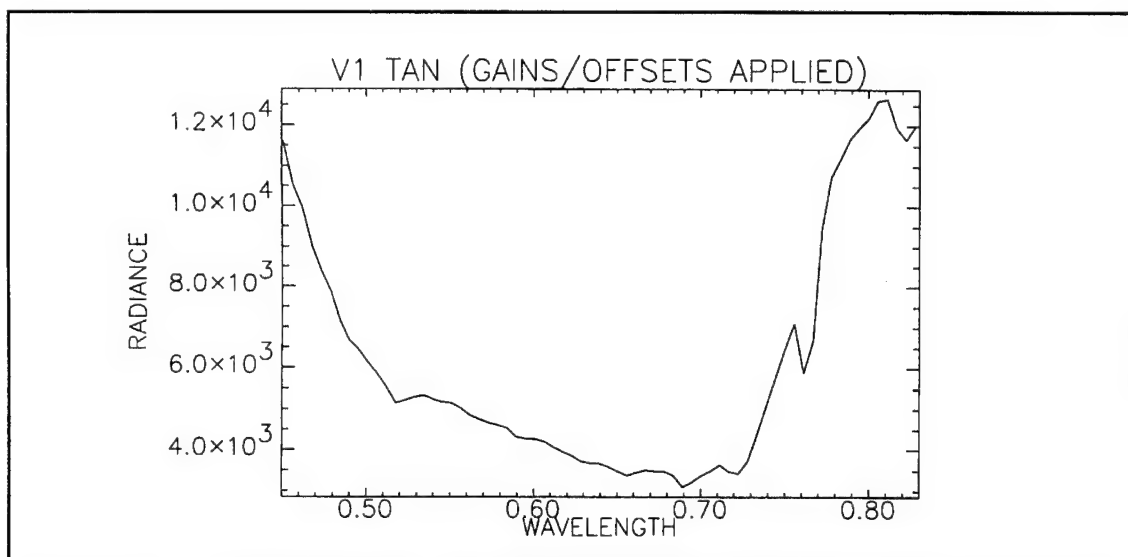


Figure 5.9 (V1 Tan spectra with AAHIS Gains/Offsets applied)

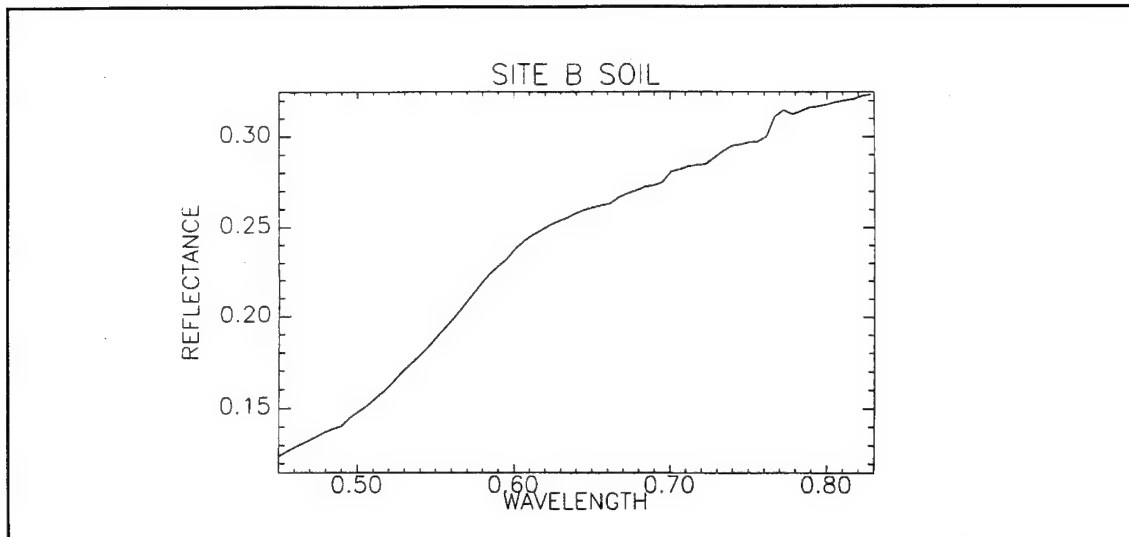


Figure 5.10 (Site B Soil from TEC ground truth -- AAHIS sensor range)

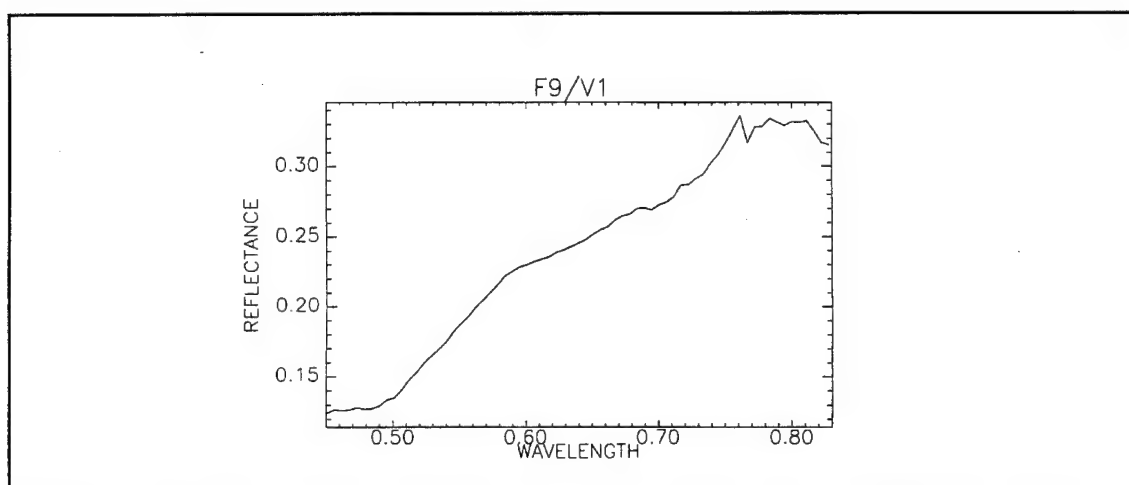


Figure 5.11 (F9 Camouflage overlaying V1 from TEC ground truth -- AAHIS sensor range)

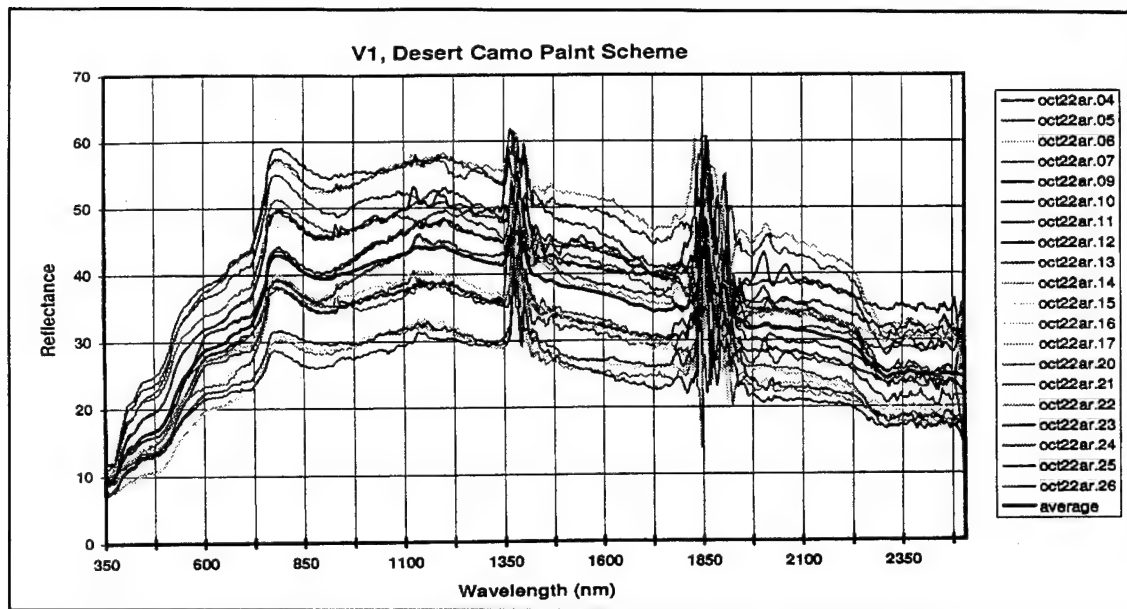


Figure 5.12 (V1 spectra from TEC ground truth -- .4 -2.5 microns)

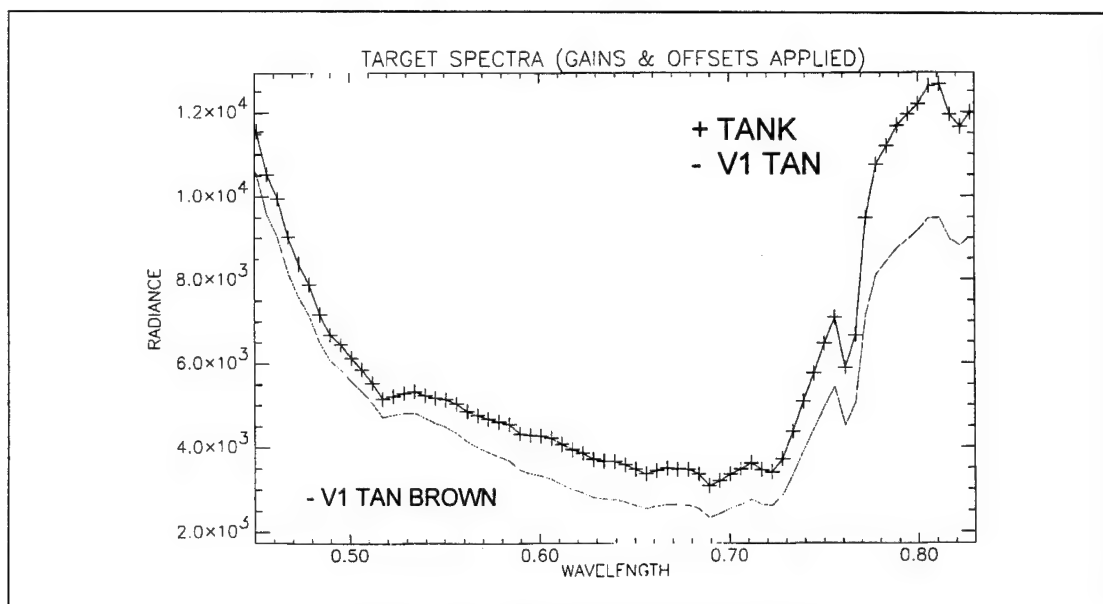


Figure 5.13 (Target spectra comparisons)

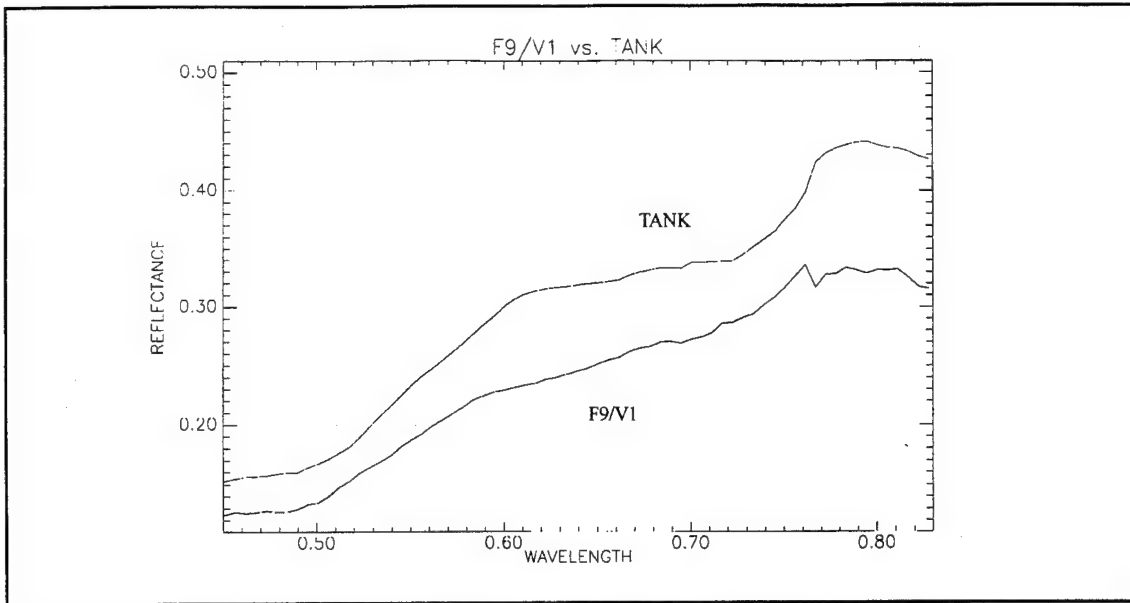


Figure 5.14 (F9 camouflage over V1 and Tank spectra comparison)

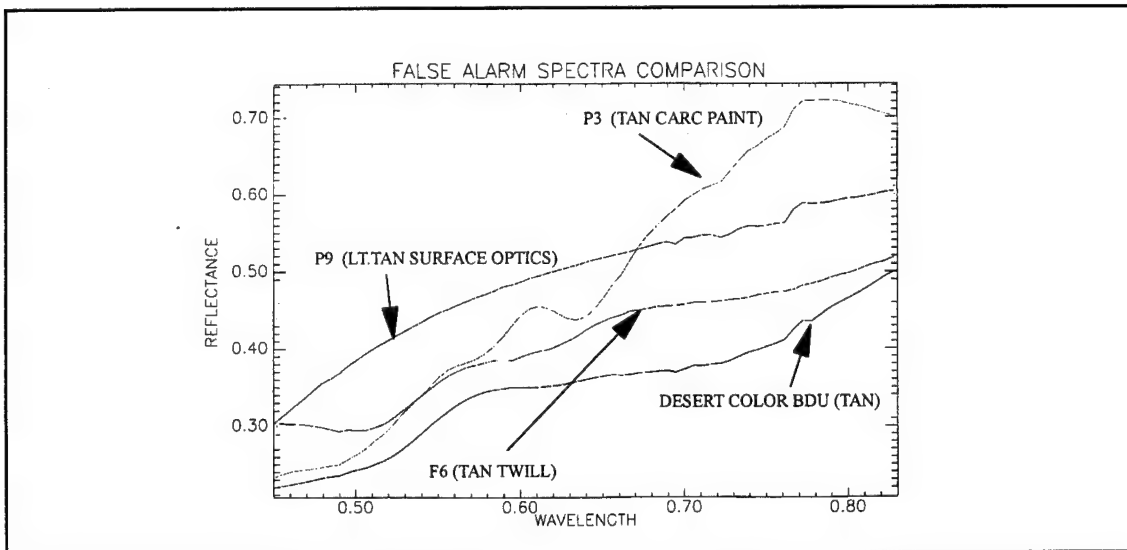


Figure 5.15 (LPD false alarm spectra comparisons)

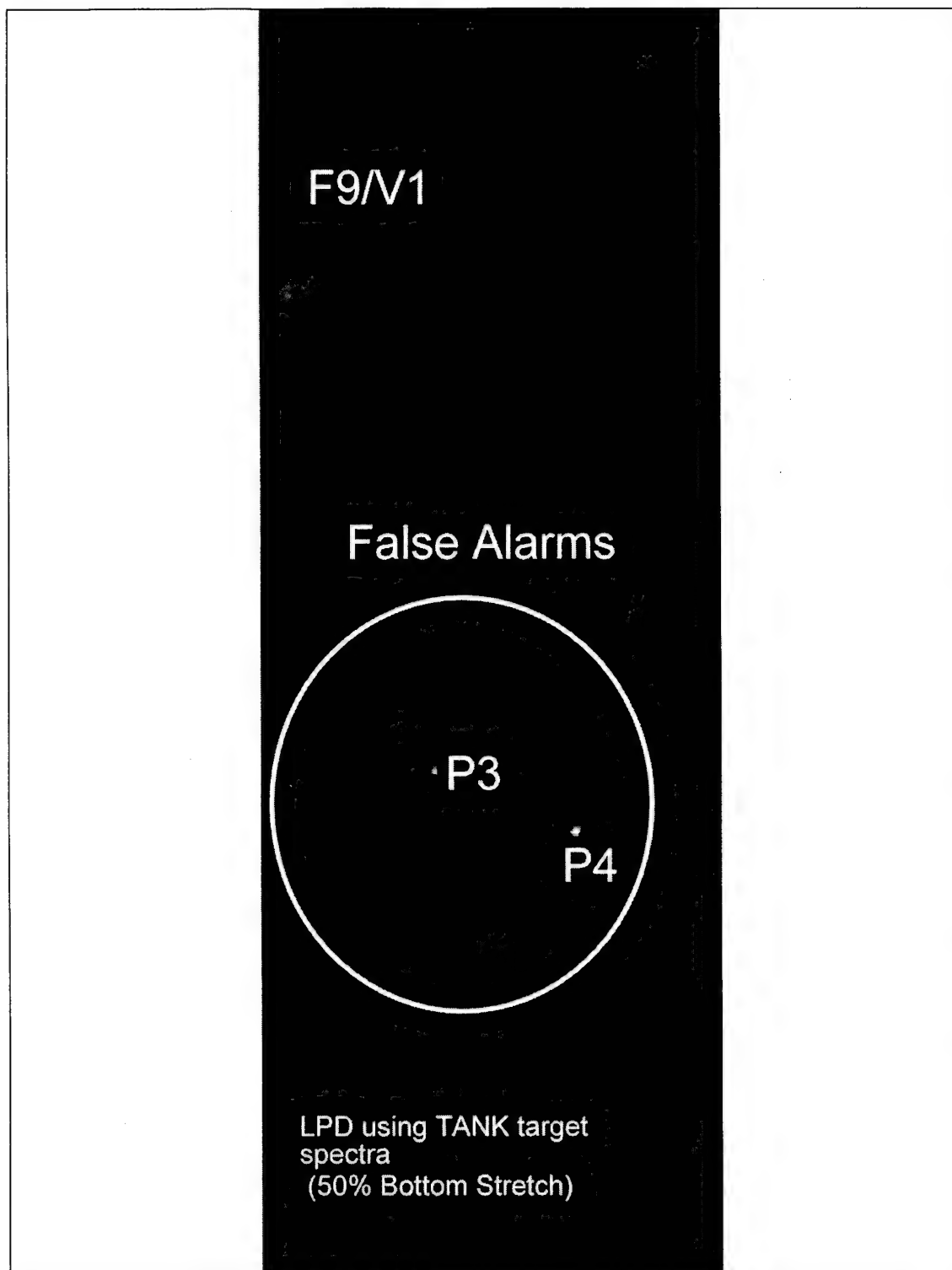


Figure 5.16 (LPD Component image-TANK Target Spectra)

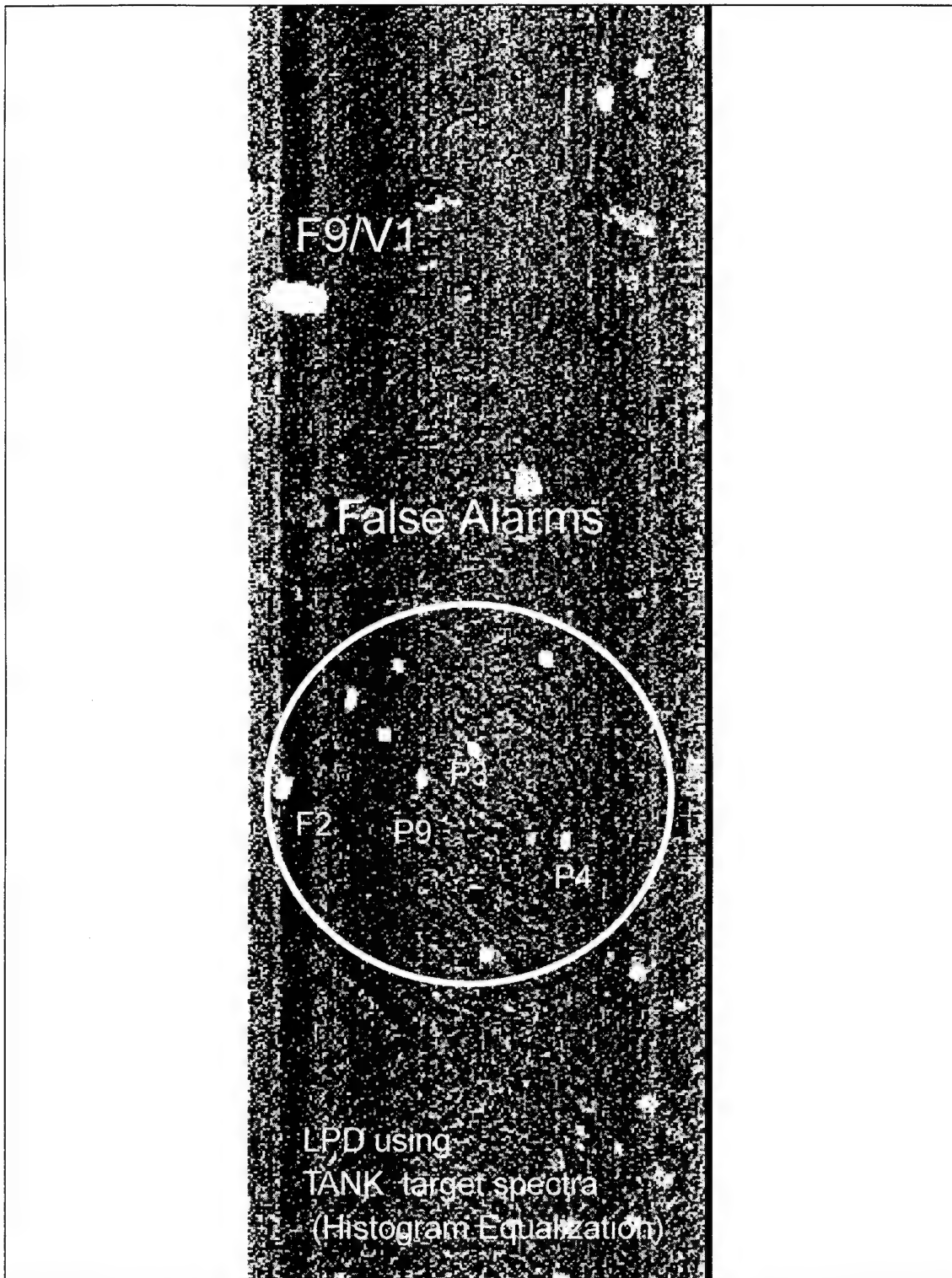


Figure 5.17 (LPD Component image--TANK Target Spectra--Histogram Eq.)

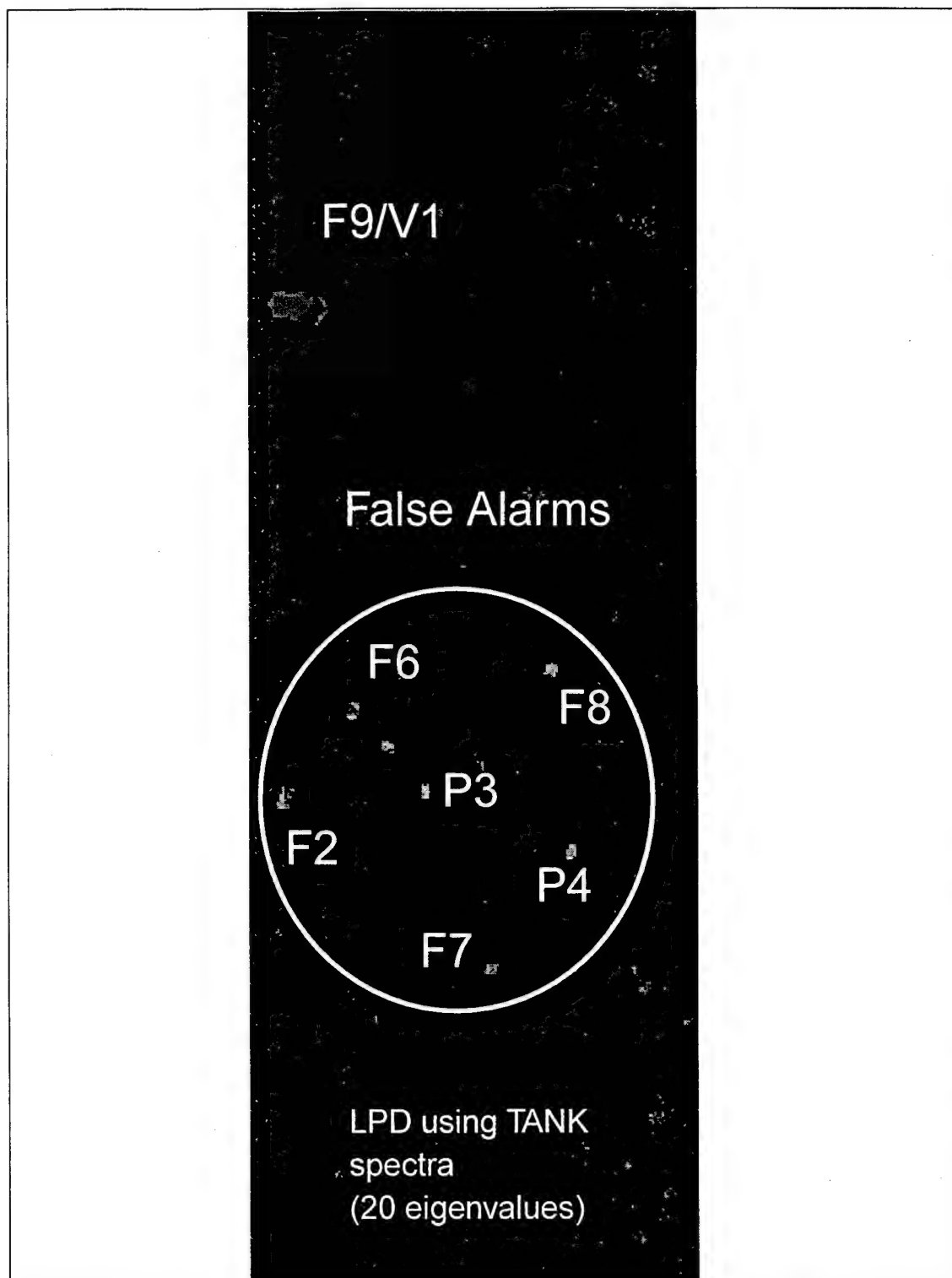


Figure 5.18 (LPD Component Image--TANK Target Spectra--20 Eigenvalues)

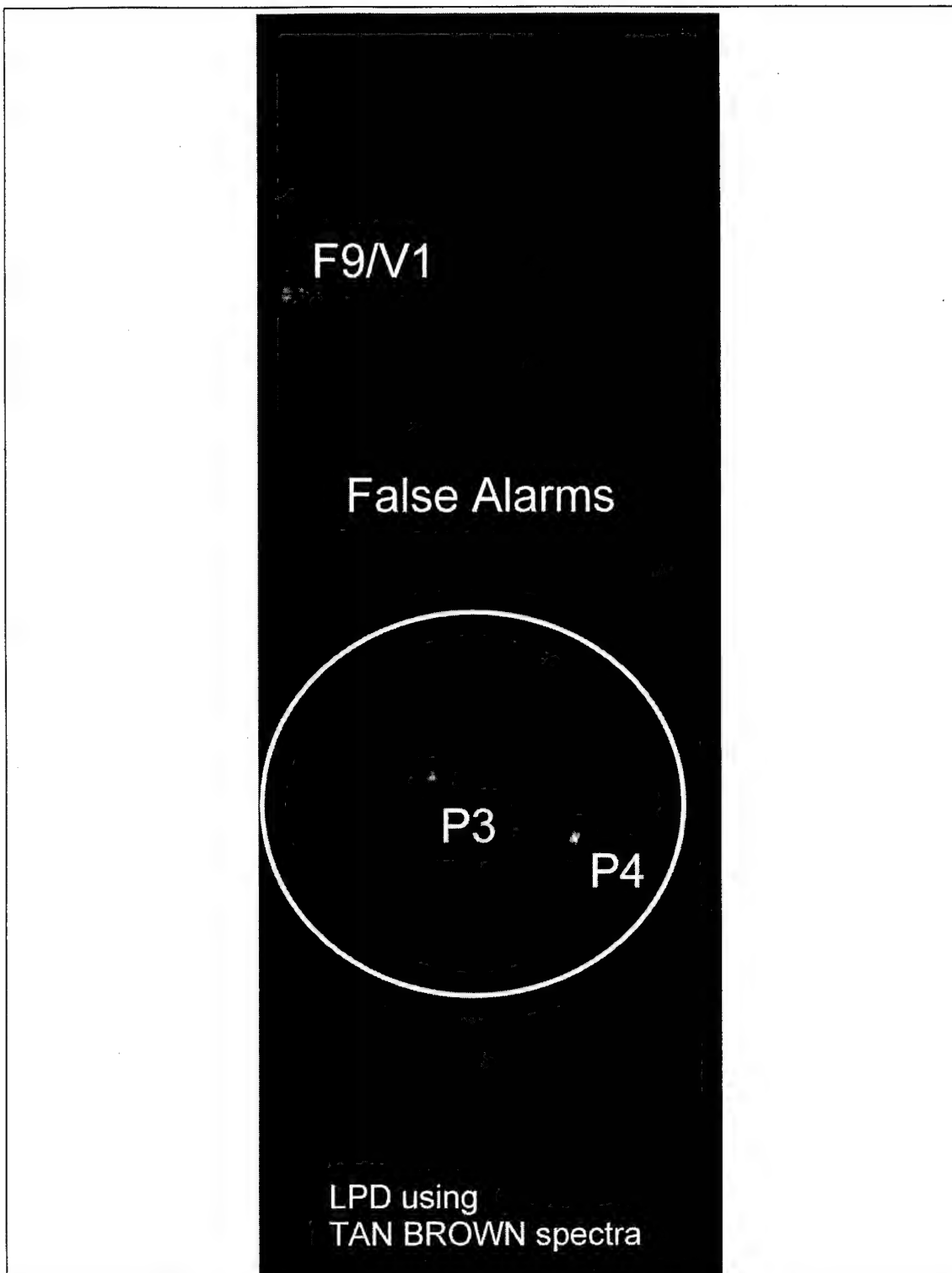


Figure 5.19 (LPD Component Image--TAN BROWN Target spectra)

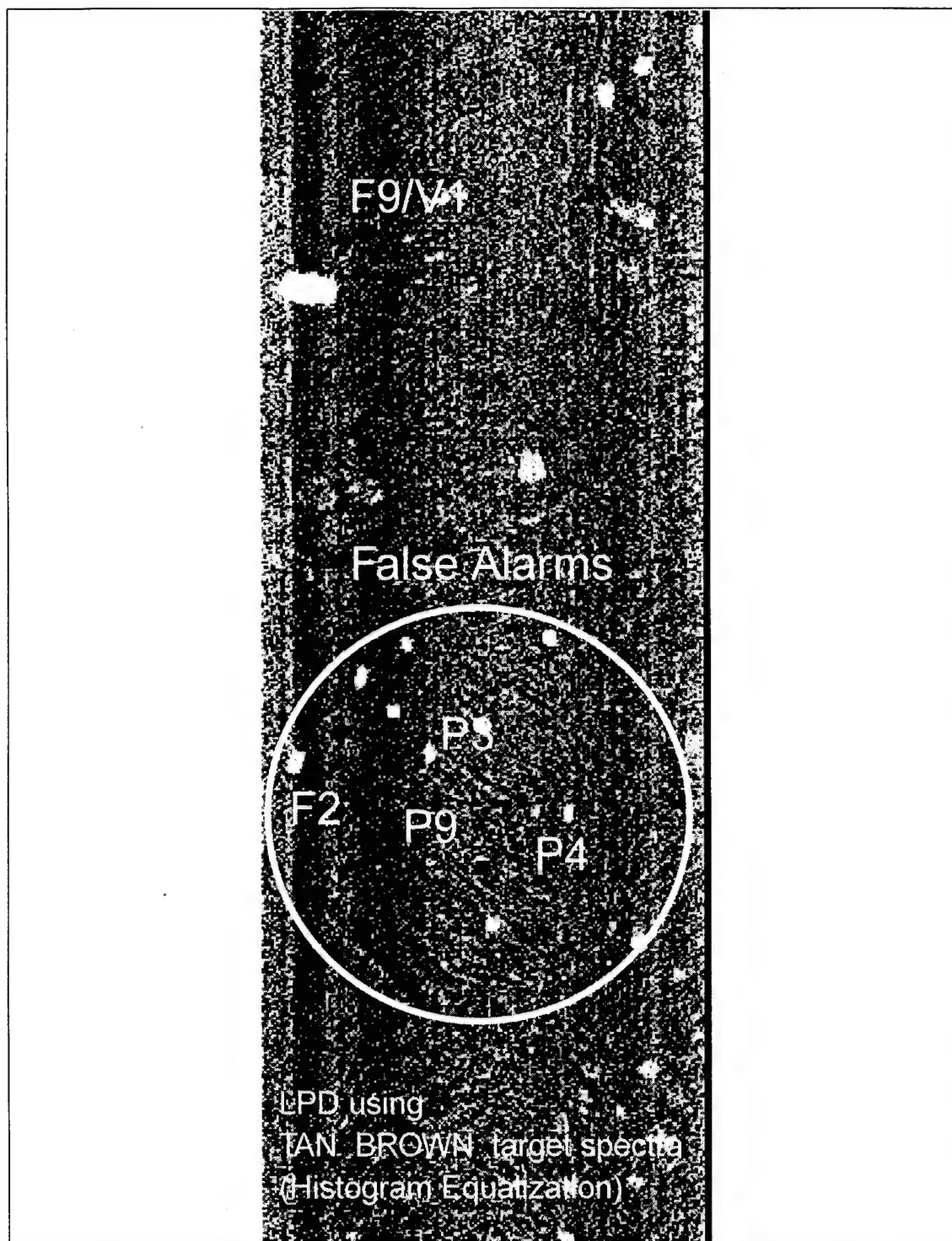


Figure 5.20 (LPD Component Image--TAN BROWN Target Spectra--Histogram Eq.)

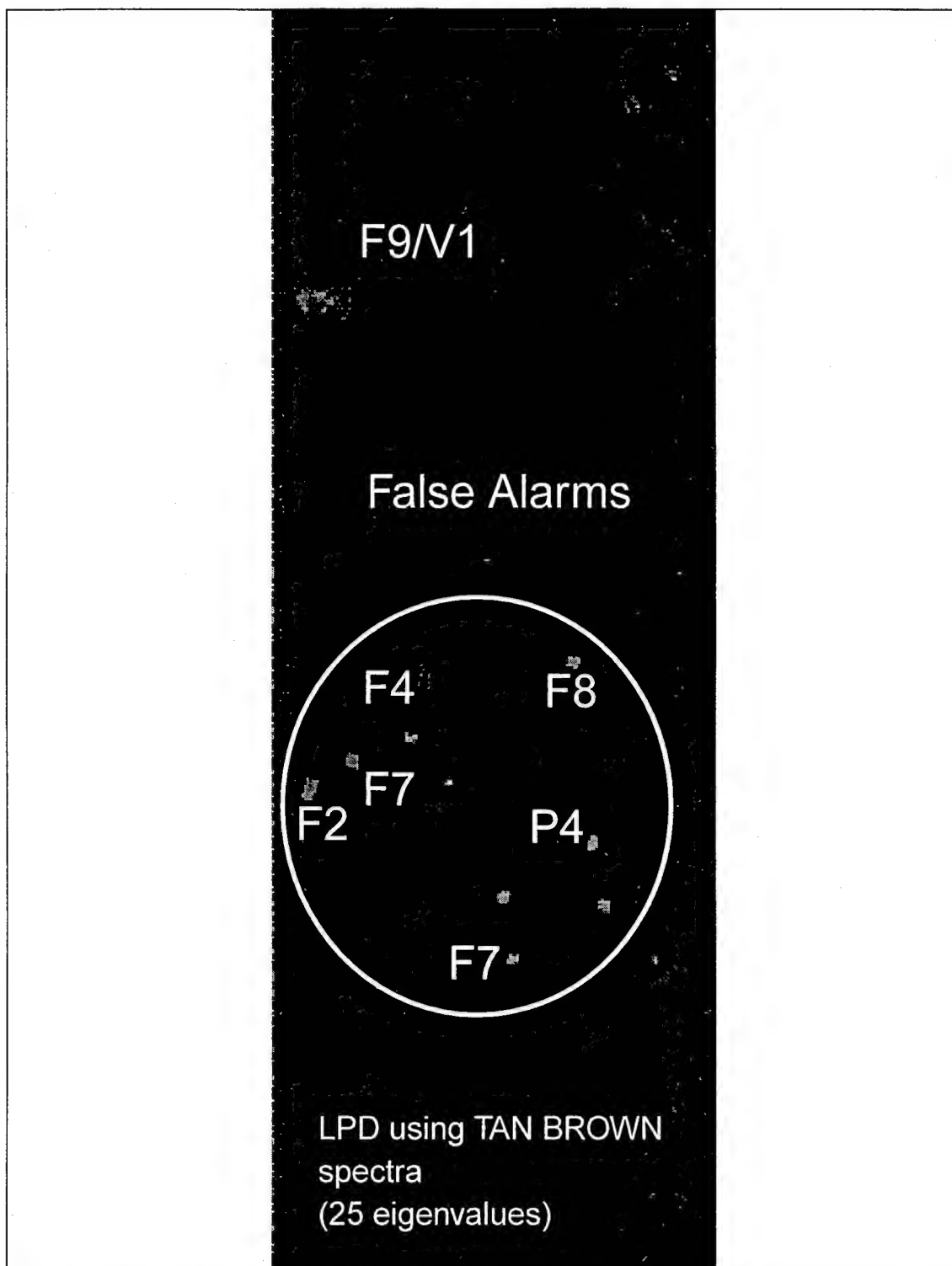


Figure 5.21 (LPD Component Image--TAN BROWN Target Spectra--25 Eigenvalues)

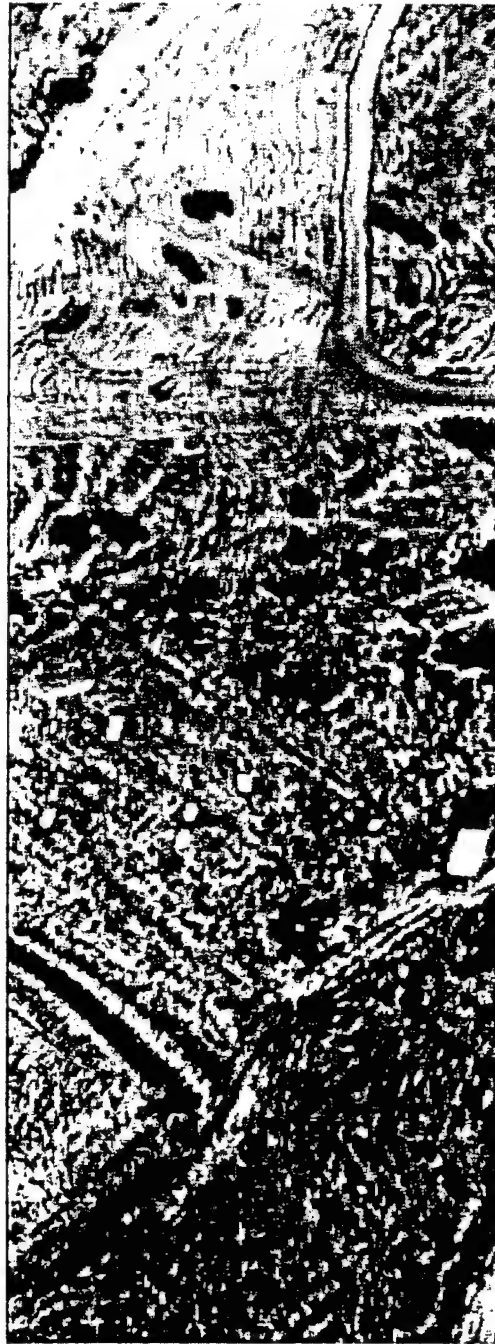


Figure 5.22 (Principle Component 1)



Figure 5.23 (Principle Component 2)



Figure 5.24 (Principle Component 8)

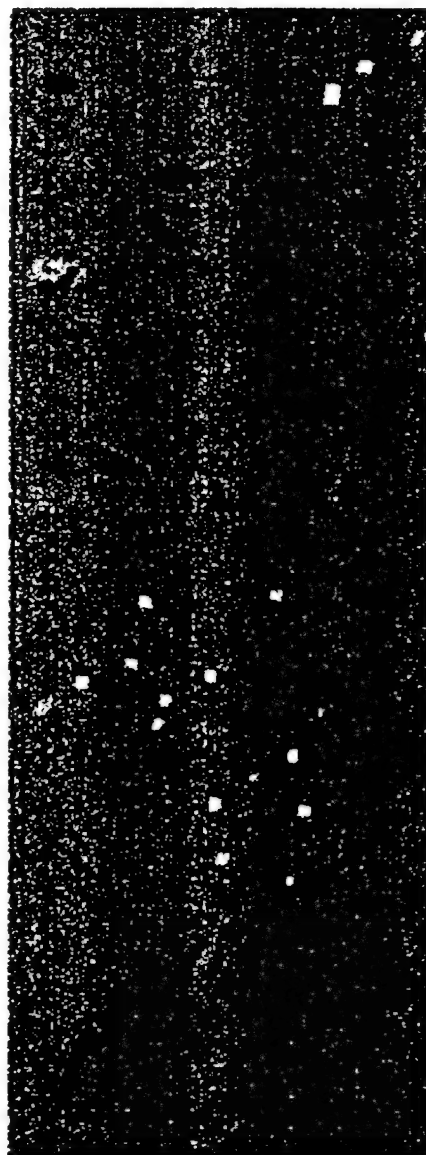


Figure 5.25 (Principle Component 10)

LIST OF REFERENCES

Anderson, M., DESERT RADIANCE, Collection and Exploitation Operations Plan (CEOP - 1), Hyperspectral MASINT Support to Military Operations, HYMSMO Program, pp. 1-110, 1995a.

Anderson, M., Program Review, Programmatics, Hyperspectral MASINT Support to Military Operations, HYMSMO Program, Book 1, 1995b.

Chrien, T.G., Eastwood, M.L., Sarture, C.M., Green, R.O., Porter, W.M., Current Instrument Status of the Airborne Visible/Infrared Imaging Spectrometer (AVIRIS), *Proceedings of the Third Annual Airborne Visible/Infrared Imaging Spectrometer (AVIRIS) Workshop*, JPL Publication 91-28, pp. 302-313, 1991.

Constance, P., Remote Sensing Use Expands to City Planning, *Aviation Week and Space Technology*, pp. 54-55, 19 September 1994.

Cracknell, A.P., Hayes, L.W.B., Introduction to Remote Sensing, Taylor and Francis Ltd., London, pg. 177, 1991.

Farrand, W.H., Harsanyi, J.C., Discrimination of Poorly Exposed Lithologies in Imaging Spectrometer Data, Submitted and Accepted for publication, *Journal of Geophysical Research - Planets*, 1995.

Farrand, W.H., Singer, R.B., Merenyi, E., Retrieval of Apparent Surface Reflectance From AVIRIS Data: A Comparison of Empirical Line, Radiative Transfer and Spectral Mixture Methods, *Remote Sensing of the Environment*, Vol. 47, pp. 311-321, 1994.

Gao, B., Goetz, A.F.H., Determination of Total Column Water Vapor in the Atmosphere at High Spatial Resolution From AVIRIS Data Using Spectral Curve Fitting and Band Ratioing Techniques, *Proceedings of the SPIE, Imaging Spectroscopy of the Terrestrial Environment*, Vol. 1298, pp. 138-148, 1990.

Green, R.O., Conel, J.E., Margolis, J.S., Carrere, V., Bruegge, C.J., Rast, M., Hoover, G., Inflight Validation and Calibration of the Spectral and Radiometric Characteristics of the Airborne Visible/Infrared Imaging Spectrometer (AVIRIS), *Proceedings of the SPIE*, Vol. 1298, pp. 18-35, 1990.

Harsanyi, J.C., Chang, C.I., Hyperspectral image Classification and Dimensionality Reduction: An Orthogonal Subspace Projection Approach, *IEEE Transactions on Geoscience and Remote Sensing*, Vol. 32, No. 4, pp. 779-785, 1994.

Harsanyi, J.C., Farrand, W.H., Chang, C.I., Detection of Subpixel Signatures in Hyperspectral Image Sequences, *American Society of Photogrammetry and Remote Sensing*, 1994.

Herring, M., The Shuttle Imaging Spectrometer Experiment (SISEX), *Proceedings of the SPIE, Imaging Spectroscopy II*, Vol. 834, pp. 181-187, 1987.

Jenson, S.K., Waltz, F.A., Principle Components Analysis and Canonical Analysis in Remote Sensing, *Proceedings of the American Society of Photogrammetry, 45th Annual Meeting*, pp. 337-348, 1979.

Kruse, F.A., Extracting Spectral Information From Imaging Spectrometer Data: A Case History From the Northern Grapevine Mountains, Nevada/California, *Proceedings From the SPIE, Imaging Spectroscopy II*, Vol. 834, pp. 119-128, 1987.

Lehmann, F., Rothfub, H., Richter, R., Evaluation of Imaging Spectrometer Data (GER) for the Analysis of an Old Vegetation Covered Waste Deposit, *Proceedings of the International Geoscience and Remote Sensing Symposium (IGARSS)*, Vol. 2, pp. 1613-1616, 1990.

Melack, J.M., Pilorz, S.H., Reflectance Spectra From Eutrophic Mono Lake, California, Measured With the Airborne Visible and Infrared Imaging Spectrometer (AVIRIS) , *Proceedings of the SPIE, Imaging Spectroscopy of the Terrestrial Environment*, Vol. 1298, pp. 202-210, 1990.

Miller, J.R., Elvidge, C.D., Rock, B.N., Freemantle, J.R., An Airborne Perspective on Vegetation Phenology From the Analysis of AVIRIS Data Sets Over the Jasper Ridge Biological Preserve, *Proceedings of the International Geoscience and Remote Sensing Symposium (IGARSS)*, Vol. 1, pp. 565-568, 1990.

Riggs, G.A., Running, S.W., Canopy Water Stress Detection in Conifers Using the Airborne Imaging Spectrometer, *Proceedings of the International Geoscience and Remote Sensing Symposium, (IGARSS)*, Vol. 1, pg. 896, 1990.

Rinker, J. N., Hyperspectral Imagery - What Is It? - What Can It Do?, Presented at the USACE Seventh Remote Sensing Symposium, 1990.

Rock, B.N., Miller, J.R., Moss, D.M., Freemantle, J.R., Boyer, M.G., Spectral Characterization of Forest Damage Occuring on Whiteface Mountain, NY. - Studies With the Fluorescence Line Imager (FLI) and Ground-based Spectrometers, *Proceedings of the SPIE, Imaging Spectroscopy of the Terrestrial Environment*, Vol. 1298, pp. 190-201, 1990.

Sarture, C.M., Chrein, T.G., Green, R.O., Eastwood, M.L., Raney, J.J., Hernandez, M.A., Airborne Visible/Infrared Imaging Spectrometer (AVIRIS): Sensor Improvements for 1994 and 1995, *Summaries of the Fifth Annual JPL Airborne Earth Science Workshop*, JPL Publication 95-1, Vol. 1, pp. 145-148, 1995.

Silvergate, P., Shu, K.L., Preston, D., Stein, J., Sileo, F., Concepts for Spaceborne Hyperspectral Imaging Using Prism Spectrometers, Hughes Danbury Optical Systems, 1994.

Stoner, W., Upward Projection of Line Spectra, Science Applications International Corporation, Personal paper, 1994.

Taranik, J.V., Mouat, D.A., Eividge, C.D., Hyperspectral Technology For Geologic Applications, *Proceedings of the International Geoscience and Remote Sensing Symposium, (IGARSS)*, Vol. 2, pp. 917-920, 1993.

Thompson, L.L., Moderate Resolution Imaging Spectrometer (MODIS) for the NASA Earth Observing System (EOS), *Proceedings of the SPIE*, Vol. 1298, pp. 105-113, 1990.

Vane, G., First Results From the Airborne Visible/Infrared Imaging Spectrometer (AVIRIS), *Proceedings of the SPIE, Imaging Spectroscopy II*, Vol. 834, pp. 166-174, 1987.

Vane, G., High Spectral Resolution Remote Sensing of the Earth, *Sensors*, December 1985.

Vane, G., Goetz, A.F.H., Terrestrial Imaging Spectrometry: Current Status, Future Trends, *Remote Sensing of the Environment*, Vol. 44, pp. 117-125, 1993.

Vane, G., Goetz, A.F.H., Terrestrial Imaging Spectroscopy, *Remote Sensing of the Environment*, Vol. 24, pp. 1-29, 1988.

Wessman, C.A., Aber, J.D., Peterson, D.L., Estimation of Forest Canopy Characteristics and Nitrogen Cycling Using Imaging Spectrometry, *Proceedings of the SPIE, Imaging Spectroscopy II*, Vol. 834, pp. 114-117, 1987.

INITIAL DISTRIBUTION LIST

	Number of Copies
1. Defense Technical Information Center Cameron Station Alexandria, Virginia 22304-6145	2
2. Library, Code 52 Naval Postgraduate School Monterey, California 93943-5101	2
3. Richard C. Olsen, Code PH/OS Department of Physics Naval Postgraduate School Monterey, California 93943-5002	5
4. Chairman, Code SP Space Systems Academic Group Naval Postgraduate School Monterey, California 93943-5002	1
5. Terry Alfrend, Code SP/AL TENCAP Chair Naval Postgraduate School Monterey, California 93943-5002	1
6. Director, Training and Education MCCDC, Code C46 1019 Elliot Road Quantico, Virginia 22134-5027	1
7. Major Matthew E. Fay 11517 Scottsbury Terrace Germantown, Maryland 20874	2
8. HYDICE Program Office Naval Research Laboratory Code 9120, Building A59 4555 Overlook Avenue, S.E. Washington, D.C. 20375-5320	3

	Number of Copies
9. Captain Thompson Office of the Chief of Naval Operations Code N63, Room 4E679, The Pentagon Washington, D.C. 20350-2000	1
10. Commander, Naval Space Command ATTN: N112 5280 4th Street Dahlgren, Virginia 22448-5300	1
11. Captain A. LeGrow Department of the Navy, CNO Code N632, Room 5P773, The Pentagon Washington, D.C. 20350-2000	1
12. Army Space Program Office ATTN: Mr. Eugene Lambert 2810 Old Lee Highway, Suite 300 Fairfax, Virginia 22031-4304	1